

Contents

Abstract	I
Acknowledgment	III
List of Figures	VII
List of Tables	IX
1 Introduction	1
2 Biological Background	5
2.1 GnRH in the Reproductive System	5
2.1.1 A Brief Experimental History	6
2.2 Electrophysiological Properties and Ca^{2+} Dynamics in GnRH Neurons	7
2.3 Experimental Data	9
2.3.1 Relationship Between Bursting and Ca^{2+} Transients	10
2.3.2 Location of Spike Initiation in GnRH Neurons	12
3 Mathematical Models	15
3.1 The van Goor model	15
3.2 The LeBeau model	16
3.3 The Roberts models	17

3.4	The Fletcher and Li model	20
3.5	The Lee model and the Duan model	21
3.6	The Cserscik model	23
3.7	Summary	24
4	Regulation of Electrical Bursting in a Spatiotemporal Model of a GnRH Neuron	29
4.1	Abstract	30
4.2	Introduction	30
4.3	Model Description	33
4.4	Results	35
4.4.1	Active and Passive Propagation	35
4.4.2	Conduction Velocity	39
4.4.3	Ca ²⁺ Transients in the Dendrite	39
4.4.4	Control of Electrical Bursting by Diffusion of Voltage	42
4.4.5	The Location of the iSite Controls Burst Properties	45
4.5	Discussion	45
5	A Computational Model of the Dendron of the GnRH Neuron	55
5.1	Abstract	56
5.2	Introduction	56
5.3	Model Description	59
5.4	Results	63
5.4.1	The Effects of Synaptic Input on Bursts	63
5.4.2	Modulation of Action Potentials by Synaptic Input	65
5.4.3	Actions of Kisspeptin on Ca ²⁺ Release	68
5.5	Discussion	71
6	Conclusions and Future Work	77
	Bibliography	94

List of Figures

2.1	Schematic representation of the HPG axis	6
2.2	Schematic diagram of the main Ca^{2+} fluxes involved in the control of cytosolic Ca^{2+} concentration	10
2.3	Relationship between bursts and Ca^{2+} transients in GnRH neurons	11
2.4	The dendrites of GnRH neurons propagate spikes	13
2.5	The site of spike initiation does not shift with somatic versus distal dendritic excitation	14
3.1	Schematic diagram of the LeBeau model	17
3.2	Computer renderings of the compartmental models used in Roberts et al. (2006, 2008, 2009)	18
3.3	Schematic diagram of the Fletcher and Li model	21
3.4	Schematic diagram of the model used in Lee et al. (2010) and Duan et al. (2011)	22
3.5	The summarized modular structure of the Cserscik model	24
4.1	Schematic diagram of the GnRH neuron model in Chen et al. (2013)	34
4.2	Active and passive propagation	37
4.3	Conduction velocity	40
4.4	Ca^{2+} transients in the dendrite	41
4.5	Intrinsic bursting and one pharmacological test (CPA) from model simulations	43
4.6	The location of the iSite controls burst properties	46

List of Figures

5.1	The effects of synaptic input on bursting behavior	64
5.2	Spatial distribution of synaptic input affects IBI	66
5.3	Interaction of synaptic input and action potentials.	67
5.4	The effects of synaptic input strength	69
5.5	Effects of different actions of kisspeptin on Ca ²⁺ release	70

List of Tables

3.1	Conductance types used in Roberts et al. (2006, 2008, 2009)	19
4.1	Parameter values of the model in Chen et al. (2013)	53
4.2	Parameter values of the voltage submodel	53
4.3	Parameter values of the Ca^{2+} submodel	54
5.1	Parameter values of the modified IPR P_o function	62
5.2	Some parameter values of the new Ca^{2+} model in Chen and Sneyd (2014) . . .	63

Co-Authorship Form

This form is to accompany the submission of any PhD that contains research reported in published or unpublished co-authored work. **Please include one copy of this form for each co-authored work.** Completed forms should be included in all copies of your thesis submitted for examination and library deposit (including digital deposit), following your thesis Acknowledgements.

Please indicate the chapter/section/pages of this thesis that are extracted from a co-authored work and give the title and publication details or details of submission of the co-authored work.

Chapter 4

Regulation of Electrical Bursting in a Spatiotemporal Model of a GnRH Neuron, Bulletin of Mathematical Biology, Volume 75 Page 1941-1960

Nature of contribution by PhD candidate: Performed the research, wrote the paper

Extent of contribution by PhD candidate (%): 75

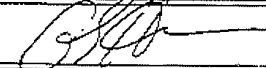
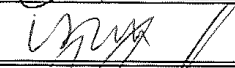
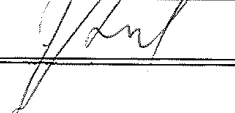
CO-AUTHORS

Name	Nature of Contribution
Karl Iremonger	Contribution of experimental data and comments (5%)
Allan Herbison	Contribution of experimental data and comments (5%)
Vivien Kirk	General supervision and comments (5%)
James Sneyd	General supervision and proof reading (10%)

Certification by Co-Authors

The undersigned hereby certify that:

- the above statement correctly reflects the nature and extent of the PhD candidate's contribution to this work, and the nature of the contribution of each of the co-authors; and
- in cases where the PhD candidate was the lead author of the work that the candidate wrote the text.

Name	Signature	Date
Karl Iremonger		3/7/14
Allan Herbison		3.7.14
Vivien Kirk		3-7-14
James Sneyd		28 July 2014

Co-Authorship Form

This form is to accompany the submission of any PhD that contains research reported in published or unpublished co-authored work. **Please include one copy of this form for each co-authored work.** Completed forms should be included in all copies of your thesis submitted for examination and library deposit (including digital deposit), following your thesis Acknowledgements.

Please indicate the chapter/section/pages of this thesis that are extracted from a co-authored work and give the title and publication details or details of submission of the co-authored work.

Chapter 5

A Computational Model of the Dendron of the GnRH Neuron, Bulletin of Mathematical Biology, Submitted.

Nature of contribution by PhD candidate	Perform the research, wrote the paper
Extent of contribution by PhD candidate (%)	90

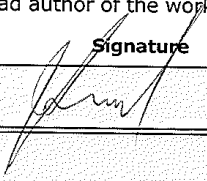
CO-AUTHORS

Name	Nature of Contribution
James Sneyd	General supervision and proof reading (10%)

Certification by Co-Authors

The undersigned hereby certify that:

- ❖ the above statement correctly reflects the nature and extent of the PhD candidate's contribution to this work, and the nature of the contribution of each of the co-authors; and
- ❖ in cases where the PhD candidate was the lead author of the work that the candidate wrote the text.

Name	Signature	Date
James Sneyd		28 July 2014

Introduction

The reproductive system is regulated by the hypothalamic-pituitary-gonadal (HPG) axis that consists of three endocrine organs: the hypothalamus, pituitary gland and gonads (Gore, 2002). Each component of the HPG axis can synthesize and release a hormone. The hypothalamus contains neurons that secrete gonadotropin-releasing hormone (GnRH; also known as luteinizing-hormone-releasing hormone) and are thus named GnRH neurons. GnRH stimulates the pulsatile release of two gonadotropins: luteinizing hormone (LH) and follicle-stimulating hormone (FSH) in the anterior pituitary, which in turn stimulate the secretion of sex hormones in the gonads, including estrogen and progesterone in females and testosterone in males. Since it plays a key role in regulating the HPG axis, GnRH is a major controller of the reproductive system.

GnRH neurons originate outside the central nervous system in the olfactory placodes and migrate to their final locations in the hypothalamic preoptic area (Schwanzel-Fukuda and Pfaff, 1989). These neurons have oval and round cell bodies, and exhibit either uni- or bipolar morphology (Gore, 2002). The dendrites of GnRH neurons can be remarkably long (i.e., more than 1.5 mm, (Campbell et al., 2005)), extending towards the median eminence from where hormones, including GnRH, are released.

The rhythmic release of GnRH is essential for reproduction, fertility, and maturation (Herbison, 2006). However, the mechanisms underlying its pulsatile releases are not well understood. Numerous experimental and theoretical studies have attempted to explain different aspects of these activities, such as the properties of electrical bursting and Ca^{2+} dynamics, which are thought to be essential for GnRH release (Moenter et al., 2003; Herbison, 2006). Previous studies have shown that some of the mechanisms for controlling the bursting behavior are lo-

cated in the soma (Lee et al., 2010). However, Iremonger and Herbison (2012) have shown that the initial 150 μm of the dendrite is highly excitable and is the site of spike initiation. Using an alternative method, Herde et al. (2013) reported that the site of spike initiation is located $89 \pm 30 \mu\text{m}$ from the soma. GnRH neuron projections have the properties of both dendrites and axons (Campbell et al., 2005; Cottrell et al., 2006; Roberts et al., 2008; Campbell et al., 2009; Iremonger and Herbison, 2012; Herde et al., 2013). In other words, these projections not only receive synaptic inputs, but they are also the site of action potential initiation and propagate action potentials to their nerve endings in the median eminence. These findings raise two questions:

- Firstly, how can electrical bursting be regulated when it is initiated at a site located some distance from the controlling mechanisms?
- Secondly, how does stochastic synaptic input along the length of the dendrite/axon affect the initiation and propagation of action potentials?

In this thesis, we used mathematical modeling to examine and answer these questions.

This thesis contains six chapters and is structured as follows.

- Chapter 2 provides a brief introduction to the biological aspects of GnRH neurons. The importance of GnRH in the reproductive system is described and some important techniques for experimental development are discussed. Based on previous experimental studies, the electrophysiological properties and Ca^{2+} dynamics in the GnRH neurons are discussed. Finally, some experimental results which motivated this research project are presented.
- Chapter 3 is a review of some earlier mathematical models of GnRH neurons. Although all these models were successful in achieving their own specific goals, reasons for why these models are not suitable for our current study are discussed.
- Chapter 4 describes a new spatiotemporal mathematical model of a GnRH neuron that includes both the soma and the dendrite. Our goal was to answer the first question raised in this thesis. We showed that the large diffusion coefficient provides a mechanism for

regulating bursting behavior by the interaction of the soma and the dendrite. The work described in Chapter 4 has been published in the *Bulletin of Mathematical Biology*; see Chen et al. (2013) in the bibliography for the full reference.

- Chapter 5 describes an expanded spatiotemporal model, which additionally incorporates stochastic synaptic input in order to study the second question raised in this thesis. We demonstrated that synaptic input along the dendrite is not a likely mechanism for controlling whether action potentials reach the synaptic terminal. Therefore, we proposed other possible ways in which synaptic input could modify Ca^{2+} release at the synaptic terminal, focusing in particular on kisspeptin. The work presented in Chapter 5 has been submitted to the *Bulletin of Mathematical Biology* for publication; see Chen and Sneyd (2014) in the bibliography for the full publication details.
- Chapter 6 summarizes major findings presented in this thesis and discusses some ideas for future study of GnRH neurons.

Biological Background

2.1 GnRH in the Reproductive System

The HPG axis consists of three endocrine organs: the hypothalamus, pituitary gland and gonads. Each level of the HPG axis produces specific hormones which are critical for reproductive function; see Figure 2.1. GnRH produced in the hypothalamus plays an important role in the HPG axis, and is the primary regulator of the entire reproductive system (Gore, 2002). For example, lack of GnRH leads to hypogonadotropic hypogonadism (i.e., a failure in the normal function of the ovaries or testes) (Weiss et al., 1989; Layman, 1999; MacColl et al., 2002).

GnRH is a neurohormone synthesized and released by GnRH neurons in the hypothalamus, which is then transported by blood to the anterior pituitary. One important role of GnRH is to regulate the release of gonadotropin from the anterior pituitary. GnRH is released in a periodic pattern that in turn stimulates the pulsatile release of two gonadotropins: LH and FSH (Clayton and Catt, 1981). High frequency GnRH pulses result in LH release, whereas low frequency GnRH pulses stimulate FSH secretion (Kaiser et al., 1997). These two hormones play important roles in communication to the gonads, such as promoting oogenesis/spermatogenesis and secretion of sex hormones in the gonads (Hillier, 2001). The sex hormones estrogen and progesterone in females and testosterone in males, act on many tissues in the body and also provide feedback to the hypothalamus and the pituitary gland to regulate the release of GnRH and gonadotropins (Hiller-Sturmhofel and Bartke, 1998). These mechanisms demonstrate the importance of GnRH for reproductive function by acting through the HPG axis; see Figure 2.1.

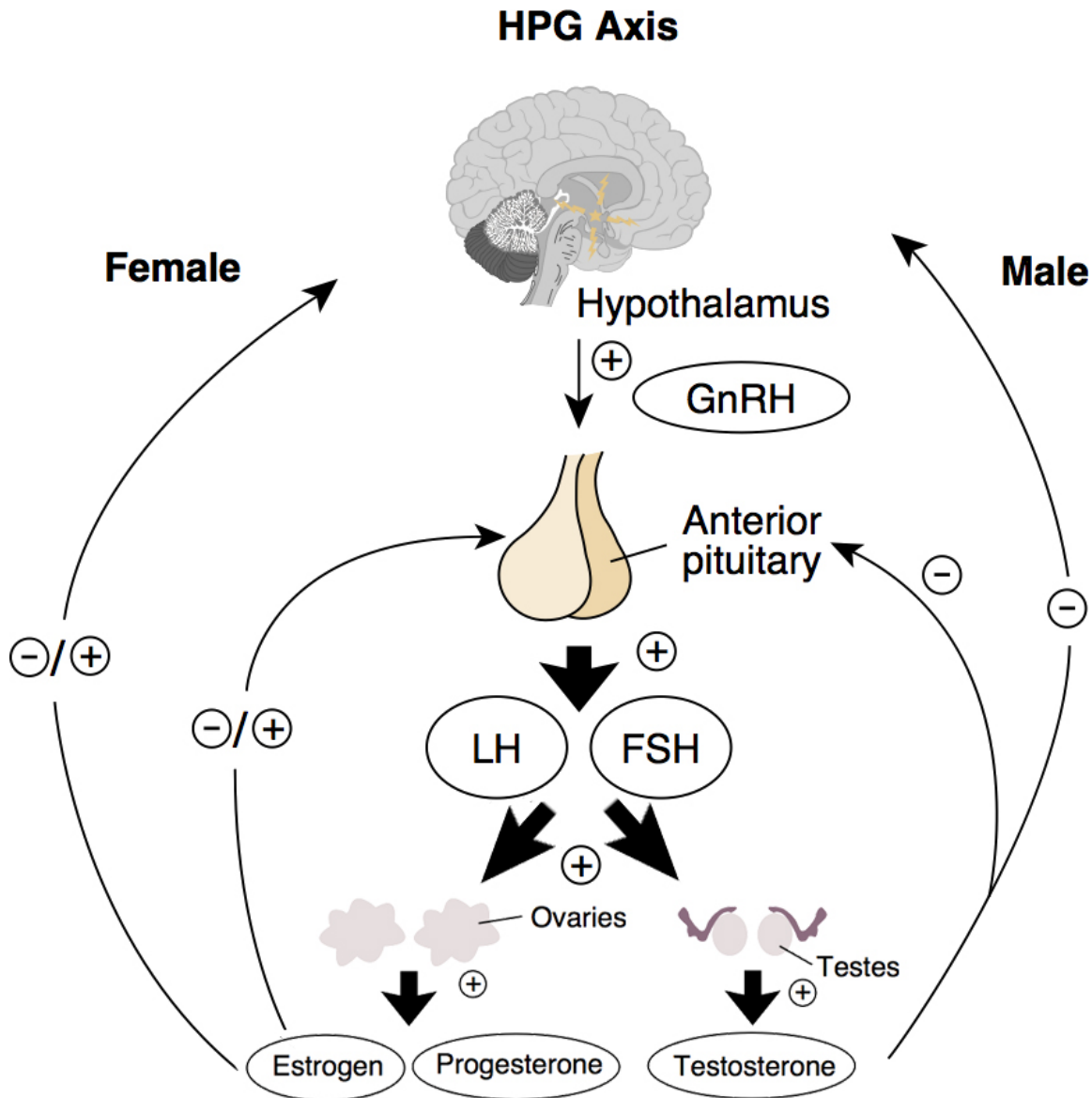


Figure 2.1 Schematic representation of the HPG axis. The hypothalamus secretes GnRH that acts on the pituitary gland. In response to those stimuli, the pituitary gland releases gonadotropins (LH and FSH). In women, LH and FSH stimulate the ovaries to produce estrogen and progesterone in the gonads. In men, LH stimulates the testes to release testosterone. The sex hormones in the gonads then send either positive or negative feedback to the hypothalamus and the pituitary gland. Figure adapted from Hiller-Sturmhofel and Bartke (1998).

2.1.1 A Brief Experimental History

Given their importance in the reproductive system, it is surprising that the number of GnRH neurons is very small, approximately 800 to 2000 neurons depending on the species (Gore, 2002). Due to the limited number and sparse distribution of GnRH neurons in the hypothalamus, experimental approaches to study these neurons were difficult and complicated before cell models (Mellon et al., 1990) were used.

In 1990, the discovery of immortalized GnRH-secreting neurons (GT1 cells) (Mellon et al., 1990) provided the opportunity to study the electrophysiological activity of GnRH neurons. Subsequent work (Constantin and Charles, 1999; Spergel et al., 1999; van Goor et al., 1999a,b) on GT1 cells have shown that bursts of action potentials are closely correlated with Ca^{2+} transients. GT1 cells are different to native GnRH neurons. For example, cultures of GT1 cells do not contain any other cell types, and hence lack many network interactions. With the development of GnRH-reporter transgenics (Herbison et al., 2001), experimentalists have had the ability to study the physiology of GnRH neurons in acute brain slice preparations. The transgenic mice models have also provided additional insight into the morphology of GnRH neurons (Suter et al., 2000; Campbell et al., 2005; Roberts et al., 2006; Campbell et al., 2009). These studies found that the dendrites of biocytin-filled GnRH neurons are very long and bundle with one another (Campbell and Suter, 2010). Other techniques were also developed to monitor Ca^{2+} dynamics and electrical bursting in GnRH neurons in a close approximation of their native environment (Nagai et al., 2001; Jasoni et al., 2007).

2.2 Electrophysiological Properties and Ca^{2+} Dynamics in GnRH Neurons

GnRH neurons represent the final output cells of the hypothalamic neuronal system regulating fertility in mammals (Herbison, 2006). Although the mechanisms underlying the pulsatile release of GnRH are not well understood at the cellular or network level, the bursting behavior of electrical activity and Ca^{2+} dynamics in GnRH neurons appears to play an important role in GnRH secretion (Moenter et al., 2003; Herbison, 2006). The understanding of the mechanisms to generate spike firing and to regulate the burst firing properties is therefore important.

Many electrophysiological studies of GnRH neurons (Spergel et al., 1999; Suter et al., 2000; Sim et al., 2001; Nunemaker et al., 2002; Kuehl-Kovarik et al., 2002; Abe and Terasawa, 2005; Han et al., 2005; Pielecka-Fortuna et al., 2008; Herbison and Moenter, 2011) have suggested that GnRH neurons can generate patterned firing activity intrinsically, but may require external or network interactions for pulsatile hormone release (Moenter, 2010).

Bundled dendrites with shared synaptic inputs (Campbell et al., 2009) provide the possibility of synchronization due to input from outside the GnRH network. GnRH neurons can respond directly to a range of neurotransmitters (Christian and Moenter, 2008; Clasadonte et al., 2008; Iremonger et al., 2010; Herbison and Moenter, 2011), while kisspeptin mediates a particularly potent one (Han et al., 2005; d'Anglemont de Tassigny et al., 2008; Keen et al., 2008). The importance of extrinsic inputs, especially kisspeptin, will be discussed in more detail in Chapter 5.

The electrical activity of GnRH neurons is determined by the ion channels present in the cell membrane. Some channels that are responsible for the action potential and burst firing have been identified in previous studies: TTX-sensitive Na^+ channels (Kusano et al., 1995; Constantin and Wray, 2008), inward rectifier, delayed rectifier and M-type K^+ channels (Kusano et al., 1995; Sim et al., 2001; DeFazio and Moenter, 2002; Chu and Moenter, 2006), voltage-gated Ca^{2+} channels (Kusano et al., 1995; Nunemaker et al., 2003; Kato et al., 2003), apamin-sensitive afterhyperpolarizing potentials (Liu and Herbison, 2008), UCL-sensitive slow afterhyperpolarizing potentials (Lee et al., 2010), hyperpolarization-gated non-specific cation channels (Chu et al., 2010), and Na^+ -dependent Ca^{2+} -activated afterdepolarization channels (Chu and Moenter, 2006).

Voltage-dependent Na^+ channels are critical for action potential generation (Kusano et al., 1995), while the voltage-dependent K^+ channels are critical for determining membrane repolarization and the interspike interval in GnRH neurons (Sim et al., 2001). Influx through Ca^{2+} channels activates pacemaker currents, including apamin-sensitive small-conductance Ca^{2+} -activated K^+ (SK) currents which are responsible for afterhyperpolarization to control the firing rates and terminate bursting (Liu and Herbison, 2008), and UCL-sensitive slow Ca^{2+} -dependent K^+ currents which are responsible for slow afterhyperpolarization to regulate the interburst interval (Lee et al., 2010). There are also two pacemaker currents, the hyperpolarization-activated cation current which was suggested to affect bursting behavior (Chu et al., 2010), and the Ca^{2+} - and Na^+ -dependent afterdepolarization current which may be important to modulate action potential firing (Chu and Moenter, 2006). These channels have been considered in previous mathematical modeling studies that will be reviewed in the next chapter.

Ca^{2+} plays a critical role in many physiological activities, such as muscle mechanics, saliva secretion, bursting oscillations, and hormone secretion (Berridge et al., 1998; Keener and Sneyd, 2008; Lee et al., 2010; Palk et al., 2010; Cao et al., 2013). Some of the major fluxes involved in Ca^{2+} dynamics are shown in Figure 2.2.

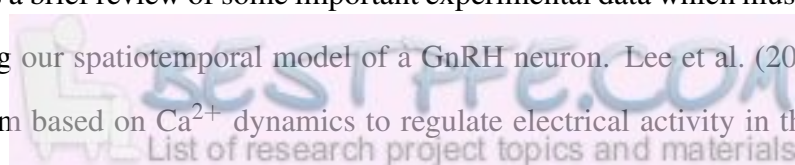
There are two pathways for Ca^{2+} to be removed from the cytosol: it can be pumped out via plasma membrane Ca^{2+} -ATPase (PMCA) and Na^{+} - Ca^{2+} exchanger (NCX) plasma membrane pumps (J_{pm}), or can be pumped from the cytosol to the endoplasmic reticulum (ER) by the sarco/endoplasmic reticulum Ca^{2+} -ATPase (SERCA) pump (J_{serca}). There are also two pathways for Ca^{2+} to enter the cytosol: one is the inflow from outside of the cell through plasma membrane Ca^{2+} channels (J_{in}), and the other is the release from internal stores (J_{release}), such as the ER, through inositol trisphosphate (IP_3) receptor.

The IP_3 receptor (IPR) is sensitive to the second messenger IP_3 , which is important in many cells including GnRH neurons. The binding of an agonist (such as a hormone or a neurotransmitter) outside the cell to a receptor on the cell membrane activates a G-protein which activates phospholipase C (PLC) (Berridge, 1993). PLC then hydrolyzes phosphatidylinositol (4,5)-bisphosphate (PIP_2) to diacylglycerol (DAG) and IP_3 (Berridge, 1993); see Figure 2.2. IP_3 diffuses through the cytosol and binds to IPR in the ER membrane, which leads to the opening of IPR and subsequent release of Ca^{2+} from the ER (Ferris et al., 1989).

The release of Ca^{2+} from the ER via IPR is an important mechanism in Ca^{2+} dynamics. The process that a small amount of Ca^{2+} entering the cell through voltage-gated Ca^{2+} channels initiates a large release of Ca^{2+} from the ER through IPR, is known as Ca^{2+} -induced Ca^{2+} release (CICR). It plays a significant role in Ca^{2+} dynamics for the bursting control mechanism in GnRH neurons (Lee et al., 2010).

2.3 Experimental Data

This section gives a brief review of some important experimental data which must be considered when constructing our spatiotemporal model of a GnRH neuron. Lee et al. (2010) provided a control mechanism based on Ca^{2+} dynamics to regulate electrical activity in the soma, while



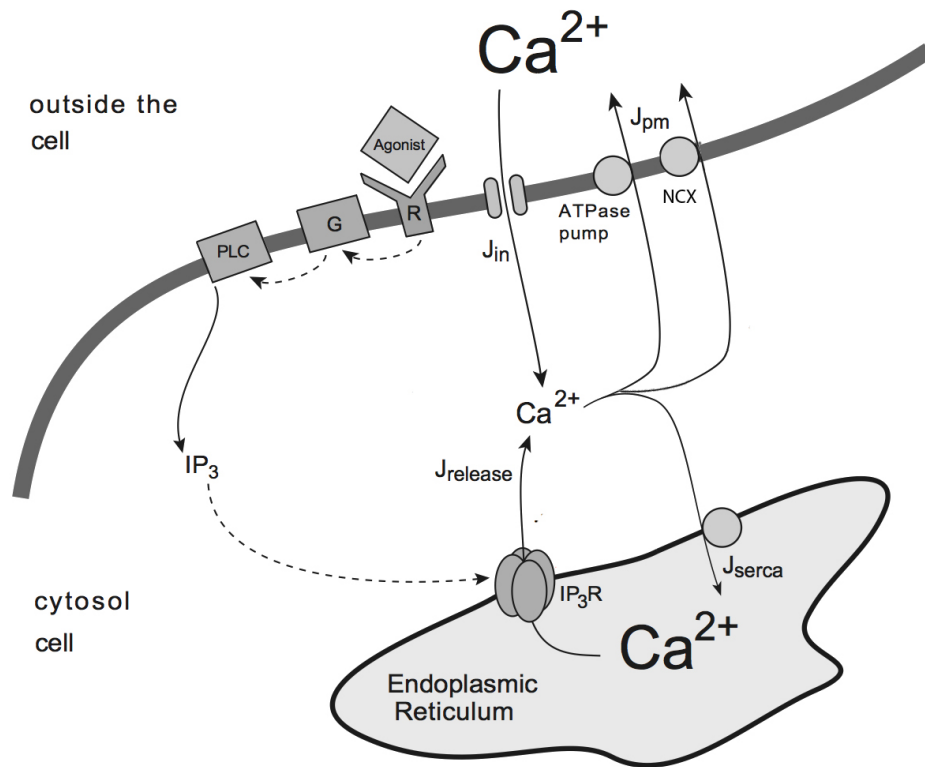


Figure 2.2 Schematic diagram of the main Ca^{2+} fluxes involved in the control of cytosolic Ca^{2+} concentration. Figure adapted from Keener and Sneyd (2008).

Iremonger and Herbison (2012) showed that the first 150 μm of dendrite is the most excitable and is the site of action potential initiation in GnRH neurons.

2.3.1 Relationship Between Bursting and Ca^{2+} Transients

Recent findings in adult GnRH neurons (Lee et al., 2010) showed that the burst firing and Ca^{2+} transients were perfectly correlated in the majority of recorded cells; see Figure 2.3. The GnRH neurons exhibited spontaneous bursts with variable interburst intervals (IBI; a mean of 40 ± 6 seconds, but with a bimodal distribution). There were about three or four action potentials in each burst, and each burst was synchronized with a Ca^{2+} transient, as shown in Figure 2.3(a). An expanded view of the relationship between a three-spike burst and corresponding Ca^{2+} transient is shown in Figure 2.3(b).

In order to further investigate the electrophysiology and Ca^{2+} dynamics of GnRH neurons, Lee et al. (2010) performed several pharmacological manipulations, such as the addi-

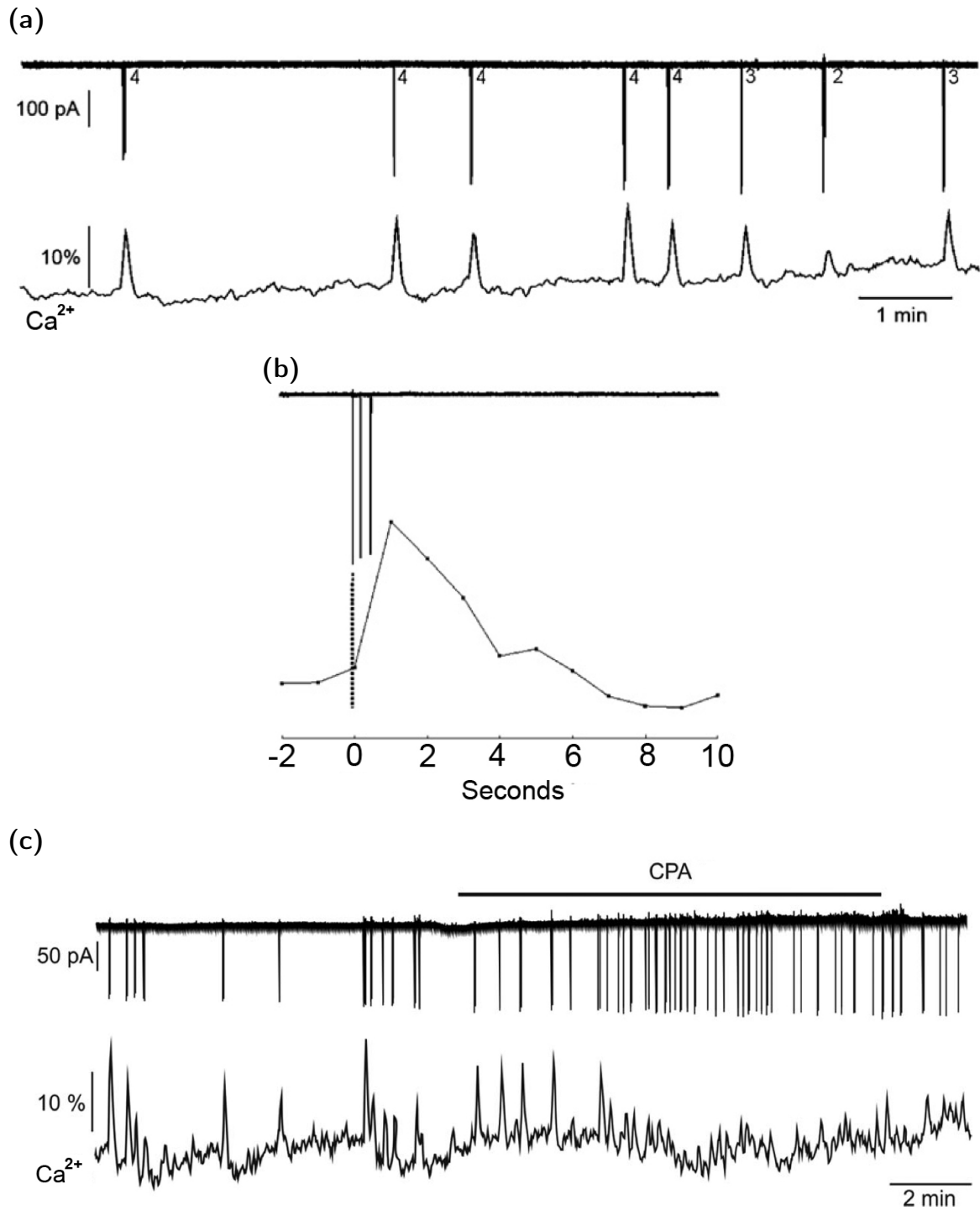


Figure 2.3 Relationship between bursts of action potential and Ca^{2+} transients in GnRH neurons. (a) Representative example of dual recordings from a burst of action potentials and corresponding intracellular Ca^{2+} transients. The numbers represent the number of action potentials in each burst in the upper trace. (b) A close-up view of the relationship between a three-spike burst and Ca^{2+} transient. (c) Representative example showing the effect of one pharmacological test (CPA). The SERCA pump inhibitor CPA decreased the amplitude of the Ca^{2+} transient and disorganized burst firing. Figures adapted from Lee et al. (2010).

tion of tetrodotoxin (TTX, a voltage-dependent Na^+ channel blocker), zero extracellular Ca^{2+} , 2-aminoethoxydiphenylborate (2-APB, IPR antagonists), cyclopiazonic acid (CPA, SERCA pump antagonists), apamin (small-conductance Ca^{2+} -activated K^+ (SK) channel blocker), and UCL2077 (slow Ca^{2+} -activated afterhyperpolarization K^+ (UCL) channel blocker). We show here only one pharmacological test (CPA) as an example; see Figure 2.3(c).

Lee et al. (2010) reported that burst firing initiates Ca^{2+} transients in GnRH neurons. They also showed that the Ca^{2+} transient depends on both external and internal Ca^{2+} concentrations. The responses to the application of apamin and UCL2077 show that the two Ca^{2+} -activated K^+ channels (SK and UCL) had distinct roles in regulating burst firing. The authors suggested that the Ca^{2+} transient arose from a voltage-dependent membrane Ca^{2+} flux which initiated CICR from the ER via IPR. This large Ca^{2+} transient activates two pacemaker K^+ currents; the SK K^+ channel terminates the spike firing, while a longer lasting hyperpolarizing UCL current determines the interburst interval.

2.3.2 Location of Spike Initiation in GnRH Neurons

Consistent with previous experimental findings in Roberts et al. (2008), Iremonger and Herbison (2012) reported that the proximal dendrites of GnRH neurons are the most excitable and are the spike initiation sites in these neurons. In order to examine the location of spontaneous action potential initiation in GnRH neurons, Iremonger and Herbison (2012) performed simultaneous on-cell recordings from the soma and dendrite. Figure 2.4 shows two examples of spiking recorded in the soma and dendrite in two different neurons. The recordings from the first neuron, as shown in Figure 2.4(a), indicate that spikes are first detected at the somatic recording electrode before the dendritic electrode, while the results for the second neuron indicate the reverse case as shown in Figure 2.4(b). Thus the authors suggested that some GnRH neurons were capable of initiating spikes spontaneously in the dendrite.

Roberts et al. (2008) reported that GnRH neurons express Na^+ channels on the dendrite and hence suggested the dendrite may be the site of action potential initiation. However, the authors could not detect changes in channel density along the dendrite. With a different approach, Iremonger and Herbison (2012) observed that the initial 150 μm of the dendrite expressed

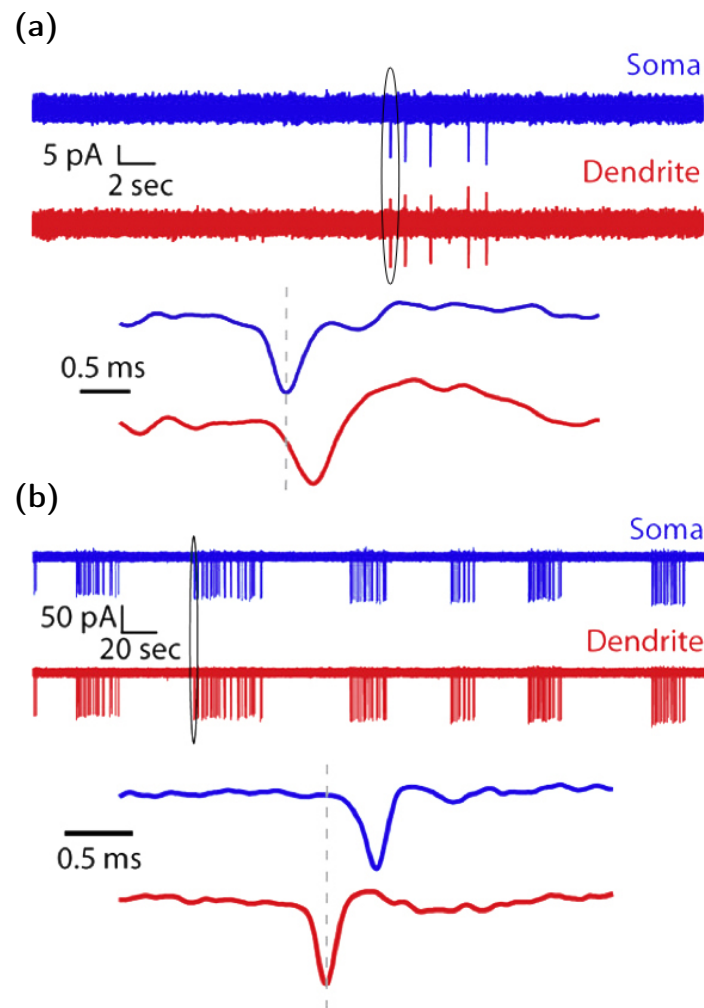


Figure 2.4 The dendrites of GnRH neurons propagate spikes. **(a)** The top panel shows a five-spike burst recorded in the soma and dendrite. The bottom panel shows an expanded view of the initial spike of the burst, which indicates the spike was detected at the somatic recording electrode before the dendritic electrode. **(b)** Recording of action potential with bursting pattern firing from a different GnRH neuron. The expanded view of a spike in the bottom panel shows the spike was observed at the dendritic recording electrode before the somatic electrode. Figures adapted from Iremonger and Herbison (2012).

a high Na^+ channel density. It was therefore suggested that proximal dendrites of the GnRH neuron are highly excitable. By using an alternative method, Herde et al. (2013) reported that the largest influx of Na^+ during a burst of action potentials was located at a distance of $89 \pm 30 \mu\text{m}$ from the soma in the projection process leading to the median eminence.

With excitatory inputs puffed onto either the soma or dendrite, that is 1 mM glutamate and glycine was injected into the cell, Iremonger and Herbison (2012) performed dual on-cell recordings in order to determine whether the site of spike initiation can shift. Figure 2.5 shows some spiking activities including spontaneous spiking, somatic-puff-evoked spiking and dendritic-puff-evoked spiking, recorded at both the soma and the dendrite of a single neuron.

There is no significant difference in latency between the somatic and dendritic recording for those three cases; see Figure 2.5(b). Iremonger and Herbison (2012) suggested that there is a relatively fixed spike initiation site. This was further confirmed by Herde et al. (2013) who found that there is only a single site of spike initiation in each GnRH neuron.

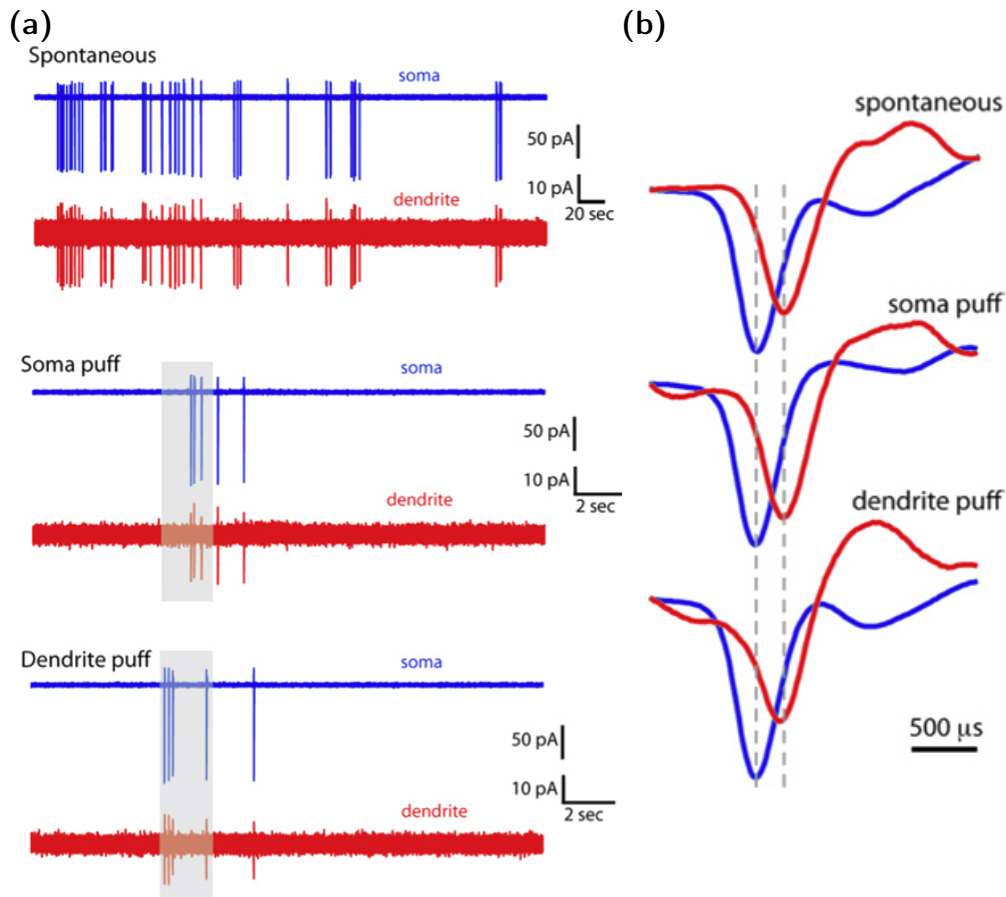


Figure 2.5 The site of spike initiation does not shift with somatic versus distal dendritic excitation. **(a)** Spikes recorded at both the soma and dendrite of a single cell in three situations: spontaneous spiking, spiking with excitatory inputs (glutamate and glycine: 1mM) added at the soma, and inputs added at the dendrite. Spikes were evoked by a 2 second puff of synaptic input at each site. **(b)** The expanded view of spikes show no significant difference in latency between the somatic and dendritic recording. Figures adapted from Iremonger and Herbison (2012).

Mathematical Models

In the last 15 years, a number of mathematical models of GnRH neurons have been developed. These models have been used to explain different aspects of GnRH neurons, such as the properties of burst electrical firing and their associated Ca^{2+} transients. Some models were constructed to explain the experimental data obtained from GT1 cells (van Goor et al., 2000; LeBeau et al., 2000; Fletcher and Li, 2009), while others were based on hypothalamic cells (Lee et al., 2010; Duan et al., 2011; Roberts et al., 2006, 2008, 2009; Cserscik et al., 2012). Some are spatially homogeneous (van Goor et al., 2000; LeBeau et al., 2000; Fletcher and Li, 2009; Lee et al., 2010; Duan et al., 2011), whereas others include a model of the dendrite, reflecting the spatiotemporal properties of GnRH neurons (Roberts et al., 2006, 2008, 2009; Cserscik et al., 2012).

This chapter gives a brief review of these mathematical models and shows the importance of mathematical models in studying GnRH neurons. However, none of these models was sufficient for our purposes, as they did not take into account the more recent data of Iremonger and Herbison (2012). As a result, we constructed a new model based partially on the older models, but also incorporating some new elements.

3.1 The van Goor model

The van Goor model is a conductance-based model of the electrical activity of a GT1 neuron, based on both experimental and modeling results, by van Goor et al. (2000). The authors explained how the GnRH neuron spiking pattern shifted from a sharp, high amplitude to a broad,

low amplitude under sustained membrane depolarization.

This model included fast, voltage-dependent currents: a TTX-sensitive Na^+ current (I_{Na}), L- and T-type Ca^{2+} currents (I_{CaL} and I_{CaT} , respectively), a delayed-rectifier-type K^+ current (I_{KDR}), an M-like K^+ current (I_{M}), an inward rectifier K^+ current (I_{ir}), and a Ca^{2+} -carrying, voltage-insensitive inward leak current I_d . All of these currents (except I_{Na}) were modeled by typical Hodgkin-Huxley equations (Hodgkin and Huxley, 1952). The authors suggested that the Hodgkin-Huxley-like Na^+ channel description was unable to accurately explain GT1 cell behavior. The model of I_{Na} was hence adapted from Kuo and Bean (1994) with a four-state Markov model. Their modeling study also indicated that the inactivation of the Na^+ channel was responsible for the spike amplitude reduction, while the decrease in K^+ current activation affected the spike broadening.

3.2 The LeBeau model

LeBeau et al. (2000) constructed a quantitative description of the regulation of action potential pacemaking and the associated Ca^{2+} signaling in GT1 cells. They extended the van Goor model by adding Ca^{2+} dynamics and Ca^{2+} -sensitive currents. With their theoretical study, LeBeau et al. (2000) reported that interplay between three pacemaker currents, I_{SOC} , I_{SK} , and I_d , could explain responses to the various stimuli in experimental tests.

A schematic diagram of the model is given in Figure 3.1. LeBeau et al. (2000) kept all the fast currents exactly the same as used in van Goor et al. (2000), except for the leak current. Based on the experimental evidence from van Goor et al. (1999a), three pacemaker currents, a SK-type Ca^{2+} -activated K^+ current (I_{SK}), a store-operated Ca^{2+} current (I_{SOC}), and an inward leak current (I_d) which is a Ca^{2+} -inactivated non-specific cation current, were added. The SK channel was modeled in the usual way, with a linear dependence on fractional activation by Ca^{2+} and voltage driving force. The description of I_{SOC} was defined in a similar way, except that it had the inverse fractional activation by shell ER Ca^{2+} concentration. I_d was assumed to be a cyclic adenosine monophosphate (cAMP)-regulated pacemaker current, controlling spontaneous electrical firing and associated Ca^{2+} signaling.

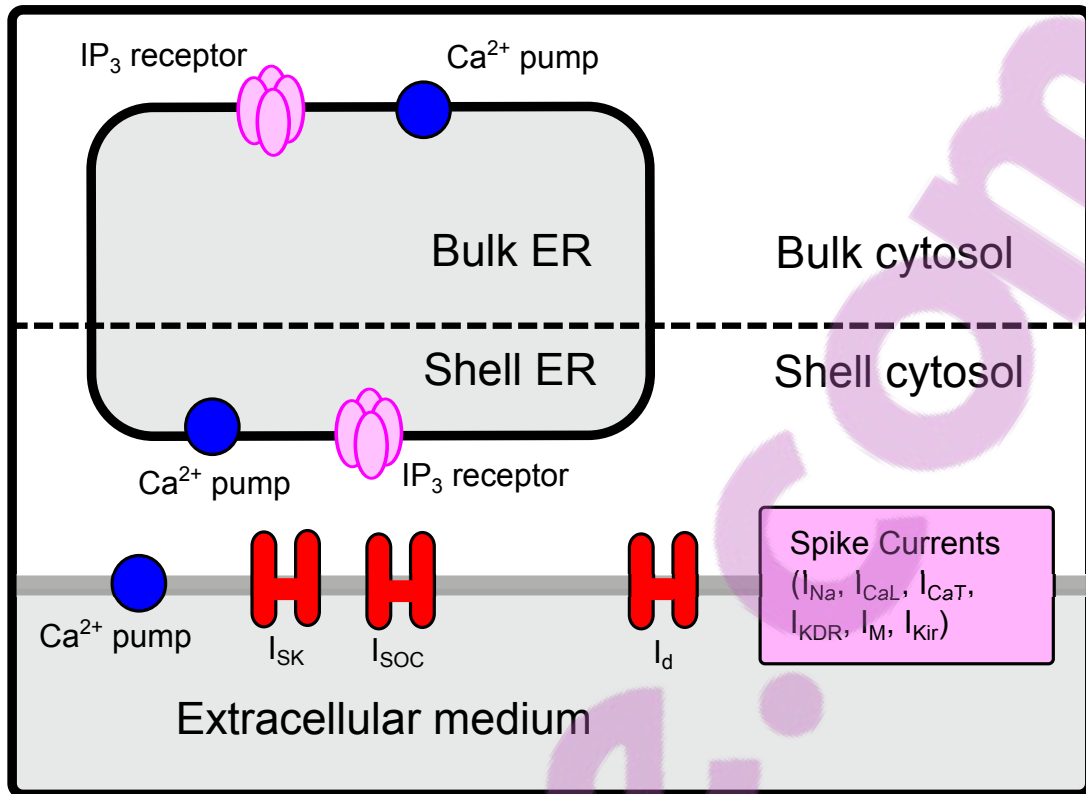


Figure 3.1 Schematic diagram of the LeBeau model. The cell was divided into two compartments, ER and cytosol. Both compartments were further separated into shell and bulk sub-compartments. The model kept all the currents used in van Goor et al. (2000), except for the leak current. The Ca^{2+} dynamics and three Ca^{2+} -sensitive pacemaker currents I_{SOC} , I_{SK} , and I_d were also added. Figure adapted from LeBeau et al. (2000).

To model Ca^{2+} dynamics, the cell was separated into ER and cytosol. These two compartments were further divided into two sub-compartments, shell and bulk; see Figure 3.1. The Ca^{2+} -sensitive currents mentioned above were coupled to the shell compartment's Ca^{2+} concentration. The Ca^{2+} dynamics included influx via plasma membrane channels (j_{in}), efflux via PMCA and NCX plasma membrane pumps (j_{eff}), release and uptake of Ca^{2+} from the shell and bulk ER (j_{rels} , j_{ups} , j_{relb} , and j_{upb} , respectively), diffusional exchange in the cytosol and ER (cyt_{ex} , ER_{ex}), and efflux and uptake from the shell and bulk mitochondria (j_{meffs} , j_{mups} , j_{meffb} , and j_{mupb} , respectively).

3.3 The Roberts models

Roberts et al. (2006) was the first study to construct multi-compartmental models of hypothalamic GnRH neurons. Electrophysiological recordings and neuronal morphology were used to

generate computer models, which studied how synaptic input to the dendrite of GnRH neurons would control firing. Figure 3.2 shows the computer renderings of the bipolar and branching GnRH neuron, where each gray shaded cylinder represents individual compartments for the soma, dendrite and axon in the model. Roberts et al. (2006) also reduced the model to a single soma compartment to understand the fundamental behavior of GnRH neurons. The kinetics of the channels were adapted from published models of GT1 cells (van Goor et al., 2000; LeBeau et al., 2000). The model of Roberts et al. (2006) only included the three strongest currents as shown in Table 3.1, the fast Na^+ current (I_{Na}), delayed rectifier K^+ current (I_{Kdr}), and L-type Ca^{2+} current (I_{CaL}), all described by typical Hodgkin-Huxley equations and applied to both soma and axon compartments. Their findings indicated that the cellular mechanisms generating spikes from GT1 cells and cultured neurons may not be the same as those in hypothalamic GnRH neurons. The authors assumed that the dendrite of the GnRH neuron is passive, which suggested that only synapses located on the soma and very proximal dendrites were capable of controlling somatic spiking. Moreover, it suggested that the dendrite may receive extensive synaptic input, but has limited effect on controlling spike firing.

The experimental work of Roberts et al. (2008) revealed voltage-gated Na^+ channels in the dendrites of GnRH neurons, and was the first study to suggest the dendrite as the site of action potential initiation. This study also constructed a multi-compartmental, morphological, conductance-based computer model of action potential generation in GnRH neurons; see

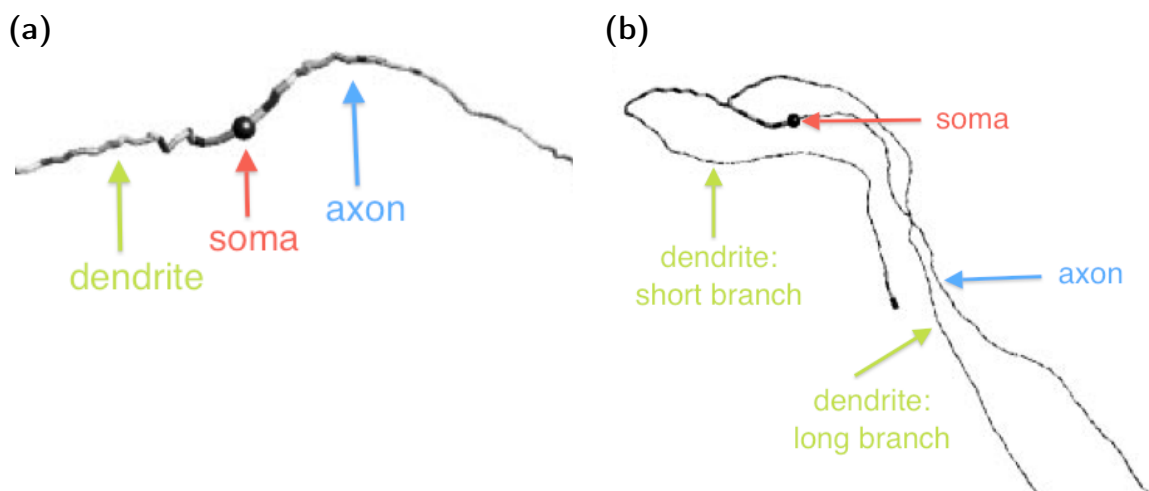


Figure 3.2 Computer renderings of the compartmental models of (a) bipolar and (b) branching GnRH neurons used in Roberts et al. (2006, 2008, 2009). The gray shaded cylinders illustrate different compartments in the model. Figures adapted from Roberts et al. (2006).

Table 3.1 Conductance types used in the three studies: I (Roberts et al., 2006), II (Roberts et al., 2008), and III (Roberts et al., 2009). The dendrite model was described as a passive model in the first study, an active model in the second study and both a passive and an active model in the third model.

Conductance type	I	II	III (a)	III (b)
soma NaF	Yes	Yes	Yes	Yes
soma Kdr	Yes	Yes	Yes	Yes
soma Kir	No	Yes	Yes	Yes
soma Km	No	No	Yes	Yes
soma CaL	Yes	Yes	Yes	Yes
soma CaT	No	No	Yes	Yes
soma NaP	No	No	Yes	Yes
axon NaF	Yes	Yes	Yes	Yes
axon Kdr	Yes	Yes	Yes	Yes
axon Nap	No	No	Yes	Yes
axon CaL	Yes	No	No	No
dendrite NaF	No	Yes	No	Yes
dendrite Kdr	No	Yes	No	No
dendrite NaP	No	No	No	Yes

Figure 3.2. The model of Roberts et al. (2008) included fast Na^+ current (I_{Na}), delayed rectifier K^+ current (I_{Kdr}), inward rectifier K^+ current (I_{ir}), and L-type Ca^{2+} current (I_{CaL}) for the soma compartments, but included only fast Na^+ current (I_{Na}) and delayed rectifier K^+ current (I_{Kdr}) for the axon and dendrite compartments; see Table 3.1. All these channels were described using equations of Hodgkin-Huxley style. This study reported that the spike initiation site depended on the location of synaptic input and dendritic properties. Their modeling study suggested that distal dendrites have a lower threshold to initiate action potentials.

The experimental and modeling approaches in Roberts et al. (2009) studied the impact of dendrites on the generation of afterdepolarization potentials (ADPs) and repetitive firing. This study also built a multi-compartmental, conductance-based model (Figure 3.2). All the voltage-gated conductances were based on the models of GT1 cells by LeBeau et al. (2000), except the persistent Na^+ channel, which was adapted from Purvis and Butera (2005); see Table 3.1. All these channels were described in the formalism of Hodgkin-Huxley. Similarly to Roberts et al. (2006) and Roberts et al. (2008), Roberts et al. (2009) did not include the Ca^{2+} dynamics and Ca^{2+} -sensitive currents. Both their modeling and experimental results indicated that neuronal morphology strongly influenced the ADP response of GnRH neurons. They suggested that

there existed a local spike generating mechanism. Their findings showed the importance of morphology and passive membrane properties of the GnRH neuron in control of firing.

3.4 The Fletcher and Li model

Fletcher and Li (2009) constructed an integrated and simplified version of the Ca^{2+} dynamics and electrical activities of GnRH neurons. Their model was based on two previous models of GT1 cells (van Goor et al., 2000; LeBeau et al., 2000), and was capable of reproducing all previous experimental results and some important new results which were not reproduced in the previous models. The Fletcher and Li model was constructed to have more realistic Ca^{2+} dynamics and a reduced number of currents and gating variables than the previous two GT1 cell models. Fletcher and Li (2009) indicated that their modeling study could help to investigate the roles of electrical firing and the associated Ca^{2+} oscillations during the pulsatile release of GnRH.

Figure 3.3 shows a schematic diagram of the Fletcher and Li model. In contrast to LeBeau et al. (2000), Fletcher and Li (2009) did not include the M-type K^+ channel and T-type Ca^{2+} channel. A TTX-sensitive Na^+ current (I_{Na}), L-type Ca^{2+} currents (I_{CaL}), a delayed rectifier K^+ current (I_{K}), and an inward rectifier K^+ current (I_{ir}) were retained and modeled in the formalism of Hodgkin-Huxley. The two pacemakers, small-conductance Ca^{2+} -activated K^+ current (I_{SK}) and store-operated Ca^{2+} current (I_{SOC}), were also retained. The other pacemaker Ca^{2+} -dependent current I_d in LeBeau et al. (2000) was replaced by I_{NSC} , a cAMP-activated, Ca^{2+} -independent, non-specific cation current.

To model Ca^{2+} dynamics, Fletcher and Li (2009) designed a single spherical soma with only two compartments, the cytosol and the ER; see Figure 3.3. The Ca^{2+} dynamics included the following fluxes: influx via plasma membrane channels (j_{in}), efflux via PMCA and NCX plasma membrane pumps (j_{out}), a leak and flux through the IPR channel (j_{rel}), and Ca^{2+} pumping via SERCA channel from the cytosol to the ER (j_{ref}).

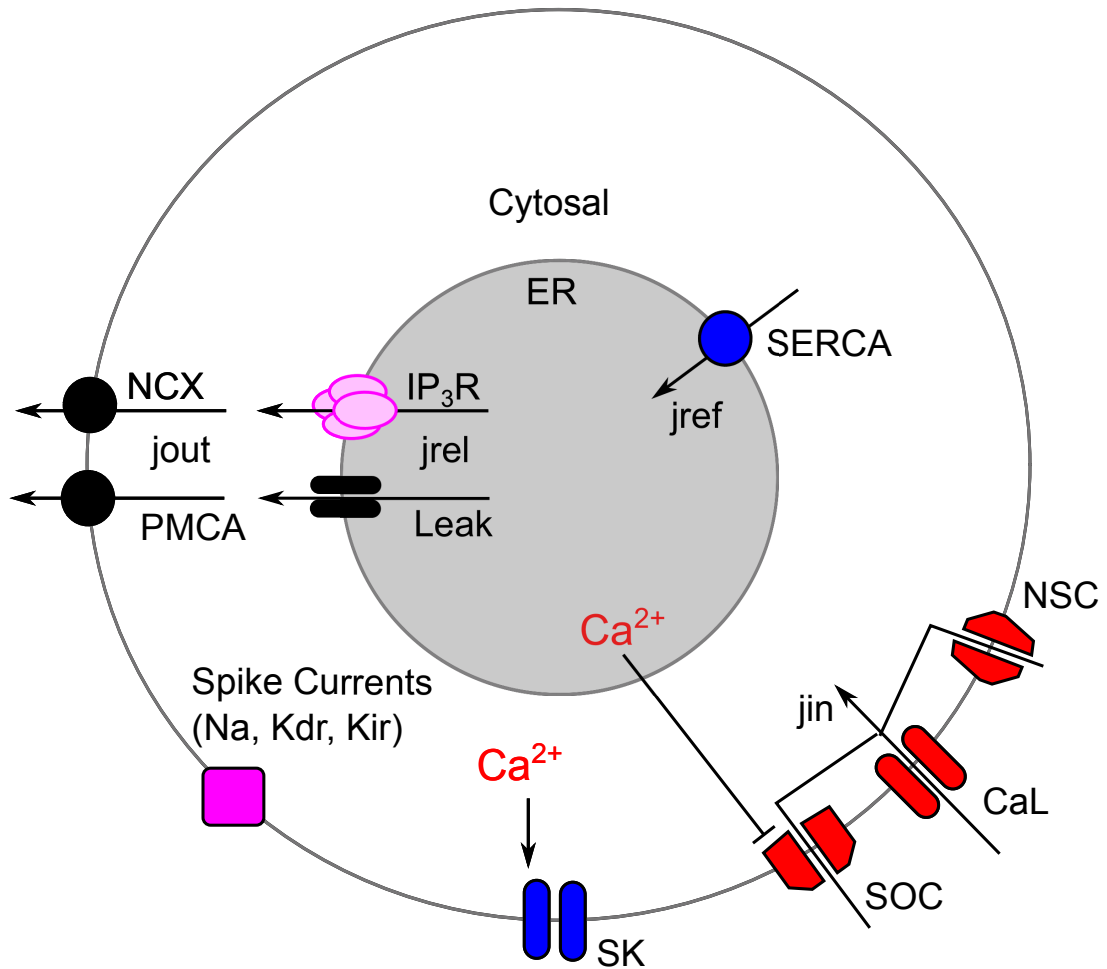


Figure 3.3 Schematic diagram of the Fletcher and Li model. The soma contained two compartments: the cytosol and the ER. Comparing to the model of LeBeau et al. (2000), Fletcher and Li (2009) kept the following currents: a TTX-sensitive Na^+ current (I_{Na}), L-type Ca^{2+} currents (I_{CaL}), a delayed rectifier K^+ current (I_{K}), and an inward rectifier K^+ current (I_{ir}). It also kept the two pacemaker currents, small-conductance Ca^{2+} -activated K^+ current (I_{SK}) and store-operated Ca^{2+} current (I_{SOC}). A cAMP-activated, Ca^{2+} -independent, non-specific cation current I_{NSC} was added. The Ca^{2+} dynamics with some Ca^{2+} fluxes were also added. Figure adapted from Fletcher and Li (2009).

3.5 The Lee model and the Duan model

Lee et al. (2010) constructed a mathematical model to help understand the electrical firing and Ca^{2+} transients in adult GnRH neurons, while Duan et al. (2011) provided a detailed bifurcation analysis of the model constructed in Lee et al. (2010). The Lee model was constructed based on a number of previous models (van Goor et al., 2000; LeBeau et al., 2000; Roberts et al., 2009; Fletcher and Li, 2009). Figure 3.4 shows a schematic diagram of the model. It included all the fast, voltage-dependent currents mentioned in the previous models: a TTX-sensitive Na^+ current (I_{naf}), L- and T-type Ca^{2+} currents (I_{cal} and I_{cat}), a delayed rectifier type K^+ current (I_{kdr}),

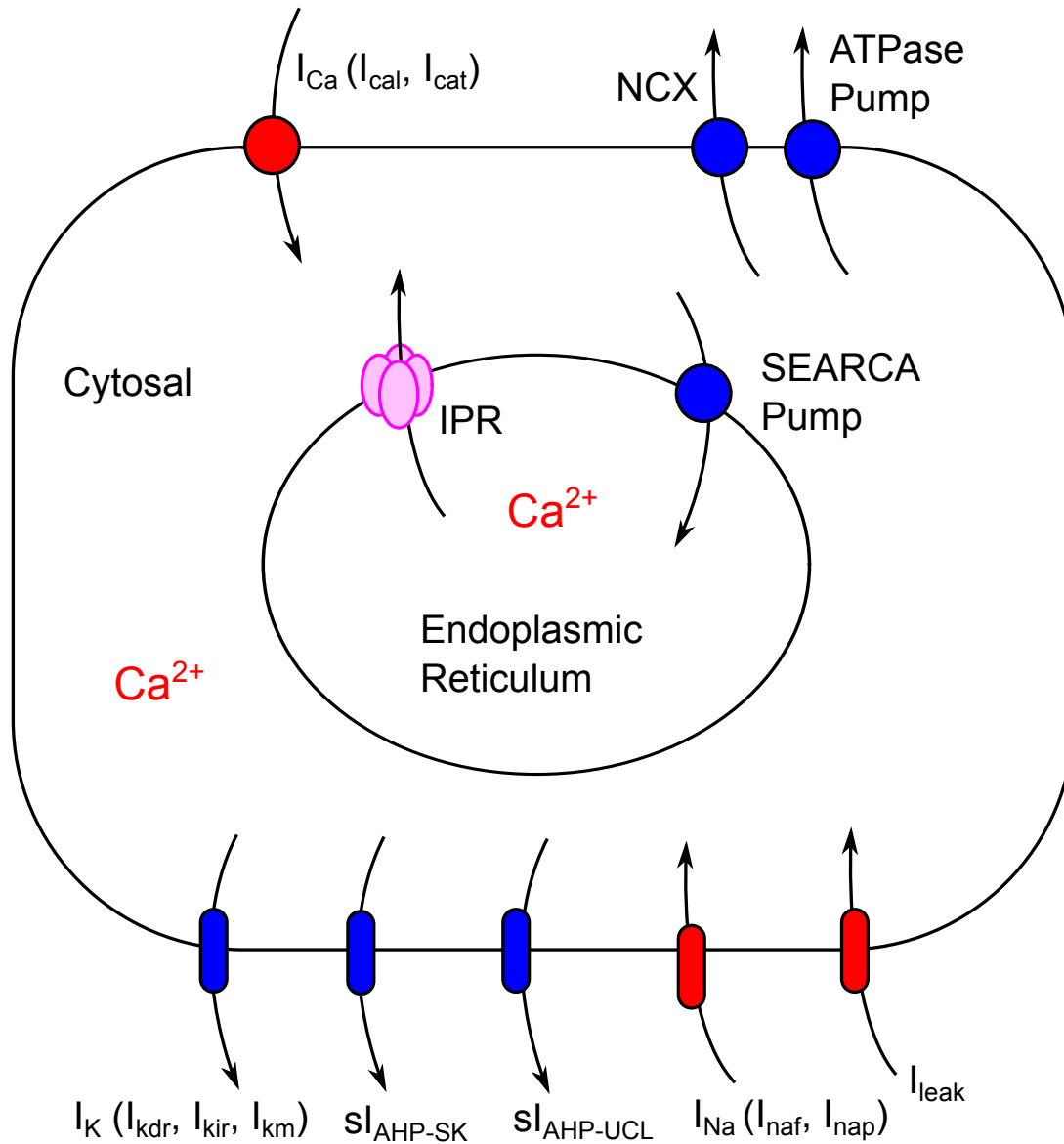


Figure 3.4 Schematic diagram of the model used in Lee et al. (2010) and Duan et al. (2011). The cell contained the cytosol and the ER. The model included the following currents: a TTX-sensitive Na^+ current (I_{naf}), L- and T-type Ca^{2+} currents (I_{cal} and I_{cat}), a delayed rectifier type K^+ current (I_{kdr}), an m-type K^+ current (I_{km}), an inward rectifier K^+ current (I_{kir}), a persistent Na^+ current (I_{nap}) and a passive membrane leakage current (I_{leak}). It also included Ca^{2+} dynamics and Ca^{2+} sensitive pacemaker currents, SK-type Ca^{2+} -activated K^+ current (sI_{AHP-SK}), and a slow Ca^{2+} -activated afterhyperpolarization current ($sI_{AHP-UCL}$). Figure adapted from Duan et al. (2011).

an m-type K^+ current (I_{km}), and an inward rectifier K^+ current (I_{kir}). Similarly to Roberts et al. (2009), the Lee model included a persistent Na^+ current (I_{nap}) and a passive membrane leakage current (I_{leak}). All these currents were described in the formalism of Hodgkin-Huxley. Similarly to LeBeau et al. (2000) and Fletcher and Li (2009), the Lee model included Ca^{2+} dynamics and Ca^{2+} -sensitive currents. It also included two pacemaker currents, SK-type Ca^{2+} -activated K^+ current (sI_{AHP-SK}), and a slow Ca^{2+} -activated afterhyperpolarization current ($sI_{AHP-UCL}$).

Lee et al. (2010) used a similar approach to Fletcher and Li (2009) to model the Ca^{2+} dynamics. The Ca^{2+} dynamics included the following fluxes: influx via plasma membrane channels (J_{in}), efflux via PMCA and NCX plasma membrane pumps (J_{pm}), release and uptake of Ca^{2+} from the ER (J_{release} , and J_{serca} respectively). They used a four-state Markov model to describe the SERCA pump. For modeling the J_{release} through IPR, the open probability of IPR model from Sneyd and Dufour (2002) was used in Lee et al. (2010), while the one from Gin et al. (2009) was used for bifurcation analysis in Duan et al. (2011).

Based on the experimental results of six different pharmacological tests (TTX, zero extracellular Ca^{2+} concentration, apamin, CPA, 2-APB and GABAzine), Lee et al. (2010) suggested a hypothetical mechanism for bursting firing and Ca^{2+} transients, and tested this hypothesis experimentally. For instance, electrical spiking brings in Ca^{2+} via voltage-gated Ca^{2+} channels, and this Ca^{2+} influx stimulates a large Ca^{2+} release from internal stores, through IPR. The large Ca^{2+} transient activates two pacemaker K^+ channels, the SK K^+ channels appear to set the burst duration, while the UCL K^+ channels appear to set the interburst interval. As a result, Lee et al. (2010) successfully predicted the existence of a Ca^{2+} -dependent slow afterhyperpolarization current ($sI_{\text{AHP-UCL}}$) which was found experimentally.

3.6 The Cserscik model

A modular model of GnRH neuronal electrophysiology was described in Cserscik et al. (2012). This study presented a three-compartmental model, including the soma, an active dendrite, and a compartment representing a passive dendrite; see Figure 3.5. It provided a simplified model to study interactions between the soma and dendrite.

Figure 3.5 shows the summarized modular structure of the model. The voltage submodel was described by an impulsive system for simplicity, while the Ca^{2+} submodel mainly relied on the model described in Lee et al. (2010). Both submodels are excitable and are coupled to each other via voltage-dependent Ca^{2+} fluxes and Ca^{2+} -dependent channels. The main objective of this modeling study was to reproduce the characteristic features of the bursting properties indicated by GnRH neurons in loose patch recordings. This model also included a Ca^{2+} -dependent

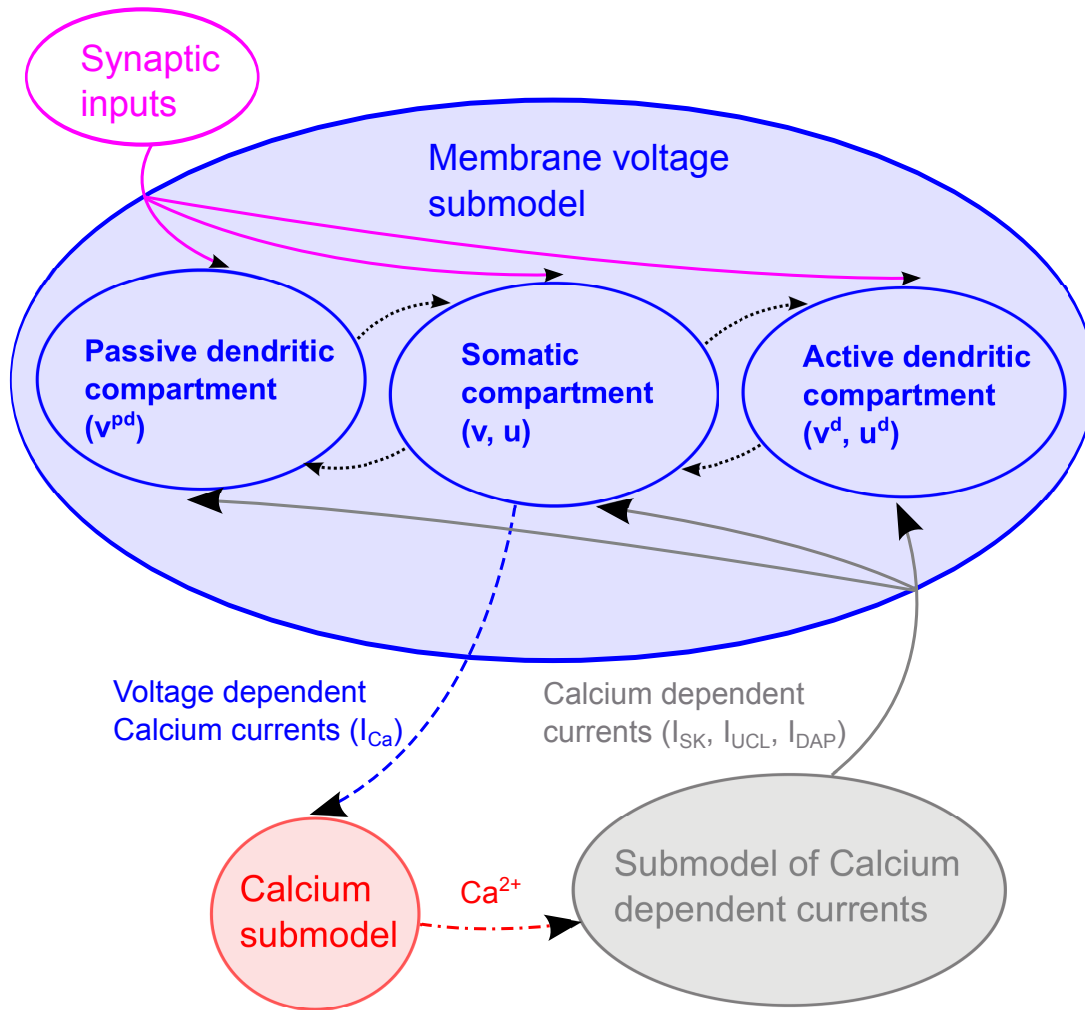


Figure 3.5 The summarized modular structure of the Cserscik model. It shows state variables and the currents connecting their dynamics. Figure adapted from Cserscik et al. (2012).

Na^+ current (I_{DAP}) to explain depolarizing afterpotentials (DAPs) or afterdepolarization potentials (ADPs). With some realistic inputs applied to the model, Cserscik et al. (2012) observed periodic bursting behavior of GnRH neuron.

3.7 Summary

All the previous models mentioned above were successful in achieving their own specific goals. These modeling and experimental studies helped us to understand many aspects of GnRH neurons, such as the properties of burst electrical firing and their associated Ca^{2+} transients. van Goor et al. (2000) studied the electrical activities of a GT1 neuron and explained how GnRH neuron spiking pattern shifted under membrane depolarization. With extension to the van Goor

model, LeBeau et al. (2000) provided a quantitative description of the regulation of action potential pacemaking and the associated Ca^{2+} signaling in GT1 cells. Based on these two pioneer studies, there were many mathematical models (Roberts et al., 2006, 2008, 2009; Fletcher and Li, 2009; Lee et al., 2010; Duan et al., 2011) developed. For instance, Roberts et al. (2006, 2008, 2009) constructed multi-compartmental models of hypothalamic GnRH neurons, which studied the functions of the dendrite of GnRH neurons on controlling spike firing. Fletcher and Li (2009) constructed an integrated and simplified version of the Ca^{2+} dynamics and electrical activity of GT1 cells, while Lee et al. (2010) and Duan et al. (2011) presented a mathematical model to help the understanding of electrical firing and Ca^{2+} transients in adult GnRH neurons. Cserscik et al. (2012) provided a simplified modular model to study interactions between the soma and the dendrite.

However, these previous models could not fully represent the latest experimental data (Iremonger and Herbison, 2012; Herde et al., 2013) as mentioned in Chapter 2. The proposed model should at least satisfy all the following properties as indicated in Roberts et al. (2006), Lee et al. (2010), Iremonger and Herbison (2012) and Herde et al. (2013):

- Ca^{2+} transients and bursts of action potentials are perfectly correlated in adult GnRH neurons (Lee et al., 2010),
- the model should reproduce all the pharmacological results as shown in Lee et al. (2010),
- in response to the influx of a small amount of Ca^{2+} , IP_3 receptors cause CICR in the soma (Lee et al., 2010),
- spikes are initiated in the dendrite (Roberts et al., 2006), and only a single site of spike initiation exists in each GnRH neuron (Iremonger and Herbison, 2012; Herde et al., 2013),
- the highest density of Na^+ channels is in the first 150 μm of dendrite (Iremonger and Herbison, 2012), especially $89 \pm 30 \mu\text{m}$ from the soma in the projection process heading toward the median eminence (Herde et al., 2013).

Consideration of these recent data raised a number of important questions that could not be addressed by previous models. Most importantly, since some of the mechanisms for controlling

the bursting properties are located in the soma, how can electrical bursting be controlled when initiated at a site located some distance from these controlling mechanisms? This was not studied in detail in previous models.

There are other reasons that those previous models are not suitable for our current study. We would like to build a model to study hypothalamic GnRH neurons, while the models of van Goor et al. (2000), LeBeau et al. (2000), and Fletcher and Li (2009) were constructed to explain the experimental data obtained from GT1 cells. These three models along with the models of Lee et al. (2010) and Duan et al. (2011) were spatially homogeneous, and thus can not be used to describe the dendritic action potential initiation. Conversely, some spatiotemporal models (Roberts et al., 2006, 2008, 2009) did not include the Ca^{2+} submodel. Unlike the results reported in Iremonger and Herbison (2012) and Herde et al. (2013) such that the proximal dendrite of GnRH neurons is the most excitable site, the modeling study in Roberts et al. (2008) suggested that the threshold to initiate action potentials is lower in the distal dendrite. Cserscik et al. (2012) tried to reproduce the important features of GnRH neurons reported previously (Roberts et al., 2008; Lee et al., 2010), but did not provide detailed investigations on the interaction between soma and dendrite. The voltage submodel in Cserscik et al. (2012) was a simplified form of Lee et al. (2010) using an impulsive system, which made it impossible to reproduce all the pharmacological results as shown in Lee et al. (2010). The three-compartmental model described with ordinary differential equations could not satisfy the latest findings (Iremonger and Herbison, 2012; Herde et al., 2013) as mentioned above. Hence, none of the models reviewed here could answer all the relevant questions, such as, where is the most excitable region, how is spiking initiated, how do the control mechanisms regulate the bursting, and how do changes at the soma affect dendritic responses, and vice versa.

The initial purpose of our model is to investigate how the controlling mechanism located in the soma could regulate the bursts initiated at a site located some distance from the soma. Based on the previous models, especially the Lee model, we hence constructed a spatiotemporal model of a GnRH neuron. The new model includes both the soma and the dendrite, as it had a particular focus on the control of bursting via the interaction between the soma and the initiation site in the dendrite. Our study showed that the diffusion coefficient for the spread of electrical

potentials in the dendrite was large enough to coordinate burst firing of action potentials when the initiation site was located at some distance from the soma. As a result, our model should be consistent with the experimental results of Lee et al. (2010) as well as those of Roberts et al. (2008), Iremonger and Herbison (2012), and Herde et al. (2013). See Chapter 4 of this thesis for more details.

The model presented in Chapter 4 was extended to be a stochastic spatiotemporal model by including synaptic input along the dendrite. Our modeling study suggests that although stochastic synaptic input along the dendrite is likely to be a major determinant of action potential initiation, it is an unlikely mechanism for controlling whether or not action potentials reach the synaptic terminal. Thus we hypothesized an alternative mechanism, based upon the secretion of kisspeptin at the synaptic terminal, for controlling the secretion of GnRH. See Chapter 5 of this thesis for more details.

Regulation of Electrical Bursting in a Spatiotemporal Model of a GnRH Neuron

In this chapter, we present a spatiotemporal mathematical model of a GnRH neuron with the aim of investigating how electrical bursting can be regulated when initiated at a site located some distance (often more than $100 \mu\text{m}$) from the controlling mechanism. What follows is a copy of the journal paper as it appears in the Bulletin of Mathematical Biology, Volume 75(10). The full reference is given in the bibliography (Chen et al., 2013).

4.1 Abstract

Gonadotropin-releasing hormone (GnRH) neurons are hypothalamic neurons that control the pulsatile release of GnRH that governs fertility and reproduction in mammals. The mechanisms underlying the pulsatile release of GnRH are not well understood. Some mathematical models have been developed previously to explain different aspects of these activities, such as the properties of burst action potential firing and their associated Ca^{2+} transients. These previous studies were based on experimental recordings taken from the soma of GnRH neurons. However, some research groups have shown that the dendrites of GnRH neurons play very important roles. In particular, it is now known that the site of action potential initiation in these neurons is often in the dendrite, over 100 μm from the soma. This raises an important question. Since some of the mechanisms for controlling the burst length and interburst interval are located in the soma, how can electrical bursting be controlled when initiated at a site located some distance from these controlling mechanisms? In order to answer this question we construct a spatiotemporal mathematical model that includes both the soma and the dendrite. Our model shows that the diffusion coefficient for the spread of electrical potentials in the dendrite is large enough to coordinate burst firing of action potentials when the initiation site is located at some distance from the soma.

4.2 Introduction

Gonadotropin-releasing hormone (GnRH) neurons are hypothalamic neurons that control the pulsatile release of GnRH that governs fertility and reproduction in mammals (Herbison, 2006). Although the mechanisms underlying the pulsatile release of GnRH are not well understood, it is likely that the bursting behavior of electrical activity in GnRH neurons plays an important role in GnRH release (Moenter et al., 2003; Herbison, 2006).

The discovery twenty years ago of immortalized GnRH-secreting neurons (GT1 cells) (Melton et al., 1990; Martinez et al., 1992) provided the opportunity to study the electrophysiological activity of GnRH neurons. Subsequent work (Constantin and Charles, 1999; Spergel et al., 1999; van Goor et al., 1999a,b) on GT1 cells showed that, in these cells, bursts of ac-

tion potentials are closely correlated with Ca^{2+} transients. More recently, the development of GnRH-reporter transgenics (Herbison et al., 2001) have given experimentalists the ability to study the physiology of postnatal GnRH neurons in acute brain slice preparations, monitoring Ca^{2+} dynamics and electrical bursting in GnRH neurons in a close approximation of their native environment (Nagai et al., 2001; Jasoni et al., 2007).

Furthermore, the transgenic animal models have provided additional insight into the morphology of GnRH neurons (Suter et al., 2000; Campbell et al., 2005, 2009; Roberts et al., 2006). These studies found that the dendrites of biocytin-filled GnRH neurons are very long and bundle with one another (Campbell and Suter, 2010). In most neurons, action potentials are initiated in the axon initial segment, as this region is the most excitable with the highest density of voltage-gated Na^+ channels (Kole et al., 2008; Schmidt-Hieber et al., 2008; Foust et al., 2010; Palmer et al., 2010; for review, see Debanne et al., 2011). However, in GnRH neurons it appears that the site of action potential initiation is in the dendrite (Roberts et al., 2008; Iremonger and Herbison, 2012).

Mathematical models also have been developed to explain different aspects of GnRH neurons, such as the properties of burst electrical firing and their associated Ca^{2+} transients. Some models were constructed to explain the experimental data obtained from GT1 cells (van Goor et al., 2000; LeBeau et al., 2000; Fletcher and Li, 2009), while others were based on hypothalamic cells (Lee et al., 2010; Duan et al., 2011). Moreover, spatiotemporal models of the GnRH neuron dendrite have also been previously constructed (Roberts et al., 2008, 2009; Cserscik et al., 2012).

Our study here focuses on the recent results from Iremonger and Herbison (2012), and addresses in particular the question of how electrical bursting is controlled. This question arises because the site of action potential initiation (in the dendrite, at a place we name the *iSite*) can be located at some distance (often more than $100\ \mu\text{m}$) from the channels in the soma that are thought to regulate the length of the electrical burst and the interburst interval (IBI). This is not necessarily always the case, but it is certainly the case in many GnRH neurons.

To appreciate the importance of this point, let us first consider the mechanisms that appear to control electrical bursting. Electrical spiking (mediated by the usual Na^+ and K^+ currents)

brings in Ca^{2+} via voltage-gated Ca^{2+} channels, and this Ca^{2+} influx initiates the release of additional Ca^{2+} from internal stores, through inositol trisphosphate receptors (IPR). This process is known as Ca^{2+} -induced Ca^{2+} release, or CICR, and results in a large Ca^{2+} transient that activates two pacemaker K^+ channels; the SK K^+ channel terminates the spiking, while a longer-lasting hyperpolarizing current, which we call the UCL current, prevents spiking during the interburst interval. Thus, the SK channels appear to set the burst duration, while the UCL channels appear to set the interburst interval.

We know that CICR is a crucial part of the control process, as if the internal stores are depleted (by the application, say, of cyclopiazonic acid, or CPA) then the bursting becomes disorganized with a smaller interburst interval and smaller Ca^{2+} transients (Lee et al., 2010). However, there is no apparent CICR at the iSite (or elsewhere in the dendrite), only at the soma (Iremonger and Herbison, 2012).

Hence the question. Since the site of initiation (the iSite) does not contain the necessary controlling mechanism (CICR), is it possible for the somatic channels to control the electrical bursting, and if so, what effect does this spatial separation have? More specifically,

- How do the soma and iSite interact to control electrical bursting?
- Does voltage and Ca^{2+} diffusion along the dendrite play an important role in control of bursting?
- How do changes at the soma (in either electrical properties or Ca^{2+} transport) affect dendritic responses, and vice versa?

To answer these questions we modify the model of Lee et al. (2010) and Duan et al. (2011) to include a spatially varying dendrite linked to a spatially homogenous soma. All the ionic channels in the soma are as in Lee et al. (2010) and Duan et al. (2011). They are described briefly in the next section and with more detail in the Appendix. Our spatial model uses the same parameters as Lee et al. (2010) and Duan et al. (2011), with only a few minor exceptions. The most important new parameter is the electrical diffusion coefficient, which is determined by fitting to experimental data. Simulations from the spatial model agree well with almost

every important experimental result, and hence help us to answer, at least partially, the above questions.

4.3 Model Description

For simplicity we model the GnRH neuron as a one-dimensional cable, with a single dendrite. Although GnRH neurons often have two dendrites, incorporation of a second dendrite is not necessary for the current simplified model. The initiation site for action potentials, called the *iSite*, is a region of high Na^+ channel density located anywhere from 100-200 μm from the soma (Iremonger and Herbison, 2012). Each GnRH neuron is likely to have only one *iSite* as suggested in Iremonger and Herbison (2012), and thus we assume that a single *iSite* is located in one particular position in the dendrite.

We set up the model as shown in Figure 4.1. The soma is the region $[0, x_1]$, the dendrite between the soma and the *iSite* is $[x_1, x_2]$, the *iSite* is $[x_2, x_3]$, and the dendrite elsewhere is $[x_3, x_4]$, where x_4 is typically much larger than x_3 . We set the size of the soma to be 30 μm , and the size of the *iSite* to be 70 μm . In our initial simulations we assume that the distance between the soma and *iSite* (L_{Si}) is 50 μm , (for instance, $x_1 = 30$, $x_2 = x_1 + L_{\text{Si}}$, and $x_3 = x_2 + 70$). The basic components of our model are taken directly from Lee et al. (2010) and Duan et al. (2011), with the addition of the diffusion of voltage and of intracellular free Ca^{2+} . One important feature is the absence of inositol trisphosphate receptors (IPR) from the *iSite*, as suggested by experimental data (Iremonger and Herbison, 2012). Since release of Ca^{2+} through the IPR is a major controller of the electrical bursting (Lee et al., 2010) this means that the bursting, which is being initiated at the *iSite*, is being controlled by the release of Ca^{2+} at a distant site (i.e., at the soma). How this could work is the subject of the present investigation. In the absence of any information to the contrary, all the other relevant ionic channels are assumed to be located at the *iSite* as well as at the soma.

For simplicity we also assume that there are no *SK* or *UCL* channels in the dendrite. This assumption can be relaxed without changing the qualitative nature of our results.

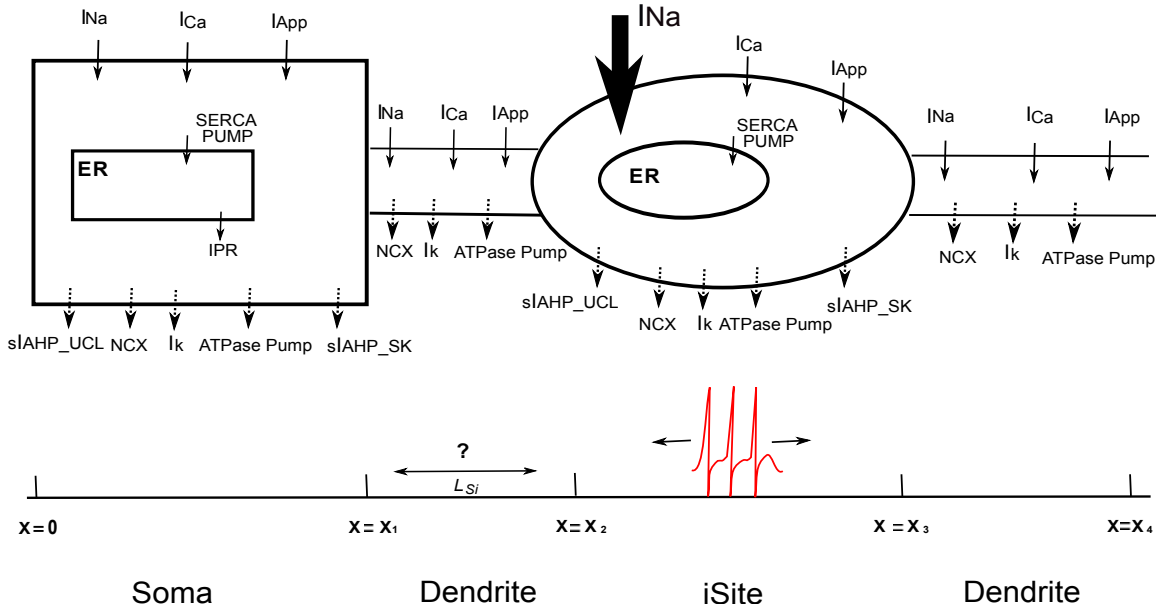


Figure 4.1 Schematic diagram of the GnRH neuron model. The soma is the region $[0, x_1]$, the iSite is $[x_2, x_3]$, and the rest is dendrite. The question mark between x_1 and x_2 indicates that we will do some model simulations by varying the length between the soma and the iSite (L_{Si}). The schematic diagram also shows the key channels and pumps in each region (see Appendix for more details). The density of sodium channels in the iSite is higher than in the other regions. The action potential is initiated in the iSite and propagates in both directions. To avoid a cluttered diagram, the dendritic ER is omitted, except in the iSite.

The equation for the membrane potential (V) is

$$\frac{\partial V(x,t)}{\partial t} = -\frac{1}{C_m} I_{\text{ionic}}(V, x, t) + D_v \frac{\partial^2 V(x,t)}{\partial x^2}, \quad (4.1)$$

where C_m is the membrane capacitance and I_{ionic} is the sum of the ionic currents. Note that, in the more traditional terminology of the cable *length constant* (λ_m) and the membrane *time constant* (τ_m), we have $D_v = \frac{\lambda_m^2}{\tau_m}$. The equation for Ca^{2+} (c) is

$$\frac{\partial c(x,t)}{\partial t} = \rho(J_{\text{in}} - J_{\text{pm}}) + J_{\text{release}} - J_{\text{serca}} + D_c \frac{\partial^2 c(x,t)}{\partial x^2}, \quad (4.2)$$

where ρ is used to scale plasma membrane and ER fluxes. J_{in} , J_{pm} , J_{release} , and J_{serca} denote the influx via plasma membrane channels, efflux via PMCA and NCX plasma membrane pumps, release of Ca^{2+} from the ER to cytosol, and Ca^{2+} pumping from the cytosol to the ER, respectively. D_c is set to be zero.

For $x \in [0, x_1]$, the currents in the soma are $I_{\text{ionic}}(V, x, t) = I_{\text{naf}} + I_{\text{nap}} + I_{\text{kdr}} + I_{\text{kir}} + I_{\text{km}} + I_{\text{cal}} +$

$I_{\text{cat}} + sI_{\text{AHP-SK}} + sI_{\text{AHP-UCL}} + I_{\text{App}}$. Each channel is described in detail in the Appendix.

For $x \in [x_2, x_3]$, the currents in the iSite are the same as in the soma, except that we use a higher conductance for I_{naf} , representing a higher density of Na^+ channels in the iSite. We use Na^+ conductance (g_{naf}) equal to 410 nS in the iSite, and 150 nS elsewhere.

For $x \in [x_1, x_2]$ and $x \in [x_3, x_4]$, the currents in the dendrite are $I_{\text{ionic}}(V, x, t) = I_{\text{naf}} + I_{\text{nap}} + I_{\text{kdr}} + I_{\text{kir}} + I_{\text{km}} + I_{\text{cal}} + I_{\text{cat}} + I_{\text{App}}$.

Calcium handling is slightly different in the soma and the iSite. At the soma, where there are IPR, calcium handling is described by the same equations as Lee et al. (2010). Hence, at the soma, the entry of a small amount of Ca^{2+} through voltage-gated channels stimulates the release of a much larger amount of Ca^{2+} through the IPR, in a process of Ca^{2+} -induced Ca^{2+} release (CICR), leading to subsequent activation of Ca^{2+} -dependent K^+ channels, termination of the burst, and a long IBI. At the iSite, however, no such CICR can occur, as there are no IPR there, and so there is no large Ca^{2+} transient. Thus, Ca^{2+} at the iSite cannot control the burst duration or the IBI.

Although our model equations do include Ca^{2+} diffusion, simulations (not shown here) show that Ca^{2+} diffusion is so slow that it plays effectively no role at all in the control of bursting, and no role in the communication between the iSite and the soma. Given that Ca^{2+} diffusion is orders of magnitude slower than the diffusion of V (Keener and Sneyd, 2008), this is entirely unsurprising. Hence, Ca^{2+} diffusion was omitted from all our model simulations.

All the ion channels and fluxes are modeled as in Lee et al. (2010), Duan et al. (2011) and references therein. The full model equations and some parameters are presented in the Appendix.

4.4 Results

4.4.1 Active and Passive Propagation

The most important new parameter in the model is the diffusion coefficient of the voltage, and this is determined from experimental data on the spread of depolarization in the GnRH neuron dendrite.

Iremonger and Herbison (2012) performed a whole-cell recording from the soma and an on-cell recording from the dendrite. Dendritic on-cell recordings were performed in different positions in eight neurons (mean distance, $227.9 \pm 36.5 \mu\text{m}$; $n = 8$) (Iremonger and Herbison, 2012). After injection of an action potential waveform into the soma, Iremonger and Herbison (2012) measured the amplitude of the spikes along the dendrite, both in the absence and presence of TTX, which blocks the voltage-gated Na^+ channels. In each case, the magnitude of the resulting spike which is a capacitive current was measured as a function of distance along the dendrite.

In the absence of TTX (the control case), the soma injection stimulated an action potential which propagated actively along the dendrite. In the presence of TTX there was no active propagation and the voltage spread entirely by passive diffusion. The ratio between the control spike height and the height of the transient after TTX is shown in Figure 4.2(a) by the cyan circles. The representative capacitive currents before and after TTX, and the first derivative of the voltage in the soma are presented in Figure 4.2(c).

In addition, the time when the capacitive current reaches its peak was compared with the time of the peak of the first derivative of somatic voltage. The latency between dendritic spikes (before and after TTX) and the first derivative of the somatic voltage is shown in Figure 4.2(e). The negative latencies indicate that the peak of the dendritic spike appeared before the peak of the somatic spike. This happens when current injection at the soma causes an initial firing at the iSite, which then spreads back to the soma. In the presence of TTX this cannot happen, as the voltage-gated Na^+ channels are blocked.

Model simulations based on these data are shown in Figure 4.2(a), (b), (d) and (f). In Figure 4.2(a) we see the result of computing the ratio of the spike height, before and after TTX, as a function of distance along the dendrite. The smooth curve was computed using $D_v = 30000 \mu\text{m}^2/\text{ms}$. We did not do a formal fit to the data, as the inverse problem is highly ill-defined. Any value of D_v between approximately 28000 and 32000 $\mu\text{m}^2/\text{ms}$ gave identical qualitative behavior, and the experimental data is not sufficient to determine a more specific value.

To calculate the space and time constants, we rearrange our model in terms of λ_m and τ_m ,

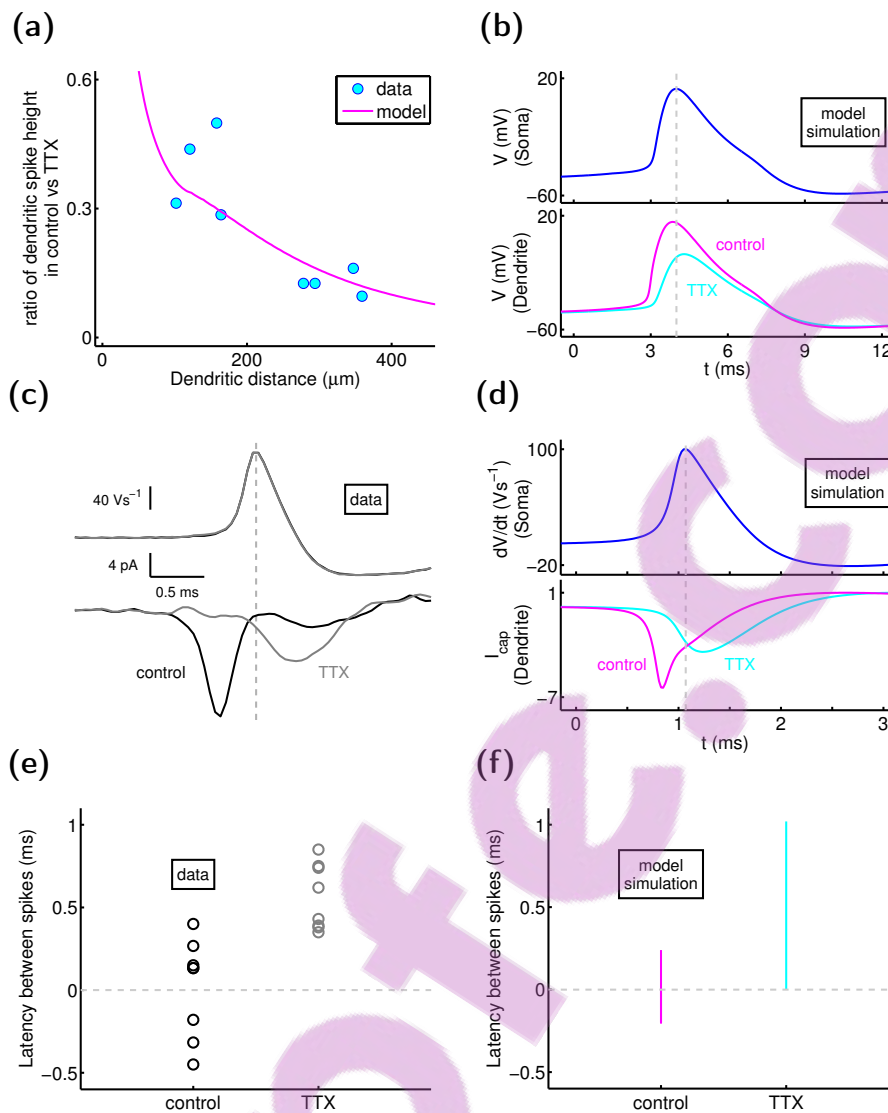


Figure 4.2 (a) The effect of TTX on dendritic spike amplitude. Experimental data (symbols) and model simulations (solid curve) showing the ratio of dendritic spike height in control conditions to the height in the presence of TTX. (b) Model simulations. Top panel is the action potential waveform injected into the soma, the bottom panel is the dendritic action potential in control conditions and in the presence of TTX. To model the action of TTX, we set the Na⁺ conductances g_{naf} and g_{nap} to zero. The dendritic voltages are measured at $x = 115 \mu\text{m}$ which is in the middle of iSite. (c) Experimental data. The soma was held in voltage clamp and an action potential waveform was injected into the cell. This action potential waveform induced a dendritic spike. The first derivative of the somatic membrane potential is shown in the top trace. In the bottom trace, the peak of the dendritic spike (capacitive current) comes before the peak of the first derivative of the somatic action potential, and the peak of spike in the presence of TTX comes after that. (d) Model simulations to match the experimental results as shown in (c). The top panel is the first derivative of the somatic membrane potential, and the bottom panel is capacitive currents (scaled to maximum current) which reflect the voltage change in dendrite in the control conditions and in the presence of TTX. We also set g_{naf} and g_{nap} to zero as in the presence of TTX. The dendritic capacitive currents are also measured at $x = 115 \mu\text{m}$. (e) Experimental data. Latency of the dendritic spike before and after TTX. The negative latency indicates that the peak of the dendritic spike appeared before the peak of the first derivative of the somatic action potential. (f) Model simulations. Latency between spikes in control conditions and in the presence of TTX. The latency is measured by the difference between the spike occurring in every positions along the dendrite (zero to $400 \mu\text{m}$ far away from the soma) and the one in the soma. Dendritic on-cell recordings were measured in different locations in eight cells (Iremonger and Herbison, 2012). Experimental results in (a), (c) and (e) are adapted from Iremonger and Herbison (2012).

where $\tau_m = C_m R_m$, and where R_m is the membrane resistance at rest. In our model $R_m = 1.35 \text{ G}\Omega$, and so $\tau_m \approx 22 \text{ ms}$ (with $C_m = 16 \text{ pF}$). Hence, λ_m is about $805 \text{ }\mu\text{m}$ if $D_v = 30000 \text{ }\mu\text{m}^2/\text{ms}$. Our value for the length constant is consistent with results reported from a range of other types of neurons. For instance, $\lambda_m \sim 85 \text{ }\mu\text{m}$ in hippocampal dentate granule cells (Krueppel et al., 2011), $\sim 220 \text{ }\mu\text{m}$ in hippocampal CA3 pyramidal neurons (Sasaki et al., 2011), $\sim 450 \text{ }\mu\text{m}$ in hippocampal mossy fibers (Alle and Geiger, 2006) or in layer 5 cortical pyramidal cells (Shu et al., 2006), $\sim 550 \text{ }\mu\text{m}$ in layer 5 pyramidal neurons (Kole et al., 2007), and even up to 1.2 mm ($1200 \text{ }\mu\text{m}$) in olfactory mitral cells (Djurisic et al., 2004). Similarly our value for the time constant is consistent with the results of Spergel et al. (1999), who estimated it to be between 20-30 ms in GnRH neurons.

Using this value of D_v we can compute the wave forms of the depolarizations (before and after TTX; Figure 4.2(b)). However, it may be not a good choice to use voltage peaks for latency analysis in the experiments. Firstly, the latency time scale is hundreds (even tens) of microseconds, and the peak of the action potential is relatively broad, which is a potential source of error in identifying the true peak (Meeks and Mennerick, 2007). Secondly, Iremonger and Herbison (2012) measured the dendritic capacitive currents experimentally. Hence, we also computed the capacitive currents before and after TTX along the dendrite and compared them with the first derivative of the action potential in the soma, as shown in Figure 4.2(d). As observed experimentally, in the control case some spikes in the dendrite appear before the somatic spike. Conversely, in the presence of TTX, the dendritic spike always follows the somatic spike. This is summarized in Figure 4.2(f).

Although qualitative agreement is good, quantitative agreement is not perfect. For instance, the amplitudes of the model dendritic spikes did not match well with the one measured in the experiment, indicating that our Na^+ channel density distributed along the dendrite is not perfect. However, determination of the correct distribution of Na^+ channel density to match these data is not the goal of this paper and is left for future work.

4.4.2 Conduction Velocity

Given our estimated value of D_v , we can also calculate the conduction velocity of action potential propagation down the dendrite. We show here two cases: one is the control case that the spontaneous bursting is initiated in the iSite and propagates to both sides, and the other one is the TTX case that the action potential waveform is injected in the soma and passively propagates along the dendrite. Figure 4.3 shows the latency (i.e., the time between the peak at the soma and the peak elsewhere) as a function of distance along the dendrite in spontaneous spiking condition and in the presence of TTX, from which information we estimate the spike velocity to be about $670 \mu\text{m/ms}$ (0.67 m/s) for the control case, while the one for the TTX case is about $270 \mu\text{m/ms}$ (0.27 m/s).

It shows that the Na^+ channel density could affect the conduction velocity. The larger the Na^+ channel density, the higher the rate of rise of the action potential, which makes the excitation faster along the dendrite and hence conduction velocity increased (Debanne et al., 2011).

The propagation speed of mammalian unmyelinated axons is generally slow. It has been reported to be about 0.25 m/s in the Schaffer collateral (Andersen et al., 2000) or in hippocampal mossy fiber axons (Kress et al., 2008; Schmidt-Hieber et al., 2008), about 0.3 m/s in the dendrite of rat neocortical pyramidal neurons (Antic, 2003), about 0.35 m/s in the dendrite of layer 5 pyramidal neurons (Nevian et al., 2007), about 0.4 m/s in CA3 pyramidal axons (Meeks and Mennerick, 2007), about 0.7 m/s in neocortical pyramidal cells (Shu et al., 2007), and up to around 1.1 m/s in Cerebellar Purkinje neurons (Foust et al., 2010) or in thalamic interneuron dendrites (Casale and McCormick, 2011).

Note that the magenta curve for the control case in Figure 4.3 has a characteristic dip at the position of the iSite, as this is where the action potentials are initiated.

4.4.3 Ca^{2+} Transients in the Dendrite

The effect of spiking on Ca^{2+} signaling in the dendrite has also been investigated in Iremonger and Herbison (2012). Spikes were evoked by somatic current injections, and propagate along the dendrite. Both single spikes and bursts of three spikes could evoke Ca^{2+} transients

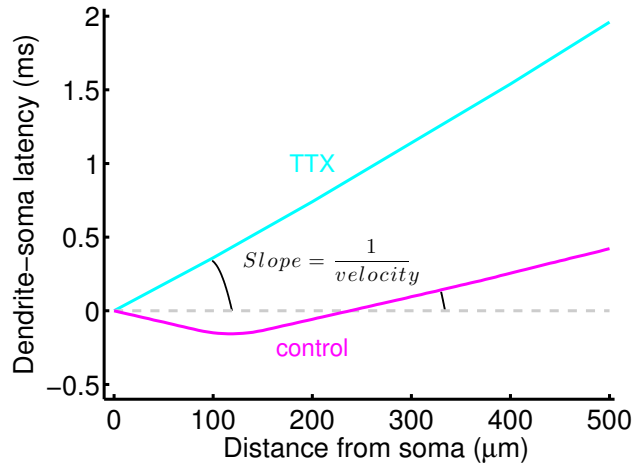


Figure 4.3 The time interval between the action potential measured at the soma and dendrite in spontaneous spiking condition (control) and in the presence of TTX. The mean conduction velocity for the control case is about $670 \mu\text{m/ms}$ (0.67 m/s), with standard deviation $134 \mu\text{m/ms}$, while the one for the TTX case is about $270 \mu\text{m/ms}$ (0.27 m/s), with standard deviation $8 \mu\text{m/ms}$.

in the dendrites. The Ca^{2+} transient evoked by three somatic current injections is shown in Figure 4.4(a). The Ca^{2+} transient was recorded in the dendrite about $450 \mu\text{m}$ from the soma. Local release of TTX on the dendrite next to the recording site decreased the local spike amplitude. Hence, a localized puff of TTX produced a significant local inhibition (a decrease of over 70%) of the spike-evoked dendritic Ca^{2+} transient (Figure 4.4(c)). This suggests that dendritic voltage spikes are responsible for the dendritic Ca^{2+} transients (Iremonger and Herbison, 2012).

Furthermore, the nonspecific Ca^{2+} channel antagonist CdCl_2 decreases the Ca^{2+} by over 70%, the L-type Ca^{2+} channel antagonist Nifedipine inhibits about half the Ca^{2+} transient, and the T- and R-type Ca^{2+} channel antagonist NiCl_2 decreases the Ca^{2+} transient to about 66%. However, the SERCA pump inhibitor cyclopiazonic acid (CPA) reduces the Ca^{2+} transient by only approximately 15% (Iremonger and Herbison, 2012). These data are shown in Figure 4.4(c).

Our model simulations agree well with those results (Figure 4.4(b) and (d)). A sample simulation is shown in Figure 4.4(b), which shows the effect of TTX on spikes and spike-evoked Ca^{2+} transients. We summarize the simulation results for other pharmacological tests in Figure 4.4(d). These results were computed in a region of dendrite situated about 420 to $480 \mu\text{m}$ from the soma. Note that, due to the absence of IPR, blocking the SERCA pump in the model

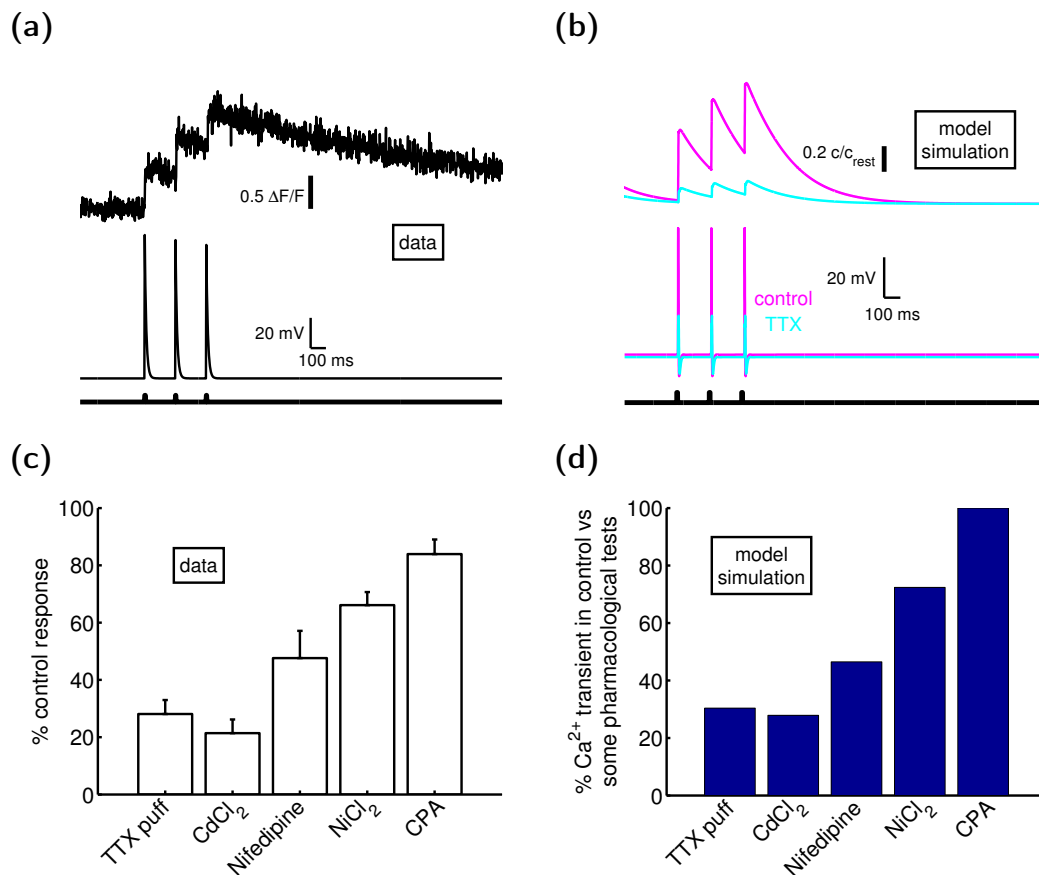


Figure 4.4 (a) Current was injected in the soma to induce three spikes, and Ca^{2+} transient was recorded in the dendrite about $450 \mu\text{m}$ from the soma. (b) Model simulation shows Ca^{2+} transient changes before and after TTX puffing in the dendrite. Ca^{2+} is normalized to its resting value. Current was injected at soma as well to depolarize the spikes. (c) Several pharmacological drugs were used to test the effect on Ca^{2+} transient, it shows the summary data about the percentage of the spike evoked Ca^{2+} in dendrite remained after adding various drugs. TTX is to block the Na^+ channel showing the importance of dendritic voltage gated Na^+ channel in evoking dendritic Ca^{2+} transients, CdCl_2 is unspecific Ca^{2+} channel antagonist, Nifedipine is to block L-type Ca^{2+} channel, NiCl_2 is to block T- and R-type Ca^{2+} channel, and CPA is SERCA pump inhibitor to test the involvement of Ca^{2+} release from internal stores. (d) Model simulation gives similar results as shown in (c). To model the TTX puffing test, we set the conductances of Na^+ (g_{naf} and g_{nap}) to be zero in the dendrite somewhere between 420 to $480 \mu\text{m}$ from soma. To model the CdCl_2 test to block unspecific Ca^{2+} channels, we set the conductances of L-type Ca^{2+} current (g_{cal}) to be half of its control value and the conductance of T-type Ca^{2+} current (g_{cat}) to be 10% of its control value together. To model the Nifedipine test to block L-type Ca^{2+} channel and NiCl_2 test to block T-type Ca^{2+} channel, we set g_{cal} to be half of its control value and g_{cat} to be 10% of its control value, respectively. Note that, due to the absence of IPR, there is no change on the magnitude of the dendritic Ca^{2+} transient by blocking the SERCA pump in the model. Experimental results in (a) and (c) are adapted from Iremonger and Herbison (2012).

has no effect on the magnitude of the dendritic Ca^{2+} transient, as there can be no CICR. This does not agree with the experimental data, which shows a significant decline of around 15% when the SERCA pumps are blocked. This is another indication either that our model is not capturing every possible Ca^{2+} handling mechanism, or that CPA does more than just block the

SERCA pumps.

These results imply that dendritic Ca^{2+} transients evoked by three spikes show no evidence of CICR. The Ca^{2+} transients are entirely the result of entry of Ca^{2+} from outside through voltage-gated Ca^{2+} channels, with no significant component of the Ca^{2+} responses arising from release from internal stores.

4.4.4 Control of Electrical Bursting by Diffusion of Voltage

Similarly to the spatially homogeneous model in Lee et al. (2010), our spatial model is also able to generate electrical bursting intrinsically. How this might happen is not immediately clear. It is important to keep in mind the mechanism underlying the control of bursting in the spatially homogeneous model. In that previous model, the neuron is in a naturally oscillatory state, due to the continual applied currents. Thus, in the absence of control mechanisms, the neuron would spike continuously. However, spiking brings in a small amount of Ca^{2+} via voltage-gated channels; this entering Ca^{2+} induces the release of a large amount of Ca^{2+} from internal stores. The resultant large Ca^{2+} transient activates two Ca^{2+} -dependent K^+ channels; the faster SK channel terminates the bursting, while the slower UCL channel prevents the bursting from recurring, thus giving a long IBI.

In our spatial model, however, the initiation site has no IPR, no possibility of CICR, and thus no way of controlling the burst length or IBI. However, the soma is still capable of controlling the burst, even when it is situated at a distance from the initiation site. With the highest density of Na^+ channels, the iSite is the first place to depolarize and hence give an action potential (or bursting). The voltage diffuses rapidly from the iSite to either side. Since the diffusion coefficient for V is large, this diffusion happens so quickly that the soma is depolarized at almost the same time as the iSite.

Once the soma begins to burst, the entry of Ca^{2+} through voltage-gated channels in the soma cause a large Ca^{2+} transient in the soma due to CICR, and a large hyperpolarizing potential, which terminates bursting in the soma (Figure 4.5). This hyperpolarizing potential then spreads backwards along the dendrite until it reaches the iSite, terminating bursting there and setting the IBI. In essence, diffusion of voltage is so fast that the iSite and the soma are practically

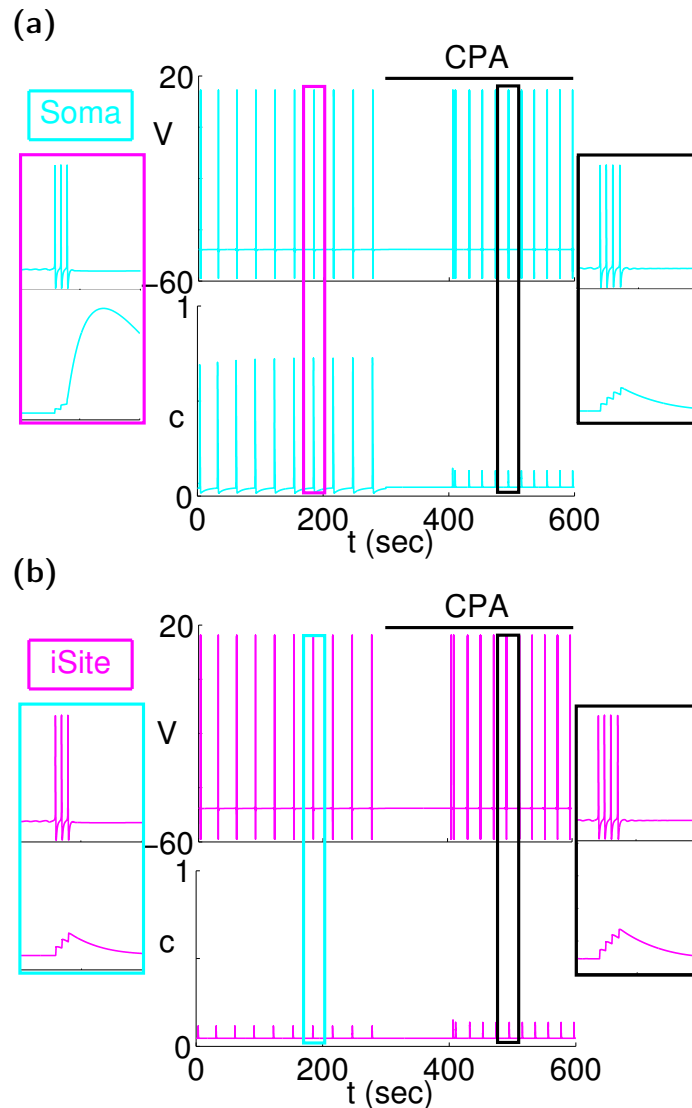


Figure 4.5 Intrinsic bursting and one pharmacological test (CPA) from model simulations. **(a)** Action potential bursting and associated Ca^{2+} transients in the soma. It shows the control case in the first 300 seconds, and CPA result by blocking SERCA pump after 300 seconds. Magenta rectangle shows one detailed bursting associated with a large Ca^{2+} transient in the control case in the soma, the black rectangle on the right hand side shows one detailed bursting associated with a faithful Ca^{2+} transient after CPA test in soma. **(b)** Simulation result detected in the iSite before and after CPA test. Cyan rectangle shows one representative bursting with small Ca^{2+} transient in the control case in the iSite, and the black rectangle shows one representative bursting with Ca^{2+} transient after CPA in the iSite.

isotonic, and thus the separation of the initiation mechanisms from the control mechanisms has no important effect.

Note that, as $D_v = \frac{\lambda_m^2}{\tau_m}$, the large diffusion of voltage indicates the large length constant. We will also investigate the impact of varying D_v and the location of the iSite on the coupling between the soma and the iSite in the next subsection.

Our spatial model can reproduce the responses to pharmacological manipulations, in the

same way as does the spatially homogenous model (Lee et al., 2010). We show here only the control result and one pharmacological test (CPA) as an example. The time trace from one position in the soma is shown in Figure 4.5(a). It shows the voltage bursts and the corresponding Ca^{2+} transient. CPA blocks the SERCA pump which controls the intake of Ca^{2+} into the ER. The bursting frequency increases, and the Ca^{2+} transient is inhibited.

Addition of CPA makes the IBI decrease significantly, to about half the value of the control case in the experiment (Lee et al., 2010). In our model, the IBI decreased from 30 seconds to about 20 seconds. Although the bursting frequency increase is qualitatively accurate, the quantitative match is not perfect. One possible explanation could be that our model may not capture every possible Ca^{2+} handling mechanism. For example, the large Ca^{2+} transients in our model do not quantitatively match the long (~ 8 seconds long) transient in Lee et al. (2010). Meanwhile, the UCL-sensitive current has a rise time similar to the time the large Ca^{2+} transient lasts. As addition of CPA suppresses the Ca^{2+} transient, our model has less effect on the slower UCL channel. Hence, the IBI decreased less after CPA test in our model than the one in Lee et al. (2010).

In addition to reproducing the response measured at the soma, our model also predicts the response in the dendrite (which is not measured experimentally, in general). We choose one typical position in the iSite and plot it as a function of time (Figure 4.5(b)). The bursting structure in the iSite is more or less the same as in the soma, with the soma spikes being only slightly delayed. The presence of CPA makes no qualitative difference to this feature of the solution. Note that, the Ca^{2+} shapes are different in the control case between the soma and the iSite. The large Ca^{2+} transient in the soma (left bottom panel in Figure 4.5(a)) is induced by CICR through IPR. As there is no IPR in the iSite in our model, the small Ca^{2+} transient (left bottom panel in Figure 4.5(a)) shows no CICR in the iSite.

Addition of CPA is one example showing how changes in Ca^{2+} handling at the soma affect the dendritic responses. Conversely, other pharmacological tests explore how changes in electrical channels in the dendrite (especially the iSite) affect somatic responses. For example, when TTX is used to block Na^+ channels in the iSite (not shown), bursts are prevented.

4.4.5 The Location of the iSite Controls Burst Properties

By changing the location of the iSite we determined how the distance (L_{Si}) from the iSite to the soma influences the properties of the bursting oscillations. The results are summarized in Figure 4.6(a) for the case that D_v is fixed at $30000 \mu m^2/ms$. As the iSite moves further from the soma, i.e., as L_{Si} increases, the IBI decreases and the number of spikes per burst increases. For instance, as L_{Si} is increased from zero to $270 \mu m$, the IBI is decreased from 43 to 2.8 seconds and the number of spikes per burst increases from 2 to 6 (Figure 4.6(a)). These results are intuitively clear. Since the burst is terminated by processes occurring in the soma, the tighter the coupling is between the soma and the iSite, the easier it is for the soma to terminate the burst. As the iSite moves away from the soma, the K^+ currents generated at the soma have less effect on the iSite, and take longer to terminate the burst, leading to an decreased IBI and more spikes in each burst. In an extreme case, it is possible for the soma to exhibit bursting while the iSite spikes continuously. However, in our model this occurs only for unphysiological parameter values.

Similarly, as D_v is increased up to $42690 \mu m^2/ms$ when L_{Si} is $270 \mu m$, the IBI increases from 2.8 to 51 seconds and the number of spikes per burst decreases from 6 to 2 (Figure 4.6(b)), for the same reason. The greater the value of D_v , the more easily the hyperpolarizing currents in the soma will spread to terminate the bursting at the iSite, leading to an increase in the IBI and an decrease in the number of spikes per burst. Conversely, a smaller value of D_v means a smaller length constant, and would make the soma decoupled from the iSite more effectively.

4.5 Discussion

We have constructed a spatial model of a GnRH neuron, including a soma and a single dendrite. The first $150 \mu m$ of the dendrite has the highest density of Na^+ channels and is thus the region that initiates the action potential. By fitting to experimental data, we estimate the diffusion coefficient of the voltage to be $30000 \mu m^2/ms$. This large diffusion coefficient provides a mechanism for regulating bursting behavior by the interaction of the soma and the iSite. In our model, electrical bursting that is initiated at the iSite spreads quickly to the soma to cause

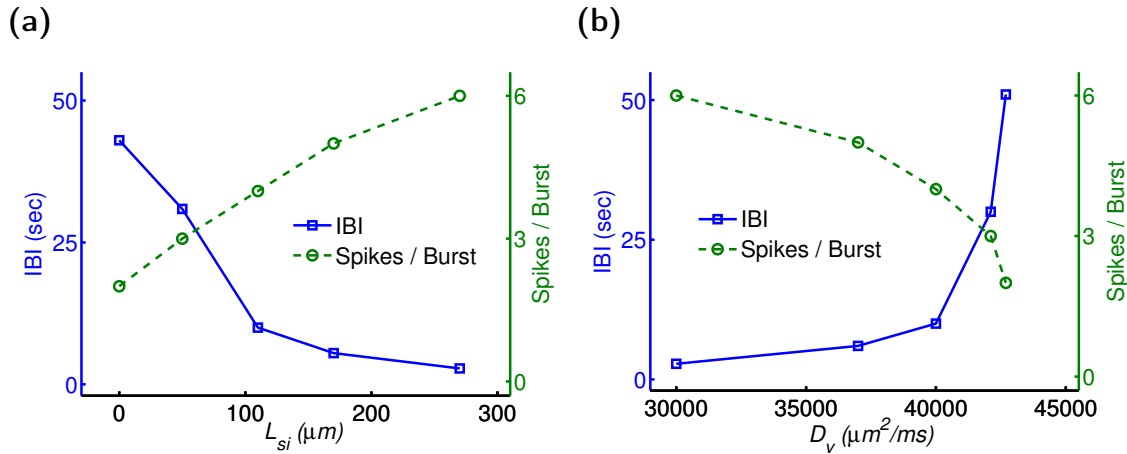


Figure 4.6 (a) Model simulations when $D_v = 30000 \mu\text{m}^2/\text{ms}$. L_{Si} is the distance from the soma to the iSite. Representative solutions for $L_{Si} = 50 \mu\text{m}$ were shown in Figure 4.5, in which there were 3 spikes in each burst with an IBI of 30 seconds. If L_{Si} is increased from this value, the IBI decreases and the number of spikes per burst increases, while the reverse is true if L_{Si} is decreased. (b) Model simulations for $L_{Si} = 270 \mu\text{m}$. The IBI is an increasing function of D_v , while the number of spikes per burst is an decreasing function of D_v . The blue solid line with squares represent the IBI, and the green dash line with circles represent the number of spikes per burst.

spiking there, and subsequent Ca^{2+} entry, which causes the release of larger amounts of Ca^{2+} via IPR located in the ER. This large somatic Ca^{2+} transient activates K^+ channels in the soma, causing a reverse spread of hyperpolarization to the iSite, termination of the burst, and control of the interburst interval. As a result, our model is consistent with the experimental results of Lee et al. (2010) as well as those of Iremonger and Herbison (2012).

Although we assume that the IPR are only in the soma, we can not explicitly rule out the possibility that there are IPR in the iSite also. However, since there is no evidence that the iSite contains IPR, and some limited evidence that they do not, we use the weakest reasonable assumption. If the iSite does in fact contain significant numbers of IPR then the problem of burst initiation and control reduces to the problem previously solved (Lee et al., 2010).

One prediction from our simulations is that GnRH neurons with the iSite located further away from the cell body would have a longer bursts and shorter IBIs than GnRH neurons with their iSite closer to the soma. However, since it is not easy to determine the precise location of the iSite, such a prediction is unlikely to be easily verifiable.

In the last decade there have been a number of other models of GnRH neurons, some of which are spatially homogeneous (van Goor et al., 2000; LeBeau et al., 2000; Fletcher and Li, 2009), others of which include a model of the dendrite (Roberts et al., 2008, 2009; Cserscik et

al., 2012). Of these, we are more interested in the models that include the dendrites, as they are more directly related to our work here. The experimental work of Roberts et al. (2008) revealed voltage-gated Na^+ channels in the dendrites of GnRH neurons, and was the first study to suggest the dendrite as the site of action potential initiation. That study also constructed a multi-compartmental, morphological, conductance-based computer model of action potential generation in GnRH neurons. Their modeling study suggested that distal dendrites have a lower threshold to initiate action potentials. Another study (Cserscik et al., 2012) presented a three-compartment model, including the soma, an active dendrite, and a compartment representing a passive dendrite. This study provides a simplified model to study interactions between the soma and the dendrite.

Our model here differs from the two previous spatial models that include both the soma and the dendrite, as it has a particular focus on the control of bursting via the interaction between the soma and the initiation site in the dendrite, a feature that was not studied in detail in either previous model. However, some aspects of those previous models, such as a detailed model of after-depolarization potentials, are not included here, as we believe them to be less relevant for soma/dendrite interactions. Another important feature that is omitted from our model is synaptic input. The most recent data (Iremonger and Herbison, 2012) indicate that synaptic input is an important part of the initiation of bursting. However, since the initiation of bursting is not our particular concern here, this feature is omitted. In future model development, it will be very important to include both after-depolarization potentials and synaptic input in order to obtain a more comprehensive model of electrical bursting in GnRH neurons.

In particular, we need to study:

- whether synaptic inputs contribute to initiate the bursting, and which type(s) of synaptic inputs is (are) the crucial driving force, and how;
- whether synaptic inputs affect the bursting behavior, and how;
- how the synaptic inputs from different locations could contribute to the bursting initiation and behaviors.

Stochastic effects are also expected to play a major role in an extended GnRH model. Synap-

tic input is, presumably, approximately random - at least at the level of detail that we consider here - and it is not yet clear how spatially distributed stochastic synaptic input will interact with the iSite and the soma to generate the observed bursting behavior. It has been reported that a Vasoactive Intestinal Polypeptide (VIP) current is one of those currents induced by those synaptic inputs (Gerhold et al., 2005; Gerhold and Wise, 2006; Christian and Moenter, 2008). Some studies have shown that a VIP current could affect the hyperpolarization-activated current (I_h) (Chu et al., 2010) that can modulate bursting, affect the after-depolarization potentials that can also modulate action potential firing (Chu and Moenter, 2006), and also affect the AHP current (Chu et al., 2010) which is so important for the control of bursting. Moreover, blockage of AMPA, NMDA and GABA_A receptors only showed some effect on bursting frequency (Liu et al., 2011; Herbison and Moenter, 2011), and hence they are not essential to initiate bursting (Lee et al., 2012). It is clear that a more detailed model of synaptic inputs will be required to try and understand how all the different inputs interact with the bursting mechanism. That, again, is left for future work.

Acknowledgements

This work was supported by the New Zealand Health Research Council, and by a University of Auckland Doctoral Scholarship to Xingjiang Chen. The author(s) wish to acknowledge the contribution of the NeSI high-performance computing facilities and the staff at the Centre for eResearch at the University of Auckland. New Zealand's national facilities are provided by the New Zealand eScience Infrastructure (NeSI) and funded jointly by NeSI's collaborator institutions and through the Ministry of Business, Innovation and Employment's Infrastructure programme. URL <http://www.nesi.org.nz>

Appendix A: Voltage Submodel

The equation for membrane potential (V) in the voltage subsystem is

$$\frac{\partial V(x,t)}{\partial t} = -\frac{1}{C_m} I_{\text{ionic}}(V,x,t) + D_v \frac{\partial^2 V(x,t)}{\partial x^2},$$

where C_m is the membrane capacitance and I_{ionic} is the sum of the ionic currents.

For $x \in [0, x_1]$, the currents in the soma are modeled as

$$I_{\text{ionic}}(V, x, t) = I_{\text{naf}} + I_{\text{nap}} + I_{\text{kdr}} + I_{\text{kir}} + I_{\text{km}} + I_{\text{cal}} + I_{\text{cat}} + sI_{\text{AHP-SK}} + sI_{\text{AHP-UCL}} + I_{\text{App}}.$$

For $x \in [x_2, x_3]$, the currents in the iSite are the same as in the soma, except that we use a higher conductance for I_{naf} , representing a higher density of Na^+ channels in the iSite. We use a Na^+ conductance (g_{naf}) of 410 nS in the iSite, and 150 nS elsewhere (Table 5.2).

For $x \in [x_1, x_2]$ and $x \in [x_3, x_4]$, the currents in the dendrite are modeled as

$$I_{\text{ionic}}(V, x, t) = I_{\text{naf}} + I_{\text{nap}} + I_{\text{kdr}} + I_{\text{kir}} + I_{\text{km}} + I_{\text{cal}} + I_{\text{cat}} + I_{\text{App}}.$$

I_{naf} and I_{nap} denote the fast, persistent Na^+ currents, I_{kdr} , I_{kir} , and I_{km} denote the delayed rectifier, inward rectifier, and m-type K^+ currents respectively, I_{cal} and I_{cat} are L-type and T-type Ca^{2+} currents, $sI_{\text{AHP-SK}}$ is an SK-type Ca^{2+} -activated K^+ current, and $sI_{\text{AHP-UCL}}$ is a slow Ca^{2+} -activated afterhyperpolarization current. I_{App} is a passive membrane leakage current. It may incorporate current from synaptic inputs, although there are no explicit synaptic inputs in our model. All the ion channels and fluxes are modeled as in Lee et al. (2010), Duan et al. (2011) and references therein.

We used a Hodgkin-Huxley formalism to model the currents. For example, I_{naf} is described as

$$I_{\text{naf}} = g_{\text{naf}} M_{\text{naf}\infty}^3 H_{\text{naf}} (V - V_{\text{na}}),$$

where g_{naf} is the maximum conductance, M_{naf} is the activation gating variable, H_{naf} is the inactivation gating variable, and V_{na} is the reversal potential for Na^+ . Similarly, equations governing

the other voltage-dependent currents are described by

$$\begin{aligned}
 I_{\text{nap}} &= g_{\text{nap}} M_{\text{nap}\infty} H_{\text{nap}\infty} (V - V_{\text{na}}), \\
 I_{\text{kdr}} &= g_{\text{kdr}} N_{\text{kdr}}^4 (V - V_k), \\
 I_{\text{kir}} &= g_{\text{kir}} N_{\text{kir}\infty} (V - V_k), \\
 I_{\text{km}} &= g_{\text{km}} N_{\text{km}} (V - V_k), \\
 I_{\text{cal}} &= g_{\text{cal}} M_{\text{cal}\infty}^2 (V - V_{\text{ca}}), \\
 I_{\text{cat}} &= g_{\text{cat}} M_{\text{cat}\infty}^2 H_{\text{cat}\infty} (V - V_{\text{ca}}).
 \end{aligned}$$

The gating variables $M_{\text{naf}}, M_{\text{nap}}, N_{\text{kir}}, M_{\text{cal}}, M_{\text{cat}}$, and H_{cat} are set to their steady-state values, while the gating variables $H_{\text{naf}}, N_{\text{kdr}}$, and N_{km} are modeled by

$$\frac{dG}{dt} = \frac{G_{\infty} - G}{\tau_G}.$$

The steady-state functions are:

$$\begin{aligned}
 M_{\text{naf}} &= \frac{1}{1 + e^{-\frac{V+40}{4.3}}}, \\
 H_{\text{naf}} &= \frac{1}{1 + e^{\frac{V+66.1}{10.8}}}, \\
 M_{\text{nap}} &= \frac{1}{1 + e^{-\frac{V+70}{4.1}}}, \\
 H_{\text{nap}} &= \frac{1}{1 + e^{\frac{V+80}{5}}}, \\
 N_{\text{kdr}} &= \frac{1}{1 + e^{-\frac{V+25}{15}}}, \\
 N_{\text{kir}} &= 0.8 \frac{1}{1 + e^{\frac{V+80}{12}}} + 0.2, \\
 N_{\text{km}} &= \frac{1}{1 + e^{-\frac{V+37}{4}}}, \\
 M_{\text{cal}} &= \frac{1}{1 + e^{-\frac{V+30}{2}}}, \\
 M_{\text{cat}} &= \frac{1}{1 + e^{-\frac{V+56.1}{10}}}, \\
 H_{\text{cat}} &= \frac{1}{1 + e^{-\frac{V+86.4}{4.7}}}.
 \end{aligned}$$

The functions for the time constants (τ_G , in ms) are:

$$\begin{aligned} H_{\text{naf}} &= 75e^{-\frac{V+80}{19}} + 2e^{-2\frac{V+80}{19}}, \\ N_{\text{kdr}} &= 21e^{-\frac{V+30}{15}} + e^{-\frac{V+30}{15}} + 1.4, \\ N_{\text{km}} &= 11.5e^{-\frac{V+30}{15}} + e^{-\frac{V+30}{15}}. \end{aligned}$$

The equation for $sI_{\text{AHP-SK}}$ is

$$sI_{\text{AHP-SK}} = g_{\text{sk}} \frac{c^{n_{\text{sk}}}}{c^{n_{\text{sk}}} + K_{\text{sk}}^{n_{\text{sk}}}} (V - V_k).$$

The equation for $sI_{\text{AHP-UCL}}$ is

$$sI_{\text{AHP-UCL}} = g_{\text{ucl}} (O_{\text{ucl}} + O_{\text{ucl}}^*) (V - V_k),$$

where O_{ucl} and O_{ucl}^* are two open states of the channel governed by the kinetic equations of the system introduced in Lee et al. (2010). We have

$$\begin{aligned} \frac{dO_{\text{ucl}}}{dt} &= k_{11}cS_{\text{ucl}} - k_{-11}O_{\text{ucl}} - k_{22}O_{\text{ucl}}, \\ \frac{dO_{\text{ucl}}^*}{dt} &= k_{22}O_{\text{ucl}} - k_{33}O_{\text{ucl}}^*, \end{aligned}$$

where $O_{\text{ucl}} + O_{\text{ucl}}^* + S_{\text{ucl}} = 1$.

Appendix B: Calcium Submodel

The equations describing the Ca^{2+} concentration in the cytosol (c) and in the endoplasmic reticulum (ER) (c_e) are as follows:

$$\begin{aligned} \frac{\partial c(x,t)}{\partial t} &= \rho (J_{\text{in}} - J_{\text{pm}}) + J_{\text{release}} - J_{\text{serca}} + D_c \frac{\partial^2 c(x,t)}{\partial x^2}, \\ \frac{dc_e(x,t)}{dt} &= \gamma (J_{\text{serca}} - J_{\text{release}}), \end{aligned}$$

where ρ is used to scale plasma membrane and ER fluxes, and γ is the volume ratio between the ER and the cytosol. J_{in} , J_{pm} , J_{release} , and J_{serca} denote the influx via plasma membrane channels, efflux via PMCA and NCX plasma membrane pumps, release of Ca^{2+} from the ER to cytosol, and Ca^{2+} pumping from the cytosol to the ER, respectively. We have

$$\begin{aligned} J_{\text{in}} &= -\alpha (I_{\text{cal}} + I_{\text{cat}}) + \beta, \\ J_{\text{pm}} &= V_p \frac{c^2}{c^2 + K_{\text{pm}}^2} + V_{\text{NaCa}} \frac{c^4}{c^4 + K_{\text{NaCa}}^4}, \\ J_{\text{release}} &= (K_f P_o + J_{\text{er}}) (c_e - c), \\ J_{\text{serca}} &= P_{\text{rate}} \frac{c - a_1 c_e}{a_2 + a_3 c + a_4 c_e + a_5 c c_e}. \end{aligned}$$

The parameter β shown in the equation of J_{in} is constant. It represents the receptor-regulated Ca^{2+} entry through the plasma membrane.

The IPR open probability (P_o) is from Gin et al. (2009):

$$P_o = \frac{q_{12} q_{32} q_{24}}{q_{12} q_{32} q_{24} + q_{42} q_{23} q_{12} + q_{42} q_{32} q_{12} + q_{42} q_{32} q_{21}},$$

where q_{12} , q_{21} , q_{24} , and q_{42} are set to their steady-state values, and where q_{23} and q_{32} are given by

$$\begin{aligned} q_{23}(c) &= a_{23} - \left(\frac{V_{23}}{k_{23}^2 + c^2} + b_{23} \right) \left(\frac{V_{-23} c^5}{k_{-23}^5 + c^5} + b_{-23} \right), \\ q_{32}(c) &= \left(\frac{V_{32}}{k_{32}^3 + c^3} + b_{32} \right) \left(\frac{V_{-32} c^7}{k_{-32}^7 + c^7} + b_{-32} \right). \end{aligned}$$

Note that, although the IPR open probability is dependent on both the Ca^{2+} and IP_3 , the P_o function used here is not IP_3 dependent. Gin et al. (2009) determined rate constants by using steady-state single-channel data which were obtained from the IPR at various Ca^{2+} concentrations at a single saturating IP_3 concentration (100 μM). A fixed value of IP_3 concentration is assumed in P_o function. The P_o function shown in the equation of J_{release} is assumed to exist in the soma only.

Since Ca^{2+} diffusion is orders of magnitude slower than the diffusion of V (Keener and Sneyd, 2008), Ca^{2+} diffusion was omitted from all our model simulations.

Appendix C: Numerical Method

We used a finite difference method to solve the model equations in MATLAB (MathWorks). We discretized the spatial derivative using the second order implicit central difference method, and the time derivative using the first order explicit Euler method. For some long time simulations we also used the method of lines, using the routine ode15s.

Appendix D: Parameter Values

Table 4.1 Parameter values of the model. These parameters are either new to this model, or have values taken from Lee et al. (2010), and Duan et al. (2011) (with very minor changes).

Parameter	Soma	Dendrite	iSite
D_v ($\mu\text{m}^2/\text{ms}$)	30000	30000	30000
g_{naf} (nS)	150	150	410
g_{nap} (nS)	20	20	20
g_{cal} (nS)	0.035	0.035	0.035
g_{cat} (nS)	2.1	2.1	2.1
g_{ucl} (nS)	963	–	963
g_{sk} (nS)	1.6	–	1.6
n_{sk}	2.6	–	2.6
k_{sk}	0.4	–	0.4
D_c ($\mu\text{m}^2/\text{ms}$)	–	–	–

Table 4.2 Parameter values of the voltage submodel.

Parameter	Value	Parameter	Value	Parameter	Value
C_m (pF)	16	V_{na} (mV)	60	k_{33}	3e-5
g_{kdr} (nS)	2	V_k (mV)	-80	k_{22}	0.5
g_{kir} (nS)	0.02	V_{ca} (mV)	100	k_{-11}	1.2
g_{km} (nS)	8	V_{leak} (mV)	100	k_{11} (μM^{-1})	1e-7
g_{leak} (nS)	0.04				

Table 4.3 Parameter values of the Ca^{2+} submodel.

Parameter	Value	Parameter	Value	Parameter	Value
a_1	1e-4	$K_{\text{pm}} (\mu\text{M})$	0.425	ρ	0.5
a_2 (ms)	35	$K_f (\text{ms}^{-1})$	1.92e-6	$\alpha (\mu\text{Mms}^{-1}\text{pA}^{-1})$	0.0048
$a_3 (\mu\text{M}^{-1}\text{ms})$	300	$K_{\text{NaCa}} (\mu\text{M})$	0.05	$\beta (\mu\text{Mms}^{-1})$	6e-6
$a_4 (\mu\text{M}^{-1}\text{ms})$	7	P_{rate}	1	γ	27
$a_5 (\mu\text{M}^{-2}\text{ms})$	35	$V_{\text{NaCa}} (\mu\text{Mms}^{-1})$	0.00035	$V_p (\mu\text{Mms}^{-1})$	0.0042
$J_{\text{er}} (\text{ms}^{-1})$	4e-7	$V_{23} (\text{nM}^2\text{ms}^{-1})$	1.08e6	k_{23} (nM)	2000
$q_{12} (\text{ms}^{-1})$	0.74	V_{-23}	0.3545	k_{-23} (nM)	72
$q_{21} (\text{ms}^{-1})$	0.11	$V_{23} (\text{nM}^3\text{ms}^{-1})$	7e6	k_{32} (nM)	520
$q_{24} (\text{ms}^{-1})$	7.84	V_{-32}	1.06	k_{-32} (nM)	150
$q_{42} (\text{ms}^{-1})$	3.60	$a_{23} (\text{ms}^{-1})$	1/1.023	$b_{23} (\text{ms}^{-1})$	2.2
b_{-23}	0.042	$b_{32} (\text{ms}^{-1})$	0.005	b_{-32}	0.03

A Computational Model of the Dendron of the GnRH Neuron

In the following chapter, we extend our previous spatiotemporal model of the GnRH neuron by considering stochastic synaptic input, in order to study the function of synaptic input along the dendrite. We also investigate other possible ways in which synaptic input could modify Ca^{2+} release at the synaptic terminal, focusing in particular on the possible role of kisspeptin. What follows is a copy of the manuscript submitted to the Bulletin of Mathematical Biology. The full reference is given in the bibliography (Chen and Sneyd, 2014).

5.1 Abstract

Gonadotropin-releasing hormone (GnRH) neurons have two major processes that have properties of both dendrites (they receive synaptic input from other neurons) and axons (they actively propagate action potentials to the synaptic terminal). These processes have thus been termed *dendrons*. We construct a stochastic spatiotemporal model of the dendron of the GnRH neuron, with the goal of studying how stochastic synaptic input along the length of the dendron affects the initiation and propagation of action potentials. We show (i) that synaptic inputs closer to the soma are effective controllers of action potential initiation and electrical bursting, and (ii) that although the effects on the amplitude and width of propagating action potentials are critically dependent on the timing and location of synaptic input addition, the effects remain small. We conclude that although stochastic synaptic input along the length of the dendron is likely to be a major determinant of action potential initiation, it is an unlikely mechanism for controlling whether or not action potentials reach the synaptic terminal. Thus, the role of synaptic inputs situated along the dendron a long way from the site of action potential initiation remains unclear. We also show that the actions of kisspeptin can result in significant modulation of the amount of calcium released by an action potential at the synaptic terminal. Furthermore, we show that the actions of kisspeptin are greatest when multiple effects operate together; a kisspeptin-induced increase in firing rate is, by itself, less effective at increasing Ca^{2+} release than is a combination of an increased firing rate, an increase in Ca^{2+} influx, and an increase in inositol trisphosphate (IP_3) production. We conclude that the inherent synergies in the various actions of kisspeptin make it a likely candidate for the precise control of Ca^{2+} transients at the synaptic terminal.

5.2 Introduction

Gonadotropin-releasing hormone (GnRH) neurons are hypothalamic neurons that represent the final output cells of the neural network regulating fertility in all mammalian species (Herbison, 2006). They send projections, extending over 1000 μm , to the median eminence to secrete GnRH (Campbell et al., 2005; Herbison, 2006; Herde et al., 2013). Although these projections

receive substantial synaptic input (Campbell et al., 2005; Cottrell et al., 2006; Campbell et al., 2009; Herde et al., 2013), they are also the site of action potential initiation in these neurons and propagate action potentials to the synaptic terminal in the median eminence (Roberts et al., 2008; Iremonger and Herbison, 2012; Herde et al., 2013). Since these GnRH neuron projections thus have the properties of both dendrites and axons, they have been termed “dendrons” (Herde et al., 2013).

We have previously studied the initiation and control of electrical bursting in the dendron of the GnRH neuron (Chen et al., 2013). Action potentials are initiated in a well-defined region (around 100 μm from the soma) that we named the *iSite*, while the control of burst length and interburst interval is carried out principally by Ca^{2+} -dependent K^{+} channels in the soma. The short electrical distance between the *iSite* and the soma allows for precise control of the bursting properties despite the relatively large physical distance between these two regions.

However, our previous study left two major questions unanswered.

- Although stochastic synaptic input along the dendron is almost certainly an important part of the initiation of bursting and propagation along the dendron, it was not included in our previous model. Thus it is not yet clear how spatially distributed stochastic synaptic input will interact with the *iSite* and the soma to generate the observed bursting behavior. There are many types of inputs that the GnRH neurons could receive and respond to. For example, studies have shown the impact of glutamate and GABA on regulating the activity of GnRH neurons (for a review, see Iremonger et al., 2010; Herbison and Moenter, 2011), while it has also been reported that Vasoactive Intestinal Polypeptide (VIP) affects GnRH neuron firing (Christian and Moenter, 2008). There are also several other inputs such as noradrenaline (Han et al., 2002), nitric oxide (Clasadonte et al., 2008) and kisspeptin (which is studied in more detail below).
- How does synaptic input along the dendron affect the arrival of action potentials at the synaptic terminal? Can synaptic inputs prevent or enhance the transmission of an action potential along the dendron, thus making it possible for synaptic inputs to control whether or not an action potential is transmitted all the way to the synaptic terminal? If this were possible, then periodic synaptic inputs along the dendron might be able to cause

the periodic transmission of action potentials to the median eminence, thus resulting in periodic secretion of GnRH.

Here, we begin by addressing these two questions. As we shall show, stochastic initiation of bursting by means of stochastic synaptic input has no qualitative effect on bursting properties, which remains essentially the same as in our previous model. Furthermore, although synaptic input can modulate the properties of the propagating action potentials, such effects are relatively small and are unlikely to provide a mechanism for allowing or preventing action potential propagation. We thus conclude that synaptic input along the length of the dendron is not a likely mechanism for the control of action potential propagation in the dendron, or for the formation of long-period patterns of GnRH secretion.

Thus motivated, in the second half of this paper we study an alternative mechanism, based upon the secretion of kisspeptin from kisspeptin neurons at the synaptic terminal, for controlling, or enhancing, the secretion of GnRH. In particular, we ask the following question; what is the most effective mechanism, or combination of mechanisms, for increasing the concentration of Ca^{2+} at the synaptic terminal, and thus, presumably, increasing GnRH secretion?

Kisspeptin and its receptor, G-protein-coupled receptor 54 (Gpr54), are known to be important for reproduction and for the regulation of GnRH secretion (Gottsch et al., 2006; Kirilov et al., 2013). Patients and mice with mutations and deletions of GPR54 have hypogonadotropic hypogonadism (infertility and reproductive failure) (de Roux et al., 2003; Seminara et al., 2003). The action of kisspeptin can be direct, since GnRH neurons express Gpr54 (Irwig et al., 2004; Han et al., 2005; Messenger et al., 2005). Kisspeptin can directly depolarize and increase the firing rate of GnRH neurons (Han et al., 2005; Liu et al., 2008; Zhang et al., 2008; Pielecka-Fortuna et al., 2008; Zhang and Spergel, 2012), and can thus activate GnRH and LH secretion (Gottsch et al., 2004; Messenger et al., 2005). In Gpr54 knockout mice, kisspeptin is unable to stimulate LH secretion (Messenger et al., 2005), and the mice are infertile (d'Anglemont de Tassigny et al., 2007). Kisspeptin neurons extend processes to the median eminence (Smith et al., 2011; Uenoyama et al., 2011), and kisspeptin can also act directly at the median eminence to regulate GnRH release via Gpr54 stimulation (d'Anglemont de Tassigny et al., 2008). Kisspeptin can even stimulate GnRH release from the synaptic terminal (Keen et al., 2008), in

the absence of the soma of the GnRH neuron, and in the presence of TTX (d'Anglemon de Tassigny et al., 2008).

Furthermore, kisspeptin can directly cause a rise in intracellular Ca^{2+} , via two principal mechanisms; firstly, by activation of PLC and production of inositol trisphosphate (IP_3), and, secondly, by the activation of transient receptor potential cation (TRPC) channels thus increasing Ca^{2+} influx. Activation of Gpr54 expressed in CHO cells causes Ca^{2+} release from intracellular stores (Kotani et al., 2001), while kisspeptin increases IP_3 formation in Cos-7 cells (Stafford et al., 2002), which mobilizes Ca^{2+} . Furthermore, Brailoiu et al. (2005) shows that kisspeptin induces an increase in intracellular Ca^{2+} concentration in cultured rat hippocampal neurons. There is evidence that, in some cell types, the kisspeptin-induced increase in Ca^{2+} concentration arises via the influx of Ca^{2+} through TRPC-like channels in the cell membrane (Zhang et al., 2008; Constantin et al., 2009; Kroll et al., 2011; Zhang and Spergel, 2012; Zhang et al., 2013a). Other studies indicate that kisspeptin induces the release of Ca^{2+} in GnRH neurons via the IP_3 -mediated release of Ca^{2+} from intracellular stores (Castellano et al., 2006; Liu et al., 2008). These studies indicate that kisspeptin activates Gpr54 to initiate a PLC-IPR- Ca^{2+} cascade (Liu et al., 2008), and hence stimulates GnRH secretion (Castellano et al., 2006).

We thus construct a model to study how the known actions of kisspeptin – increasing the bursting rate, increasing Ca^{2+} influx, and the formation of IP_3 – could interact, and what are their relative effects on the release of Ca^{2+} at the synaptic terminal. Although these actions of kisspeptin are known to occur at the cell body of GnRH neurons, here we assume they also occur at the synaptic terminal, and study the consequences of this assumption. We shall show that the actions of kisspeptin synergize effectively, such that, although each effect by itself causes some increase in Ca^{2+} transients at the synaptic terminal, the combination of all three actions has a more potent effect.

5.3 Model Description

The model of electrical bursting is the same as that in Chen et al. (2013). Synaptic inputs are modeled as applied current, where the conductance takes the form of a double exponential

function $g_{SI}(t) = \bar{g}_{SI}(e^{-\frac{t}{\tau_1}} - e^{-\frac{t}{\tau_2}})$, where the variables τ_1 and τ_2 are the rise and fall time constants, t is the time, and g_{SI} is the conductance amplitude. The synaptic input current is modeled by using Ohm's law $I_{SI} = g_{SI}(V - E_{SI})$, where V is the membrane potential of the neuron, and E_{SI} is the reversal potential of the synaptic input. We use $E_{SI} = -70$ mV as the reversal potential for an inhibitory synaptic input, and 0 mV for an excitatory synaptic input. Finally, we generate synaptic input at random times and at random positions along the dendron. We use a simple Poisson process with rate at 3 Hz.

For the first set of results we generate multiple synaptic inputs and study how the summation of multiple inhibitory and excitatory synaptic input leads to the generation of bursts of action potentials. In our second set of results we add only a single synaptic input at a specified place along the dendron, we generate an action potential artificially, and then study how the timing between the arrival of an action potential and the peak of the synaptic input affects action potential propagation along the dendron.

For our final set of results we construct a simple model of cellular Ca^{2+} dynamics that includes Ca^{2+} influx (through TRPC channels as well as through voltage-gated channels), IP_3 -induced release of Ca^{2+} from the ER, and pumping of Ca^{2+} back into the ER or to outside the cell. Kisspeptin is assumed to be applied continuously during the period of application. (Modification of this assumption – to include, for example, spikes of kisspeptin application corresponding to spiking of kisspeptin neurons – makes no qualitative difference to the results.)

The production of IP_3 is assumed to be an increasing function of kisspeptin concentration. Hence,

$$\frac{dIP_3}{dt} = K_p - K_i IP_3, \quad (5.1)$$

where K_p represents the kisspeptin concentration and K_i is a constant. The value of K_p in our model is essentially arbitrary. kisspeptin has no effect when $K_p = 0$, and spiking is continuous when $K_p = 7.5$, but this choice of 7.5 is entirely arbitrary. All that matters is the relationship between, for example, the increase in the rate of firing caused by an increase in kisspeptin, and the associated increase in Ca^{2+} influx given by the same value of kisspeptin. Here, we

have chosen the parameters so that the maximal increase in firing rate (to continuous spiking) corresponds to physiologically reasonable increases in Ca^{2+} influx and IP_3 concentration.

The equations describing the Ca^{2+} concentration in the cytosol (c) and in the endoplasmic reticulum (ER)(c_e) take a standard form, and are as follows:

$$\frac{dc}{dt} = \rho (J_{\text{in}} - J_{\text{pm}}) + J_{\text{release}} - J_{\text{serca}}, \quad (5.2)$$

$$\frac{dc_e}{dt} = \gamma (J_{\text{serca}} - J_{\text{release}}), \quad (5.3)$$

where ρ is used to scale plasma membrane and ER fluxes, and γ is the volume ratio between the ER and the cytosol. J_{in} , J_{pm} , J_{serca} , and J_{release} denote the influx via plasma membrane channels, efflux via plasma membrane pumps, Ca^{2+} pumping from the cytosol to the ER, and release of Ca^{2+} from the ER to cytosol, respectively. We have

$$J_{\text{in}} = -\alpha I_{\text{ca}} + J_{\text{TRPC}}, \quad (5.4)$$

$$J_{\text{pm}} = V_{\text{pm}} c, \quad (5.5)$$

$$J_{\text{serca}} = P_{\text{rate}} \frac{c - a_1 c_e}{a_2 + a_3 c + a_4 c_e + a_5 c c_e}, \quad (5.6)$$

$$J_{\text{release}} = (K_f P_o + J_{\text{er}}) (c_e - c). \quad (5.7)$$

We use a Hodgkin-Huxley formalism to model the I_{ca} , that is:

$$I_{\text{ca}} = g_{\text{ca}} M_{\text{ca}\infty}^2 (V - V_{\text{ca}}). \quad (5.8)$$

The gating variable $M_{\text{ca}\infty}$ can be modeled as $M_{\text{ca}\infty} = \frac{1}{1 + e^{-\frac{V+30}{2}}}$, where V is the membrane potential. The Ca^{2+} influx through TRPC channels (J_{TRPC}) can be modeled as $J_{\text{TRPC}} = g_{\text{TRPC}} \frac{K_p^2}{K_p^2 + 1^2}$. The IPR open probability (P_o) is from Palk et al. (2010), which is modified as both IP_3 and Ca^{2+} dependent from Gin et al. (2009). The modified P_o function used here is given by

$$P_o = \frac{q_{12} q_{32} q_{24}}{q_{12} q_{32} q_{24} + q_{42} q_{23} q_{12} + q_{42} q_{32} q_{12} + q_{42} q_{32} q_{21}}. \quad (5.9)$$

The rate constants between the states were investigated for their dependence on both the Ca^{2+}

and IP_3 concentrations and are given by,

$$\begin{aligned}
 q_{12} &= 0.74 \text{ ms}^{-1} & q_{21} &= \Phi_{21}(IP_3) \text{ ms}^{-1}, \\
 q_{23} &= \alpha_{23} \Psi_{23}(c) \Phi_{23}(IP_3) \text{ ms}^{-1} & q_{32} &= \alpha_{32} \Psi_{32}(c) \Phi_{32}(IP_3) \text{ ms}^{-1}, \\
 q_{24} &= 7.84 \text{ ms}^{-1} & q_{42} &= 3.6 \text{ ms}^{-1},
 \end{aligned}$$

where

$$\begin{aligned}
 \Phi_{21}(IP_3) &= \frac{V_{p21}}{1 + k_{p21}IP_3^3} + b_{p21}, \\
 \Psi_{23}(c) &= a_{23} - \left(\frac{V_{23}}{k_{23}^2 + c^2} + b_{23} \right) \left(\frac{V_{m23}c^5}{k_{m23}^5 + c^5} + b_{m23} \right), \\
 \Phi_{23}(IP_3) &= \frac{V_{p23}}{1 + k_{p23}IP_3^3} + b_{p23}, \\
 \Psi_{32}(c) &= \left(\frac{V_{32}}{k_{32}^3 + c^3} + b_{32} \right) \left(+ b_{m32} \right), \\
 \Phi(IP_3) &= \frac{V_{p32}IP_3^3}{1 + k_{p32}IP_3^3} + b_{p32}.
 \end{aligned}$$

The rate constants q_{23} and q_{32} depend on both Ca^{2+} and IP_3 . The dependence of the rate constants on Ca^{2+} was established at a fixed IP_3 concentration in Gin et al. (2009). Scaling factors and several modified parameters introduced in Palk et al. (2010) ensure the modified model matches the experimental data. Parameter values can be found in Table 5.1.

To model the action of kisspeptin on the bursting rate, we define the interburst interval (IBI) to be a simple decreasing function of K_p ; thus, $IBI_V = 30 - 4K_p$. With no kisspeptin stimulation,

Table 5.1 Parameter values of the modified IPR P_o function used in the new Ca^{2+} model at the termianl.

Parameter	Value	Parameter	Value	Parameter	Value
b_{p21} (ms^{-1})	0.11	b_{p23} (ms^{-1})	0.001	b_{p32}	0
k_{p21} (nM^{-3})	5e-10	k_{p23} (nM^{-3})	5e-9	k_{p32} (nM^{-3})	1.5e-10
V_{p21} (nM^3ms^{-1})	0.0949	V_{p23} (nM^3ms^{-1})	0.162	V_{p32} (nM^3ms^{-1})	3e-12
a_{23} (ms^{-1})	1/1.023	α_{23}	1000	α_{32}	50
V_{23} (nM^2ms^{-1})	1.08e-6	k_{23} (nM)	2000	b_{23} (ms^{-1})	2.2
V_{m23}	0.3545	k_{m23} (nM)	72	b_{m23}	0.042
V_{32} (nM^3ms^{-1})	7e+6	k_{32} (nM)	520	b_{32} (ms^{-1})	0.005
V_{m32}	1.06	k_{m32} (nM)	150	b_{m32}	0.03

the IBI is 30 seconds. As K_p increases, the IBI decreases until bursting is continuous. Clearly, there is an upper limit for the value of kisspeptin, a technical restriction which could easily be removed by the use of a saturating function for the relationship between K_p and the IBI. However, the simpler linear relationship is accurate enough for our purposes here.

For simplicity, this model of Ca^{2+} dynamics is assumed to be driven by square-wave pulses of voltage (V). Use of a more realistic wave form for an action potential results merely in increased computational time, with no qualitative change to the results.

New parameter values in this study are shown in Table 5.2. Other parameter values can be found in Chapter 4 of this thesis.

Table 5.2 Some parameter values of the new Ca^{2+} model.

Parameter (unit)	\bar{g}_{SI} (nS)	τ_1 (ms)	τ_2 (ms)	K_p ($\mu\text{M}/\text{ms}$)	K_i (ms^{-1})	V_{pm} ($\mu\text{M}/\text{ms}$)	g_{ca} (nS)	g_{TRPC} (nS)
Values	varies	1	10	varies	0.001	0.02	0.06	0.0001

5.4 Results

5.4.1 The Effects of Synaptic Input on Bursts

The control case (with no synaptic input) has an IBI of around 30 seconds, with 3 spikes per burst. These bursts arise as the result of intrinsic oscillatory properties of the neuron, as modeled by Chen et al. (2013). In Figure 5.1 we see the effect of synaptic input on bursting behavior. Compared to the control case, excitatory synaptic input gives earlier initiation for the first burst, more bursts, smaller IBI and more spikes per burst, while the inhibitory synaptic input gives the opposite results, as shown in Figure 5.1(a). An expanded view of the first burst (for both the control case and for excitatory synaptic input) is shown in Figure 5.1(b). The first spikes from each burst are artificially aligned to allow for comparison of the structure within each burst. Excitatory synaptic input causes smaller inter spike intervals than the control case. The effects of excitatory synaptic input and inhibitory synaptic input on bursting behavior are also shown in Figure 5.1(c) and (d). The more excitatory synaptic input gives smaller IBI and makes it easier

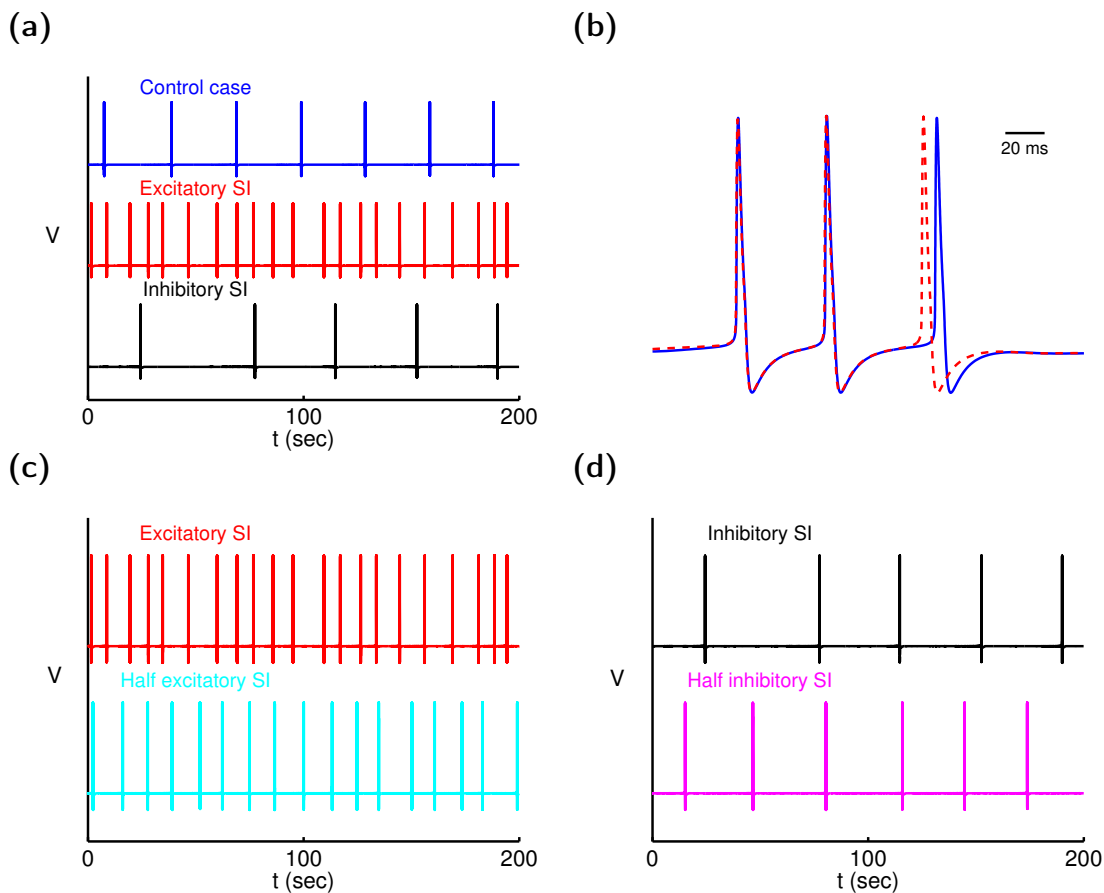


Figure 5.1 The effects of synaptic input on bursting behavior. **(a)** Excitatory synaptic input gives more bursts compared to the control case, while the inhibitory synaptic input gives fewer bursts. The excitatory synaptic input makes bursts with smaller IBI, and about 3 or 4 spikes per burst. The inhibitory synaptic input makes bursts with larger IBI, and about 2 or 3 spikes per burst. The excitatory synaptic input initiates the first burst earlier than the control case, while the inhibitory synaptic input initiates the first burst a little bit later. **(b)** The first bursts from the excitatory synaptic input case and control case as shown in **(a)**. The first spikes from each burst are aligned gives the different burst structure of each case. The excitatory synaptic input case has smaller inter spike interval than the control case. **(c)** The effect of excitatory synaptic input on bursting behavior. The top panel shows the bursts with more synaptic input, while the bottom panel with less excitatory synaptic input. The more excitatory synaptic input gives smaller IBI and makes it earlier to spike. **(d)** The effect of inhibitory synaptic input on bursting behavior. The top panel shows the bursts with more inhibitory synaptic input, while the bottom panel with less inhibitory synaptic input. The more inhibitory synaptic input gives larger IBI and makes it harder to spike. Note: SI stands for synaptic input in all the figures.

to spike, while the more inhibitory synaptic input gives larger IBI and makes it harder to spike.

Although the results in Figure 5.1 are entirely predictable they do serve to demonstrate that stochastic synaptic input distributed over the dendron suffices to initiate bursting at the iSite, with the same qualitative properties as the bursting generated by the deterministic model of Chen et al. (2013). As expected, the mean IBI can be modulated by varying the proportion of excitatory to inhibitory inputs.

We next tested the effects of synaptic input spatial distribution on bursting. The dendron was divided into 5 regions, each of length $80 \mu\text{m}$, see Figure 5.2(a). Region I is the region $0\text{-}80 \mu\text{m}$ from the soma, region II is the region $80\text{-}160 \mu\text{m}$ from the soma (and thus contains the iSite), etc. The burst properties were then determined as a function of which region the synaptic inputs were added to (Figure 5.2(b)). Surprisingly, when the synaptic inputs are distributed closer to the soma (i.e., in region I), the IBI is larger, while the IBI is smaller when the synaptic inputs are located further from the soma (Figure 5.2(b)). Hence, synaptic inputs close to the soma are *less* effective at initiating bursting than are synaptic inputs further away from the soma.

The reason for this counterintuitive result can be seen in Figure 5.2(c), where we plot the soma Ca^{2+} concentration for two bursts, one with synaptic input close to the soma (Region I), the other with synaptic input further from the soma (Region III). Note that both sets of inputs are the same average distance from the iSite (Region II), where the burst is initiated. When the synaptic input is close to the soma, the Ca^{2+} transient in the soma is higher. This higher Ca^{2+} transient in the soma causes more activation of the Ca^{2+} -dependent K^+ channels that determine the IBI, and thus cause an increase in IBI. In other words, since it is the Ca^{2+} transient in the soma that controls the IBI (Lee et al., 2010; Chen et al., 2013), any synaptic input that increases this soma Ca^{2+} transient will also increase the IBI.

5.4.2 Modulation of Action Potentials by Synaptic Input

In general, dendrons receive synaptic input at the same time they propagate bursts of action potentials, which raises the possibility that synaptic input can disrupt or enhance action potential propagation. In particular, we investigate how carefully timed synaptic input can affect action potential propagation.

We solved the model numerically on the dendron, with no iSite or soma. A single action potential was added at the left boundary and propagates along the dendron. One synaptic input was added in different positions, with different timing and different strengths. Changes in the action potential amplitude and width, measured at the site of synaptic input, are shown in Figures 5.3 and 5.4.

An example is shown in Figure 5.3(a). Here, a single synaptic input was added at $600 \mu\text{m}$

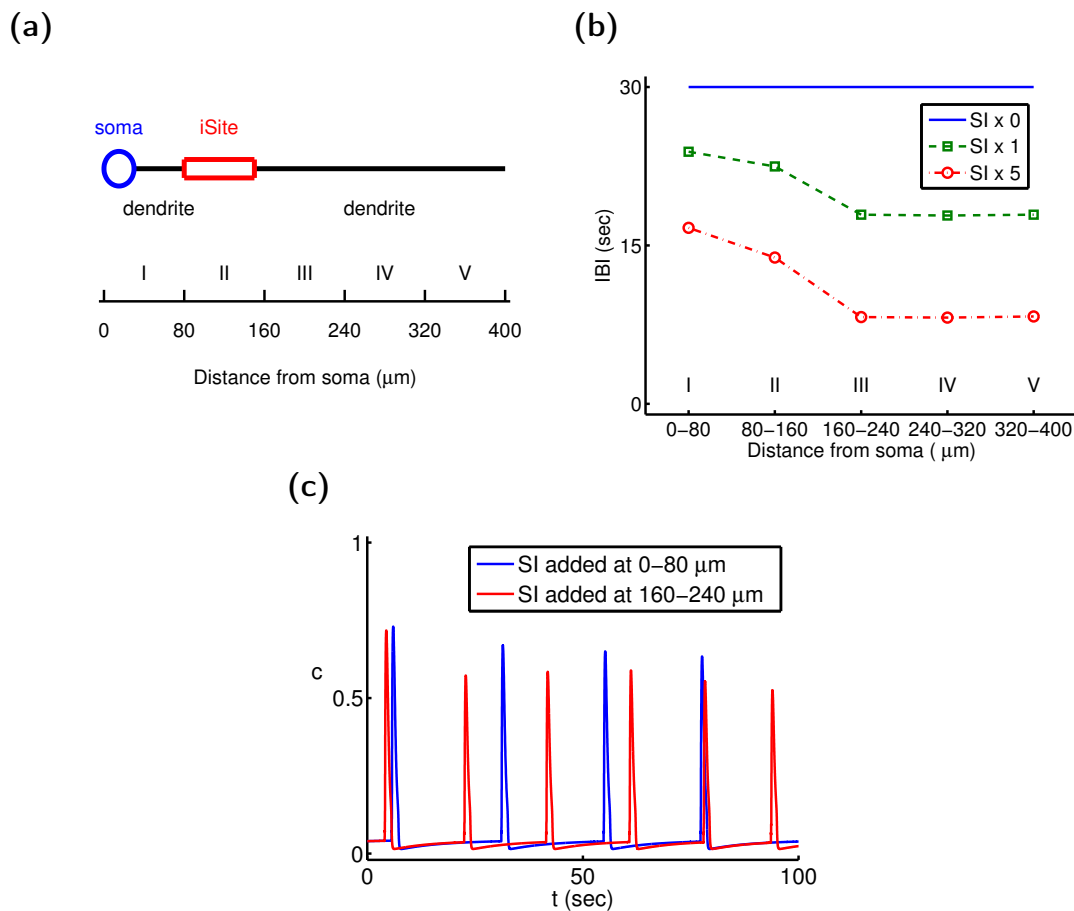


Figure 5.2 Spatial distribution of synaptic input affects IBI. **(a)** Schematic diagram of the dendron of the GnRH neuron. The dendron was divided into 5 regions, each of length 80 μm . **(b)** The IBI for different cases with different strength of synaptic input added at different regions along the dendron. Synaptic input closer to the soma results in a larger IBI, while synaptic input further away from the soma results in a smaller IBI. **(c)** Two examples of the soma Ca^{2+} traces with synaptic input added at different regions. Synaptic input added closer to the soma gives a larger Ca^{2+} transient and hence a larger IBI.

along the dendron with $g_{\text{SI}} = 0.6 \text{ nS}$. The excitatory synaptic input, as expected, causes an increase in the amplitude and width of the propagating action potential. Figure 5.3(b) shows action potentials for which the synaptic input is added slightly earlier or slightly later. The black spike indicates the control case, and the red spike shows the spike with the greatest amplitude change. The amplitude changes are summarized in Figure 5.3(c), where we see that the greatest effect on action potential amplitude occurs when the synaptic input precedes the action potential by approximately 3 ms. Note that, since the density of Na^+ channels is not constant along the dendron, the shape of the action potential will change slightly as it propagates, and thus the effects of the synaptic input upon the action potential will depend on where the synaptic input occurs. For instance, the injected action potential at the left boundary is generated with

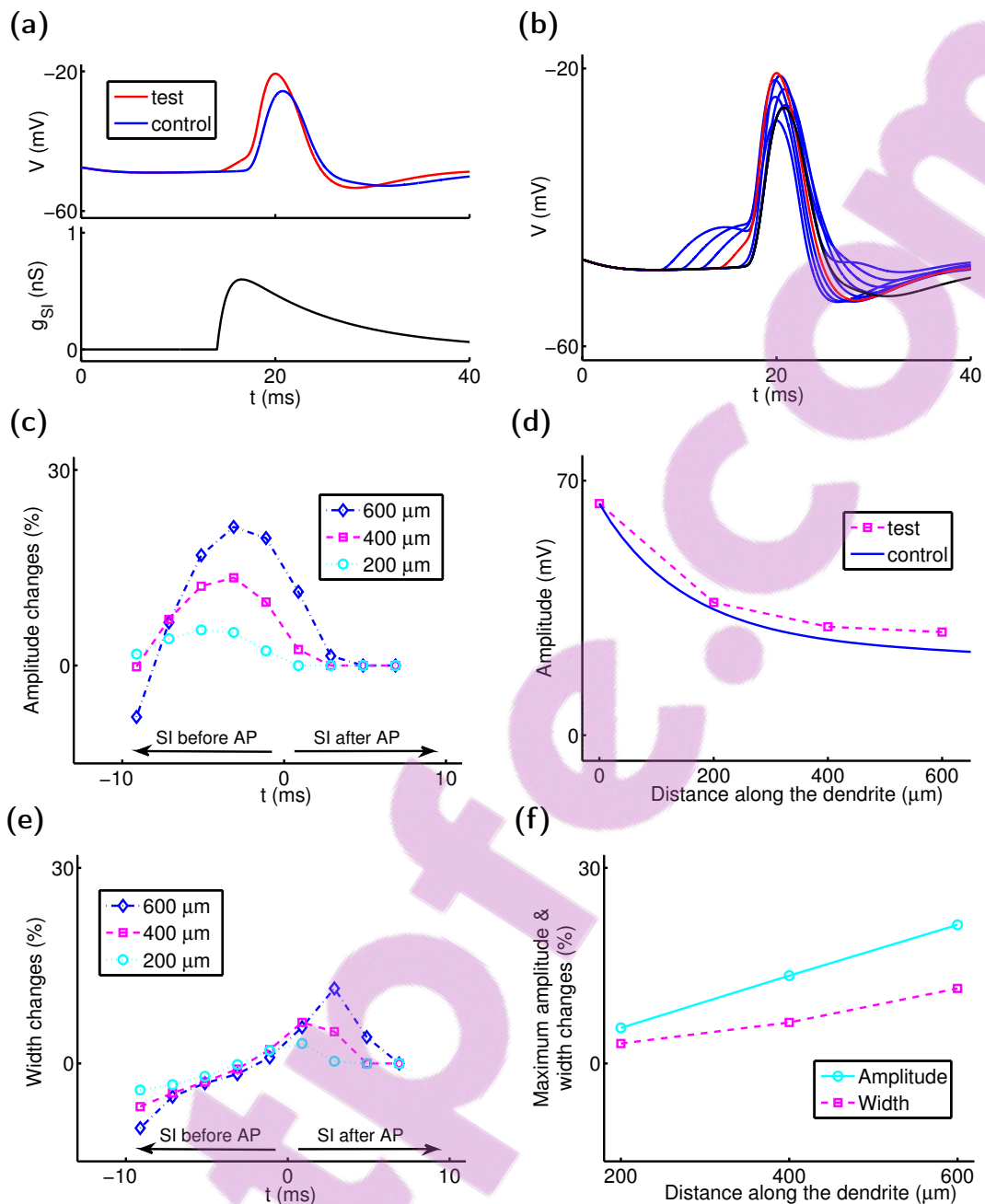


Figure 5.3 Interaction of synaptic input and action potentials. **(a)** One synaptic input added at $600 \mu\text{m}$ along the dendron with $g_{SI} = 0.6 \text{ nS}$. Bottom panel shows one example of the conductance of synaptic input added at about 14 ms. Top panel shows two action potentials with and without the synaptic input. For the added action potential at the left boundary the time to peak is about 17 ms. We define this peak time of the action potential at the left boundary as the origin (zero). Thus, for example, the test case with synaptic input added at 14 ms will be treated as synaptic input added 3 ms before the action potential. **(b)** Superimposed sweeps of examples similar to **(a)** with synaptic input added at different times. The black spike indicates the control case, and the red spike shows the spike with the greatest amplitude change. **(c)** The amplitude changes (%) for the action potentials with synaptic input added at $600 \mu\text{m}$ along the dendron as in **(b)** can be measured as shown in blue dash dot with diamond. The similar tests with synaptic input added at 200 and $400 \mu\text{m}$ along the dendrite were shown in cyan dotted line with cycle and magenta dashed line with square respectively. **(d)** For each case as shown in **(c)**, the maximum amplitude of the spike is shown relative to the control case. **(e)** The width changes (%) for the action potentials with synaptic input added at $600 \mu\text{m}$ along the dendrite as in **(b)** can be measured as shown in blue dash dot with diamond. **(f)** The maximum amplitude and width changes (%) for synaptic input added at three different positions. Note: AP stands for action potential in all the panels.

higher Na^+ conductance (180 nS), and it will experience a transition to reach a steady state amplitude spike when propagating along the dendrite with lower Na^+ conductance (26 nS). From Figure 5.3(d), we see that synaptic input further away from the soma has a greater effect on action potential amplitude, due to the lower density of Na^+ channels.

Similarly, we can determine the effects of synaptic input on action potential width; see Figure 5.3(e). As before, the excitatory synaptic input increases the action potential width, with the greatest effect occurring when the synaptic input and action potential are simultaneous. The effects on both amplitude and width, as functions of distance along the dendron, are summarized in Figure 5.3(f).

The effects of synaptic input strength are summarized in Figure 5.4. As expected, action potential amplitude and width are both increasing functions of synaptic input strength.

In summary, although synaptic input will affect the amplitude and width of action potentials propagating along the dendron, the effects are small. The maximal effects occur only when the action potential is smaller (further from the soma), and are only around a 25% increase at best.

5.4.3 Actions of Kisspeptin on Ca^{2+} Release

Although synaptic input can modulate action potential amplitude and width, these changes are small at most, and highly dependent upon the precise timing of synaptic input. Moreover, if the spike changes occur far away from the synaptic terminal the spike would quickly regain its normal shape during propagation along the dendron. It is possible, of course, that very large hyperpolarizing synaptic inputs could eliminate action potentials completely, but these would have to be unphysiologically large. We conclude that synaptic input along the dendron is not a likely mechanism for the direct control of Ca^{2+} transients at the synaptic terminal, and thus of GnRH secretion.

An alternative hypothesis is that the release of kisspeptin at the GnRH neuron synaptic terminal can act as a precise controller of Ca^{2+} transients there. Our model of this hypothesis includes the three known actions of kisspeptin; increasing the bursting rate, increasing Ca^{2+} influx, and the formation of IP_3 . These actions interact synergistically to modulate Ca^{2+} release (Figure 5.5).

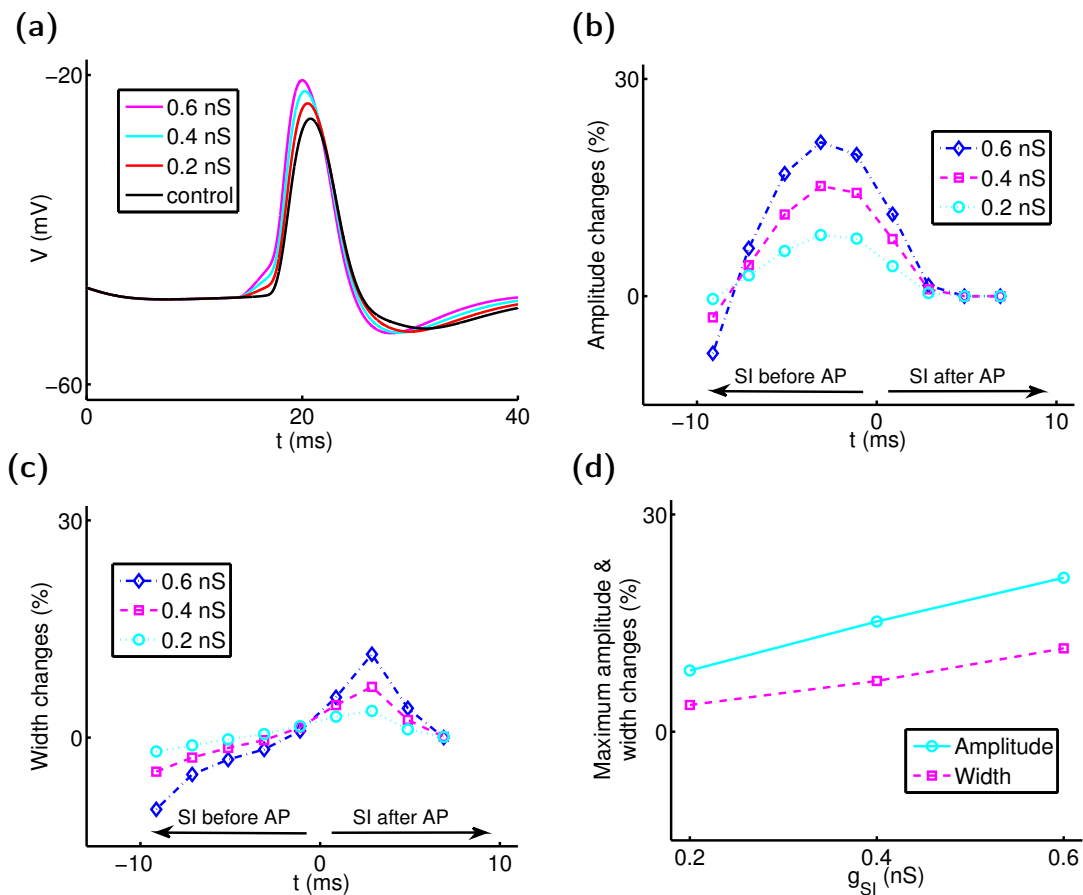


Figure 5.4 One action potential and one synaptic input added at $600 \mu\text{m}$ along the dendron with different timing and different strength. **(a)** Superimposed sweeps of synaptic input with different strength recorded $600 \mu\text{m}$ along the dendron evoked together with controlled action potential at the optimum timing for action potential amplification. **(b)** Action potential amplitude changes (%) versus the time difference between synaptic input and controlled action potential onset for synaptic input with different strength. **(c)** Action potential width changes (%) versus the time difference between synaptic input and controlled action potential onset for synaptic input with different strength. **(d)** The maximum amplitude and width changes (%) for three different strength of synaptic input added at the same location are summarized.

We here consider 6 different combinations of kisspeptin action. In the control case (no kisspeptin), the bursting has an IBI around 30 seconds, with 3 spikes per burst. In our model simulations, kisspeptin changes IP_3 , Ca^{2+} influx, and the frequency of bursting, either separately, or in any combination.

To quantify the response, we measure either the integral of the total Ca^{2+} release, or the maximum amplitude of the Ca^{2+} transient. For the integral of Ca^{2+} , each kisspeptin action occurring alone has a smaller effect, while the combination of all three actions causes the greatest Ca^{2+} release (Figure 5.5(a)). In addition, the effects interact synergistically. For example, when $K_p = 3 \mu\text{M}/\text{ms}$, the total Ca^{2+} response caused by all three mechanisms operating si-

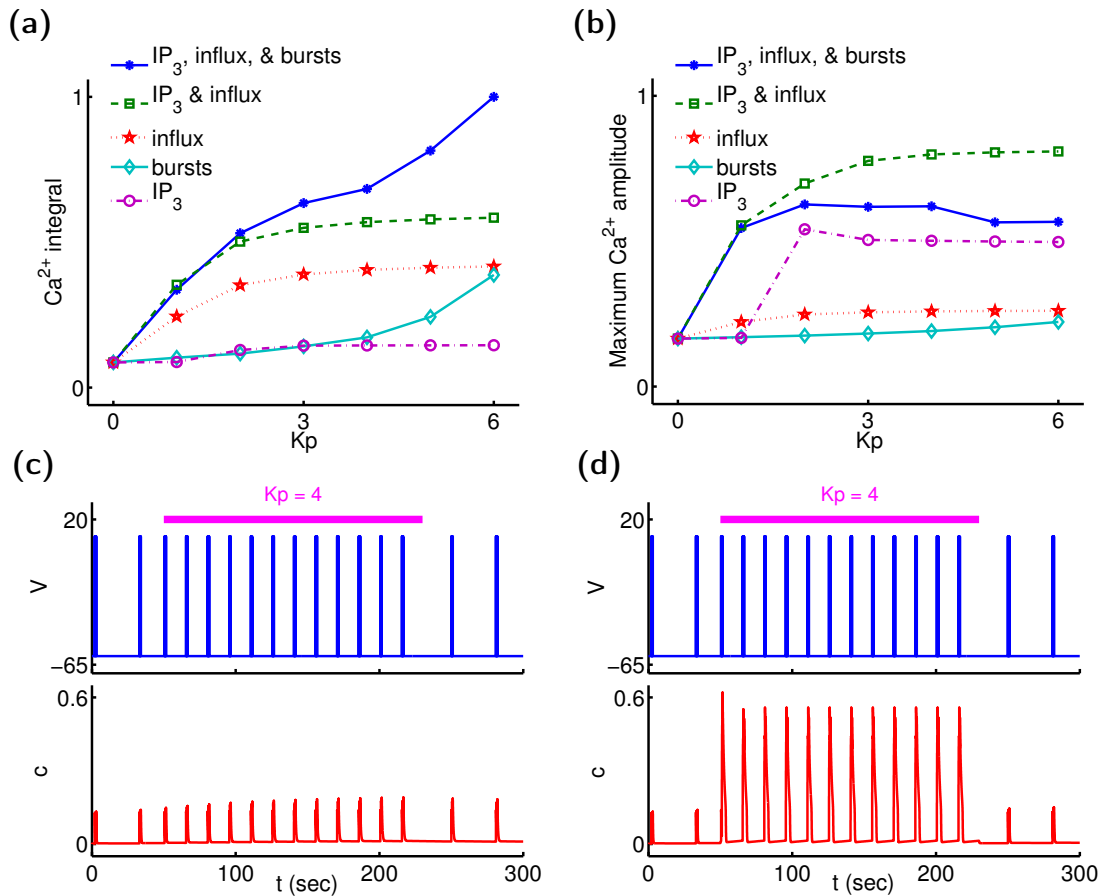


Figure 5.5 Effects of different actions of kisspeptin on Ca^{2+} release. The values for K_p are arbitrary, with 0 representing no effect of kisspeptin, and 7.5 representing the value of K_p that gives continuous spiking. **(a) - (b)** The result in the left bottom corner denotes the control case, that is, the bursting series has an IBI around 30 second, with 3 spikes per burst. Kisspeptin was added at 50 seconds and lasted 180 seconds. The magenta dash dot with circles shows the case where kisspeptin increases the level of IP_3 only. The cyan solid line with diamond denotes the case that kisspeptin increases bursting rate only. The red dotted line with pentagram represents the case that kisspeptin increases the Ca^{2+} influx only. The green dashed line with square indicates the case that kisspeptin increases both the IP_3 and Ca^{2+} influx at the same time. The blue solid line with asterisks shows the case that kisspeptin increases all three actions at the same time. **(a)** Ca^{2+} integrals under different actions of kisspeptin. **(b)** The maximum Ca^{2+} amplitude under different actions of kisspeptin. **(c) - (d)** Two examples showing the voltage and Ca^{2+} traces with $K_p = 4 \mu\text{M}/\text{ms}$. Panel (c) shows a simulation where kisspeptin only increases the rate of bursting, while panel (d) shows a simulation involving all three actions of kisspeptin.

multaneously (the top trace) is greater than the sum of the traces of the three effects operating separately. When considering the total Ca^{2+} response, the greatest single effect is that caused by the increase in Ca^{2+} influx, even at K_p values where the spiking is almost continuous.

Most interestingly, an increase in bursting rate caused by kisspeptin is relatively ineffective at increasing synaptic terminal Ca^{2+} transients, even when the bursting is almost continuous. Thus, in studying the effects of kisspeptin, the model predicts that simple membrane depolarization, and thus initiation of bursting, is possibly considerably less important than more direct

effects on the intracellular Ca^{2+} dynamics.

In contrast, when considering the maximal Ca^{2+} response, it is the change in IP_3 that has the greatest effect (Figure 5.5(b)). This is because production of IP_3 leads to a large initial Ca^{2+} transient, followed by smaller transients. Unlike the effect on the integral of Ca^{2+} , all three actions of kisspeptin at once, does not give the maximum Ca^{2+} amplitude. A shorter burst (smaller IBI) means a shorter time for Ca^{2+} to decrease between the bursts, less Ca^{2+} pumping into the ER, and hence less release through the IP_3 receptor (IPR) for the next Ca^{2+} transient.

Figure 5.5(c) and (d) shows two examples of the voltage and Ca^{2+} traces with $K_p = 4 \mu\text{M}/\text{ms}$ added at 50 seconds and lasting 180 seconds. Panel (c) shows a simulation where kisspeptin only increases the rate of bursting, while panel (d) shows a simulation involving all three actions of kisspeptin. Ca^{2+} -induced Ca^{2+} release through the IPR is clearly evident in the second case, while the enhanced Ca^{2+} influx magnifies the responses.

5.5 Discussion

GnRH neurons have a highly unusual structure, in that only two processes leave the soma. One of these processes extends to the median eminence, over 1000 μm from the cell body, to form the synaptic terminal where GnRH is secreted. Action potentials travel along this process, but it is also the site of synaptic input (Campbell et al., 2005, 2009; Cottrell et al., 2006; Herde et al., 2013). It thus has properties of both a dendrite and an axon, and so has been termed a dendron. Because a single process is both the output and the input stage of the neuron, it is important to understand how synaptic input will interact with and modify the transmission of the action potentials. This question is similar in principle to the study of how back-propagating action potentials modulate synaptic input in dendrites, but with a focus on action potential transmission rather than synaptic modification.

We showed, firstly, that stochastic synaptic input can initiate and modify electrical bursting (which is initiated at the iSite, around 80-150 μm from the soma). Excitatory synapses, unsurprisingly, cause a decrease in the interburst interval (IBI), while inhibitory synapses have the opposite effect. However, most interestingly, we showed that excitatory synaptic input close to

the soma is *less* effective at initiating bursting; the further the synaptic input is from the soma, the lower is the IBI. This is because excitatory synaptic input causes a small depolarization, thus resulting in a small amount of Ca^{2+} influx into the soma. This small Ca^{2+} influx is sufficient to activate the Ca^{2+} -sensitive K^+ channels that regulate the IBI, thus causing an increase in the IBI.

Secondly, we showed that synaptic input will modify the properties of the propagating action potential, but that these modifications are small. If an excitatory synaptic input peaks and the peak of the action potential are almost simultaneous, the action potential width and amplitude is increased by between 5-25% (depending on the strength and position of the synaptic input). If the timing of the synaptic input is shifted by 10 ms before or after the action potential, the effects are much smaller.

Interactions between backpropagating action potentials and synaptic inputs have been studied in other cell types. With appropriate timing and amplitude, synaptic input can amplify backpropagating action potentials in neocortical pyramidal neurons (Stuart and Häusser, 2001), while presynaptic action potential broadening induced by synaptic input (glutamate) can affect Ca^{2+} transients and facilitate synaptic transmission to postsynaptic neurons in hippocampal CA3 pyramidal neurons (Sasaki et al., 2011). Action potential broadening contributes to facilitation of Ca^{2+} changes measured in single neurosecretory terminals in the slices of the rat posterior pituitary, and may also contribute to hormone release (Jackson et al., 1991). Our results are broadly similar to these, although specialized to the particular case of the GnRH dendron.

The question then remains; what purpose is served by synaptic inputs along the dendron, as much as 1000 μm from the iSite? Presumably, such inputs are less effective at initiating bursting than are inputs closer to the iSite. However, our model suggests that they play only a minor role in determining the properties of action potential propagation along the dendron. Although it is possible that concerted major hyperpolarizations of the dendron by synaptic input could prevent action potential propagation entirely, such synaptic input would have to be large and sustained, effectively maintaining a hyperpolarized state for a considerable period of time.

The question of what controls the periodic secretion of GnRH with a period of around an

hour, remains one of the most important questions in the study of GnRH neurons. Although it is possible that synaptic input along the dendron plays a role in the generation of such long periodicity, our results suggest that synaptic input along the dendron is unlikely to be a major controlling factor. In other words, our results suggest that long-period synaptic input cannot act as a gating mechanism, either preventing or allowing the propagation of action potentials to the synaptic terminal. Thus, the function of the many synaptic inputs, situated along the dendron a long way from the iSite, remains unclear. It is possible that, despite their distance from the iSite, they continue to play some role in initiation of bursting. It is also possible that they can modify transmission of action potentials in important ways that are not captured by our model. Resolution of this question awaits a more detailed experimental investigation of these synapses and their function.

We thus investigated other possible ways in which synaptic input could modify Ca^{2+} release at the synaptic terminal, focusing in particular on the possible role of kisspeptin. Although GnRH neurons can receive different extrinsic inputs, kisspeptin mediates a particularly potent one (Han et al., 2005). Kisspeptin can act directly on GnRH neurons (Han et al., 2005; Messenger et al., 2005; Liu et al., 2008; Pielecka-Fortuna et al., 2008; Zhang et al., 2008; Zhang and Spergel, 2012), and can even act directly at the median eminence to regulate GnRH release (Keen et al., 2008) in the absence of GnRH neuronal cell bodies (d'Anglemont de Tassigny et al., 2008).

There are at least three known actions of kisspeptin on GnRH neurons (Castellano et al., 2006; Liu et al., 2008; Pielecka-Fortuna et al., 2008; Zhang et al., 2008; Constantin et al., 2009; Kroll et al., 2011; Zhang and Spergel, 2012; Zhang et al., 2013a,b), although these actions are not known to occur at the synaptic terminal specifically. Firstly, kisspeptin inhibits K^+ channels, and/or activates nonspecific cation channels, leading to cell depolarization and, presumably, the initiation of spiking (Liu et al., 2008; Pielecka-Fortuna et al., 2008; Zhang et al., 2008, 2013b). Secondly, kisspeptin activates TRPC channels which allow Ca^{2+} to flow into the cell, thus raising the cytoplasmic Ca^{2+} concentration (Zhang et al., 2008; Constantin et al., 2009; Kroll et al., 2011; Zhang and Spergel, 2012; Zhang et al., 2013a). Thirdly, kisspeptin stimulates the formation of inositol trisphosphate, via activation of PLC, which leads to the release of Ca^{2+}

from internal stores (Castellano et al., 2006; Liu et al., 2008). Similar actions of kisspeptin on Ca^{2+} dynamics are also seen in a variety of other cell types (Kotani et al., 2001; Stafford et al., 2002; Brailoiu et al., 2005).

We showed that the effects of kisspeptin on Ca^{2+} release (which we assumed to be at the synaptic terminal) are most potent when all three of these actions occur simultaneously. An increase in firing rate alone has limited effect on Ca^{2+} release, but there is considerable synergy between the three actions. An increased Ca^{2+} influx primes the IP_3 receptor (IPR), leading to a larger release of Ca^{2+} from internal stores when IP_3 is produced. Additionally, the Ca^{2+} -induced Ca^{2+} release, initiated by an action potential, is greatly enhanced in the presence of a greater Ca^{2+} influx and a higher basal concentration of IP_3 .

These actions of kisspeptin are consistent with the experimental evidence. The model predicts that kisspeptin alone (in the absence of membrane depolarization) can stimulate significant Ca^{2+} release, which is consistent with the observations that kisspeptin can stimulate GnRH secretion even in the absence of GnRH cell bodies, and in the presence of TTX. However, depolarization of the membrane by kisspeptin will lead to an enhanced rate of firing, and thus increased GnRH release. Keen et al. (2008) study the periodic changes in kisspeptin and GnRH release in the monkey median eminence. They showed an increase in pulsatile release of kisspeptin along with a pubertal increase in GnRH release.

We thus conclude that kisspeptin is a possible candidate for the control of long-period GnRH secretion. Long-period variations in kisspeptin concentration at the median eminence would lead to long-period variations in the rate of GnRH release, superimposed on a low basal level of GnRH release caused by the spontaneous firing of GnRH neurons. Of course, this leaves unresolved how such long-period variations in kisspeptin concentration could come about. In effect, the question of what causes long period oscillations of GnRH secretion is not solved, merely shifted to a different neuronal population

Nevertheless, our model serves to refine the investigation of this question by showing, firstly, that synaptic input along the dendron is unlikely to be a controlling factor, while the action of kisspeptin at the synaptic terminal is a far more powerful and plausible controller.

Acknowledgements

We thank Dr Karl J. Iremonger and Prof. Allan E. Herbison for their helpful comments. This work was supported by the New Zealand Health Research Council, and by a University of Auckland Doctoral Scholarship to Xingjiang Chen. The author(s) wish to acknowledge the contribution of the NeSI high-performance computing facilities and the staff at the Centre for eResearch at the University of Auckland. New Zealand's national facilities are provided by the New Zealand eScience Infrastructure (NeSI and funded jointly by NeSI's collaborator institutions and through the Ministry of Business, Innovation and Employment's Infrastructure programme. URL <http://www.nesi.org.nz>

Conclusions and Future Work

GnRH neurons represent the final output cells of the hypothalamic neuronal system regulating fertility in mammals (Herbison, 2006). GnRH released in rhythmic patterns by GnRH neurons is the central regulator of the reproductive system, acting through the HPG axis (Gore, 2002). Although the mechanisms underlying the pulsatile release of GnRH are not well understood, it has been suggested that the bursting behavior of electrical activity and Ca^{2+} dynamics play an important roles in GnRH secretion (Moenter et al., 2003; Herbison, 2006). Many studies, including both experimental work and mathematical modeling (see Chapter 3 for review), have been developed to explain different aspects of these activities. However, the earlier models could not fully represent the latest experimental data (Iremonger and Herbison, 2012; Herde et al., 2013) as mentioned in Chapter 2. Consideration of these recent data raised a number of important questions that could not be addressed by previous models.

In this thesis (Chapter 4 and 5), we used mathematical modeling, along with some important experimental data, to study and answer the questions stated in the Introduction. Our most important conclusions are summarized as follows:

- Firstly, we constructed a spatiotemporal mathematical model that includes both the soma and the dendrite. The most important new parameter, the electrical diffusion coefficient, was introduced and determined by fitting experimental data to the model. The model shows that the large diffusion coefficient provides a mechanism for regulating bursting behavior by the interactions of the soma and the iSite. In our model, electrical bursting initiated at the iSite spreads quickly to the soma to cause spiking there, and subsequent Ca^{2+} entry, which causes the large Ca^{2+} release via IP_3 receptor (IPR). This large somatic

Ca^{2+} transient activates K^+ channels in the soma, causing a reverse spread of hyperpolarization to the iSite, termination of the burst, and control of the interburst interval. Our modeling study supports this somatic burst controlling mechanism proposed in the previous model (Lee et al., 2010), and also agrees with the latest experimental data (Iremonger and Herbison, 2012; Herde et al., 2013). Our modeling study made one prediction that GnRH neurons with an iSite located further away from the cell body would have longer bursts and shorter interburst intervals than GnRH neurons with their iSite closer to the soma. This prediction remains to be verified experimentally.

- Secondly, we extended our spatiotemporal model by adding stochastic synaptic input, in order to study the function of synaptic input along the dendrite. We showed that synaptic input could modify the properties of the propagating action potential, but these modifications are small. We concluded that synaptic input along the dendrite is not a likely mechanism for the control of action potential propagation in the dendrite, or for the control of GnRH secretion.
- Thirdly, we thus investigated other possible ways in which synaptic input could modify Ca^{2+} release at the synaptic terminal, focusing in particular on the possible role of kisspeptin. Although GnRH neurons can receive different extrinsic inputs, kisspeptin mediates a particularly potent one (Han et al., 2005). We constructed a model of synaptic Ca^{2+} dynamics to study how the three actions of kisspeptin could interact, and what are their relative effects on the release of Ca^{2+} at the synaptic terminal. These actions – increasing the bursting rate, increasing Ca^{2+} influx, and the formation of IP_3 – are known to occur at the cell body of GnRH neurons. In our model we assume that these known actions of kisspeptin also occur at the synaptic terminal, which needs to be verified experimentally. Our modeling study showed that the effects of kisspeptin on Ca^{2+} release are limited when only one action occurs, and are most potent when all three of these actions occur simultaneously. For example, Ca^{2+} -induced Ca^{2+} release, initiated by an action potential, is greatly enhanced in the presence of a greater Ca^{2+} influx and a higher basal concentration of IP_3 . We conclude that the inherent synergies in the various actions of kisspeptin make it a likely candidate for the precise control of Ca^{2+} transients at the

synaptic terminal, and hence for the control of long-period GnRH secretion.

Our model did not include some aspects of previous models, such as a detailed model of afterdepolarization potentials (ADP) and hyperpolarization-activated current (I_h), as we believe them to be less relevant for the questions studied in this thesis. However, both currents have been identified experimentally. It has been reported that I_h can affect bursting behavior (Chu et al., 2010) and the ADP current can contribute to repetitive firing (Chu and Moenter, 2006). It will be important to consider both currents in future model development in order to obtain a more comprehensive model of electrical bursting in GnRH neurons.

GnRH neurons can intrinsically generate burst firing activity, but may require external or network interactions for hormone release (Moenter, 2010). Vasoactive intestinal polypeptide (VIP) current is an important current induced by neuromodulators (i.e., extrinsic inputs) (Gerhold et al., 2005; Gerhold and Wise, 2006; Christian and Moenter, 2008). VIP could activate I_h to modulate action potential burst firing, acting through cAMP (Gerhold et al., 2005; Chu et al., 2010). I_h could also affect the afterhyperpolarization potential (AHP) which is important for the control of bursting, and may interact with the ADP current to modulate action potential firing (Chu et al., 2010).

Another important neuromodulator, kisspeptin, is the most potent in exciting GnRH neurons (Han et al., 2005; Piet et al., 2014). For example, kisspeptin excites GnRH neurons to open canonical transient receptor potential cation (TRPC) channels and closes Kir channels (Liu et al., 2008; Zhang et al., 2008), and also inhibits an apamin-insensitive slow afterhyperpolarization current, to regulate burst firing (Zhang et al., 2013b).

Although it is known that burst firing, kisspeptin and Ca^{2+} are essential for GnRH secretion, the mechanisms involved are not very clear. Recently, some groups have studied the electrophysiological and Ca^{2+} dynamics of GnRH and kisspeptin neurons, not only in the cell body, but also along the long dendron towards the median eminence. For example, there are two different Ca^{2+} transients evoked by kisspeptin reported from two groups. Kroll et al. (2011) used isolated individual rat GnRH neurons without synaptic coupling and reported an elevated Ca^{2+} transient, while Liu et al. (2008) used an acute brain slice preparation of mouse GnRH neurons and reported a Ca^{2+} transient with a quick increase followed by a sudden decline. Interestingly,

our model presented in Chapter 5 can reproduce these two Ca^{2+} transients. For example, increasing the Ca^{2+} influx gives the elevated Ca^{2+} transient, while the formation of IP_3 gives the quick increase followed by the sudden decline.

The recording of Ca^{2+} transients far away from the soma (or close to the median eminence) is much more difficult than measurements at the soma, due to the thinness of the dendron. Our modeling study provides some predictions, particularly to do with the interaction of the various actions of kisspeptin on the Ca^{2+} dynamics, but our model assumptions remain in need of experimental verification, and our predictions need to be tested.

Although many studies, including both experimental and modeling studies, have been developed to study the GnRH secretion, the mechanisms underlying the pulsatile release of GnRH are not well understood (Brown et al., 1994; Terasawa et al., 1999a,b; Duittoz et al., 2000; Funabashi et al., 2000; Nunemaker et al., 2001; Khadra and Li, 2006; Clément and Françoise, 2007; Vidal and Clément, 2010; Constantin, 2011; Gay et al., 2012; Krupa et al., 2013). In order to investigate what roles burst firing and Ca^{2+} play in the mechanism that underlies the pulsatile release of GnRH, our model could be further extended by consideration of GnRH secretion. We can determine the spike firing rates under different conditions (i.e., from continuous spiking to bursts of electrical firing with different interburst intervals) and compare with the frequency of GnRH secretion. With bundled dendrites (Campbell et al., 2009), it is possible that network interactions play a role in the synchronization, and generation of rhythmic patterns (Moenter et al., 2003). A GnRH network model could be built to evaluate how network interactions might affect or control secretion. We could examine whether the synchronization of Ca^{2+} oscillations at the network level could provide a mechanism to match the rhythmic pattern of GnRH release. For example, network synchronizations could produce Ca^{2+} transients with interpeak intervals similar to pulses of GnRH release. By determining the intrinsic activities of GnRH neurons (i.e., burst firing and Ca^{2+} transients) and the network interactions (i.e., GnRH neuron to GnRH neuron and extrinsic inputs to GnRH neuron), we can study the possible mechanisms of underlying rhythmic GnRH secretion that governs the reproductive system.

Bibliography

- Abe, H., & Terasawa, E. (2005). Firing pattern and rapid modulation of activity by estrogen in primate luteinizing hormone releasing hormone-1 neurons. *Endocrinology*, *146*, 4312-4320.
- Alle, H., & Geiger, J. R. P. (2006). Combined Analog and Action Potential Coding in Hippocampal Mossy Fibers. *Science*, *311*, 1290-1293.
- Andersen, P., Soleng, A. F., & Raastad, M. (2000). The hippocampal lamella hypothesis revisited. *Brain Research*, *886*, 165-171.
- Antic, S. D. (2003). Action potentials in basal and oblique dendrites of rat neocortical pyramidal neurons. *The Journal of Physiology*, *550*(1), 35-50.
- Berridge, J. M. (1993). Inositol trisphosphate and calcium signalling. *Nature*, *361*, 315-325.
- Berridge, J. M., Bootman, M. D., & Lipp, P. (1998). Calcium—a life and death signal. *Nature*, *395*, 645-648.
- Brailoiu, G. C., Dun, S. L., Ohsawa, M., Yin, D., Yang, J., Chang, J. K., Brailoiu, E., & Dun, N. J. (2005). KiSS-1 Expression and Metastin-Like Immunoreactivity in the Rat Brain. *The Journal of Comparative Neurology*, *481*, 314-329.
- Brown, D., Herbison, A. E., Robinson, J. E., Marrs, R. W., & Leng, G. (1994). Modelling the luteinizing hormone-releasing hormone pulse generator. *Neuroscience*, *63*(3), 869-879.
- Campbell, R. E., Gaidamaka, G., Han, S. K., & Herbison, A. E. (2009). Dendro-dendritic bundling and shared synapses between gonadotropin-releasing hormone neurons. *Proceedings of the National Academy of Sciences of the United States of America*, *106*, 10835-10840.

- Campbell, R. E., Han, S. K., & Herbison, A. E. (2005). Biocytin filling of adult gonadotropin releasing hormone neurons in situ reveals extensive, spiny, dendritic processes. *Endocrinology*, *146*, 1163-1169.
- Campbell, R. E., & Suter, K. J. (2010). Redefining the Gonadotrophin-Releasing Hormone Neurone Dendrite. *Journal of Neuroendocrinology*, *22*, 650-658.
- Cao, P., Donovan, G., Falcke, M., & Sneyd, J. (2013). A stochastic model of calcium puffs based on single-channel data. *Biophysical Journal*, *105*, 1133-1142.
- Casale, A. E., & McCormick, D. A. (2011). Active Action Potential Propagation But Not Initiation in Thalamic Interneuron Dendrites. *The Journal of Neuroscience*, *31*(50), 18289-18302.
- Castellano, J. M., Navarro, V. M., Fernández-Fernández, R., Castaño, J. P., Malagón, M. M., Aguilar, E., Dieguez, C., Magni, P., Pinilla, L., & Tena-Sempere, M. (2006). Ontogeny and mechanisms of action for the stimulatory effect of kisspeptin on gonadotropin-releasing hormone system of the rat. *Molecular and Cellular Endocrinology*, *257-258*, 75-83.
- Chen, X., Iremonger, K., Herbison, A., Kirk, V., & Sneyd, J. (2013). Regulation of Electrical Bursting in a Spatiotemporal Model of a GnRH Neuron. *Bulletin of Mathematical Biology*, *75*, 1941-1960.
- Chen, X., & Sneyd, J. (2014). A Computational Model of the Dendron of the GnRH Neuron. *Bulletin of Mathematical Biology*, Submitted for publication.
- Christian, C. A., & Moenter, S. M. (2008). Vasoactive Intestinal Polypeptide Can Excite Gonadotropin-Releasing Hormone Neurons in a Manner Dependent on Estradiol and Gated by Time of Day. *Endocrinology*, *149*(6), 3130-3136.
- Chu, Z., & Moenter, S. M. (2006). Physiologic Regulation of a Tetrodotoxin-Sensitive Sodium Influx That Mediates a Slow Afterdepolarization Potential in Gonadotropin-Releasing Hormone Neurons: Possible Implications for the Central Regulation of Fertility. *The Journal of Neuroscience*, *26*(46), 11961-11973.
- Chu, Z., Takagi, H., & Moenter, S. M. (2010). Hyperpolarization-Activated Currents in Gonadotropin-Releasing Hormone (GnRH) Neurons Contribute to Intrinsic Excitability and Are Regulated by Gonadal Steroid Feedback. *The Journal of Neuroscience*, *30*(40), 13373-13383.

- Clasadonte, J., Poulain, P., Beauvillain, J., & Prevot, V. (2008). Activation of Neuronal Nitric Oxide Release Inhibits Spontaneous Firing in Adult Gonadotropin-Releasing Hormone Neurons: A Possible Local Synchronizing Signal. *Endocrinology*, *149*(2), 587-596.
- Clayton, R.N., & Catt, K.J. (1981). Gonadotropin releasing hormone receptors: Characterization, physiological regulation and relationship to reproductive function. *Endocrine Reviews*, *2*, 186-209.
- Clément, F., & Françoise, J. P. (2007). Mathematical Modeling of the GnRH Pulse and Surge Generator. *SIAM Journal on Applied Dynamical Systems*, *6*(2), 441-456.
- Constantin, S. (2011). Physiology of the Gonadotrophin-Releasing Hormone (GnRH) Neurone: Studies from Embryonic GnRH Neurons. *Journal of Neuroendocrinology*, *23*, 542-553.
- Constantin, J., & Charles, A. (1999). Spontaneous Action Potentials Initiate Rhythmic Intercellular Calcium Waves in Immortalized Hypothalamic (GT1-1) Neurons. *Journal of Neurophysiology*, *82*, 429-435.
- Constantin, S., Caligioni, C. S., Stojilkovic, S., & Wray, S. (2009). Kisspeptin-10 Facilitates a Plasma Membrane-Driven Calcium Oscillator in Gonadotropin-Releasing Hormone-1 Neurons. *Endocrinology*, *150*(3), 1400-1412.
- Constantin, S., & Wray, S. (2008). Gonadotropin-releasing hormone-1 neuronal activity is independent of hyperpolarization-activated cyclic nucleotide- modulated channels but is sensitive to protein kinase a-dependent phosphorylation. *Endocrinology*, *149*, 3500-3511.
- Cottrell, E. C., Campbell, R. E., Han, S., & Herbison, A. E. (2006). Postnatal Remodeling of Dendritic Structure and Spine Density in Gonadotropin-Releasing Hormone Neurons. *Endocrinology*, *147*(8), 3652-3661.
- Cserscik, D., Farkas, I., Hrabovszky, E., & Liposits, Z. (2012). A simple integrative electrophysiological model of bursting GnRH neurons. *Journal of Computational Neuroscience*, *32*, 119-136.
- d'Anglemont de Tassigny, X., Fagg, L. A., Carlton, M. B. L., & Colledge, W. H. (2008). Kisspeptin Can Stimulate Gonadotropin-Releasing Hormone (GnRH) Release by a Direct Action at GnRH Nerve Terminals. *Endocrinology*, *149*(8), 3926-3932.

- d'Anglemont de Tassigny, X., Fagg, L. A., Dixon, J. P. C., Day, K., Leitch, H. G., Hendrick, A. G., Zahn, D., Franceschini, I., Caraty, A., Carlton, M. B. L., Aparicio, S. A. J. R., & Colledge, W. H. (2007). Hypogonadotropic hypogonadism in mice lacking a functional *Kiss1* gene. *Proceedings of the National Academy of Sciences of the United States of America*, *104*(25), 10714-10719.
- Debanne, D., Campanac, E., Bialowas, A., Carlier, E., & Alcaraz, G. (2011). Axon Physiology. *Physiological Reviews*, *91*, 555-602.
- DeFazio, R. A., & Moenter, S. M. (2002). Estradiol feedback alters potassium currents and firing properties of gonadotropin-releasing hormone neurons. *Molecular Endocrinology*, *16*, 2255-2265.
- de Roux, N., Genin, E., Carel, J., matsuda, F., Chaussain, J., & Milgrom, E. (2003). Hypogonadotropic hypogonadism due to loss of function of the Kiss1-derived peptide receptor GPR54. *Proceedings of the National Academy of Sciences of the United States of America*, *100*(19), 10972-10976.
- Djurisic, M., Antic, S., Chen, W. R., & Zecevic, D. (2004). Voltage Imaging from Dendrites of Mitral Cells: EPSP Attenuation and Spike Trigger Zones. *The Journal of Neuroscience*, *24*(30), 6703-6714.
- Duan, W., Lee, K., Herbison, A. E., & Sneyd, J. (2011). A mathematical model of adult GnRH neurons in mouse brain and its bifurcation analysis. *Journal of Theoretical Biology*, *276*, 22-34.
- Duittoz, A. H., & Batailler, M. (2000). Pulsatile GnRH secretion from primary cultures of sheep olfactory placode explants. *Journal of Reproduction and Fertility*, *120*, 391-396.
- Ferris, C. D., Haganir, R. L., Supattapone, S., & Snyder, S. H. (1989). Purified inositol 1,4,5-trisphosphate receptor mediates calcium flux in reconstituted lipid vesicles. *Nature*, *342*, 87-89.
- Fletcher, P., & Li, Y. (2009). An integrated model of electrical spiking, bursting, and calcium oscillations in GnRH neurons. *Biophysical Journal*, *96*, 4514-4524.

- Foust, A., Popovic, M., Zecevic, D., & McCormick, D. A. (2010). Action Potentials Initiate in the Axon Initial Segment and Propagate through Axon Collaterals reliably in Cerebellar Purkinje Neurons. *The Journal of Neuroscience*, 30(20), 6891-6902.
- Funabashi, T., Daikoku, S., Shinohara, K., & Kimura, F. (2000). Pulsatile Gonadotropin-Releasing Hormone (GnRH) Secretion Is an Inherent Function of GnRH Neurons, as Revealed by the Culture of Medial Olfactory Placode Obtained from Embryonic Rats. *Neuroendocrinology*, 71, 138-144.
- Gay, V. L., Hemond, P. J., Schmidt, D., O'Boyle, M. P., Hemond, Z., Best, J., O'Farrell, L., & Suter, K. J. (2012). Hormone secretion in transgenic rats and electrophysiological activity in their gonadotropin releasing-hormone neurons. *American Journal of Physiology - Endocrinology and Metabolism*, 303, E243-E252.
- Gerhold, L. M., Rosewell, K. L., & Wise, P. M. (2005). Suppression of Vasoactive Intestinal Polypeptide in the Suprachiasmatic Nucleus Leads to Aging-Like Alterations in cAMP Rhythms and Activation of Gonadotropin-Releasing Hormone Neurons. *The Journal of Neuroscience*, 25(1), 62-67.
- Gerhold, L. M., & Wise, P. M. (2006). Vasoactive Intestinal Polypeptide Regulates Dynamic Changes in Astrocyte Morphometry: Impact on Gonadotropin-Releasing Hormone Neurons. *Endocrinology*, 147(5), 2197-2202.
- Gin, E., Falcke, M., Wagner II, L. E., Yule, D. I., & Sneyd, J. (2009). A kinetic model of the inositol trisphosphate receptor based on single-channel data. *Biophysical Journal*, 96, 4053-4062.
- Gore, A. (2002). *GnRH: The Master Molecule of Reproduction*. Kluwer Academic Publishers.
- Gottsch, M. L., Clifton, D. K., & Steiner, R. A. (2006). Kisspeptin-GPR54 signaling in the neuroendocrine reproductive axis. *Molecular and Cellular Endocrinology*, 254-255, 91-96.
- Gottsch, M. L., Cunningham, M. J., Smith, J. T., Popa, S. M., Acohidio, B. V., Crowley, W. F., Seminara, S., Clifton, D. K., & Steiner, R. A. (2004). A Role for Kisspeptins in the Regulation of Gonadotropin Secretion in the Mouse. *Endocrinology*(9), 4073-4077.

- Han, S. K., Chong, W., Li, L. H., Lee, I. S., Murase, K., & Ryu, P. D. (2002). Noradrenaline Excites and Inhibits GABAergic Transmission in Parvocellular Neurons of Rat Hypothalamic Paraventricular Nucleus. *Journal of Neurophysiology*, *87*, 2287-2296.
- Han, S. K., Gottsch, M. L., Lee, K. J., Popa, S. M., Smith, J. T., Jakawich, S. K., Clifton, D. K., Steiner, R. A., & Herbison, A. E. (2005). Activation of Gonadotropin-Releasing Hormone Neurons by Kisspeptin as a Neuroendocrine Switch for the Onset of Puberty. *The Journal of Neuroscience*, *25*(49), 11349-11356.
- Herbison, A. E. (2006). Physiology of the GnRH neuronal network. In: J.D. Neill (Ed.), *Knobil and Neill's Physiology of Reproduction*, third ed. (pp. 1415-1482). San Diego: Academic Press.
- Herbison, A. E., & Moenter, S. M. (2011). Depolarising and Hyperpolarising Actions of GABA_A Receptor Activation on Gonadotrophin-Releasing Hormone Neurones: Towards and Emerging Consensus. *Journal of Neuroendocrinology*, *23*, 557-569.
- Herbison, A. E., Pape, J. R., Skynner, S. X., & Sim, J. A. (2001). Molecular and cellular properties of GnRH neurons revealed through transgenics in the mouse. *Molecular and Cellular Endocrinology*, *185*, 185-194.
- Herde, M. K., Iremonger, K. J., Constantin, S., & Herbison, A. E. (2013). GnRH Neurons Elaborate a Long-Range Projection with Shared Axonal and Dendritic Functions. *The Journal of Neuroscience*, *33*(31), 12689-12697.
- Hiller-Sturmhofel, S., & Bartke, A. (1998). The endocrine system: An overview. *Alcohol Health & Research World*, *22*, 153-164.
- Hillier, S. G. (2001). Gonadotropic control of ovarian follicular growth and development. *Molecular and Cellular Endocrinology*, *179*(1-2), 39-46.
- Hodgkin, A. L., & Huxley, A. F. (1952). A quantitative description of membrane current and its application to conduction and excitation in nerve. *The Journal of Physiology*, *117*, 500-544.
- Iremonger, K. J., Constantin, S., Liu, X., & Herbison, A. E. (2010). Glutamate regulation of GnRH neuron excitability. *Brain Research*, *1364*, 35-43.

- Iremonger, K. J., & Herbison, A. E. (2012). Initiation and propagation of action potentials in GnRH neuron dendrites. *The Journal of Neuroscience*, 32(1), 151-158.
- Irwig, M. S., Fraley, G. S., Smith, J. T., Acohido, B. V., Popa, S. M., Cunningham, M. J., Gottsch, M. L., Clifton, D. K., & Steiner, R. A. (2004). Kisspeptin Activation of Gonadotropin Releasing Hormone Neurons and Regulation of KiSS-1 mRNA in the Male Rat. *Neuronendocrinology*, 80, 264-272.
- Jackson, M. B., Konnerth, A., & Augustine, G. J. (1991). Action potential broadening and frequency-dependent facilitation of calcium signals in pituitary nerve terminals. *Proceedings of the National Academy of Sciences of the United States of America*, 88, 380-384.
- Jasoni, C. L., Todman, M. G., Strumia, M. M., & Herbison, A. E. (2007). Cell type-specific expression of a genetically encoded calcium indicator reveals intrinsic calcium oscillations in adult gonadotropin-releasing hormone neurons. *The Journal of Neuroscience*, 27, 860-867.
- Kaiser, U. B., Jakubowiak, A., Steinberger, A., & Chin, W. W. (1997). Differential effects of gonadotropin-releasing hormone (GnRH) pulse frequency on gonadotropin subunit and GnRH receptor messenger ribonucleic acid levels in vitro. *Endocrinology* 138, 1224-1231.
- Kato, M., Ui-Tei, K., Watanabe, M., & Sakuma, Y. (2003). Characterization of voltage-gated calcium currents in gonadotropin-releasing hormone neurons tagged with green fluorescent protein in rats. *Endocrinology*, 144, 5118-5125.
- Keen, K. L., Wenger, F. H., Bloom, S. R., Ghatei, M. A., & Terasawa, E. (2008). An Increase in Kisspeptin-54 Release Occurs with the Pubertal Increase in Luteinizing Hormone-Releasing Hormone-1 Release in the Stalk-Median Eminence of Female Rhesus Monkeys *in Vivo*. *Endocrinology*, 149(8), 4151- 4157.
- Keener, J., & Sneyd, J. (2008). *Mathematical physiology*, Ed 2. New York: Springer.
- Khadra, A., & Li, Y. X. (2006). A Model for the Pulsatile Secretion of Gonadotropin-Releasing Hormone from Synchronized Hypothalamic Neurons. *Biophysical Journal*, 91, 74-83.
- Kirilov, M., Clarkson, J., Liu, X., Roa, J., Campos, P., Porteous, R., Schütz, G., & Herbison, A. E. (2013). Dependence of fertility on kisspeptin-Gpr54 signaling at the GnRH neuron. *Nature Communications*, 4(2492), doi:10.1038/ncomms3492.

- Kole, M. H. P., Ilshner, S. U., Kampa, B. M., Williams, S. R., Ruben, P. C., & Stuart, G. J. (2008). Action potential generation requires a high sodium channel density in the axon initial segment. *Nature Neuroscience*, *11*, 178-186.
- Kole, M. H. P., Letzkus, J. J., & Stuart, G. (2007). Axon Initial Segment Kv1 Channels Control Axonal Action Potential Waveform and Synaptic Efficacy. *Neuron*, *55*, 633-647.
- Kotani, M., Detheux, M., Vandenbogaerde, A., Communi, D., Vanderwinden, J., Le Poul, E., Brézillon, S., Tyldesley, R., Suarez-Huerta, N., Vandepun, F., Blanpain, C., Schiffmann, S. N., Vassart, G., & Parmentier, M. (2001). The Metastasis Suppressor Gene KiSS-1 Encodes Kisspeptins, the Natural Ligands of the Orphan G Protein-coupled Receptor GPR54. *The Journal of Biological Chemistry*, *276*(37), 34631-34636.
- Kress, G. J., Dowling, M., Meeks, J. P., & Mennerick, S. (2008). High Threshold, Proximal Initiation, and Slow Conduction Velocity of Action Potentials in Dentate Granule Neuron Mossy Fibers. *Journal of Neurophysiology*, *100*, 281-291.
- Kroll, H., Bolsover, S., Hsu, J., Kim, S., & Bouloux, P. (2011). Kisspeptin-Evoked Calcium Signals in Isolated Primary Rat Gonadotropin-Releasing Hormone Neurons. *Neuroendocrinology*, *93*, 114-120.
- Krueppel, R., Remy, S., & Beck, H. (2011). Dendritic Integration in Hippocampal Dentate Granule Cells. *Neuron*, *71*, 512-528.
- Krupa, M., Vidal, A., & Clément, F. (2013). A Network Model of the Periodic Synchronization Process in the Dynamics of Calcium Concentration in GnRH Neurons. *Journal of Mathematical Neuroscience*, *3*(4), doi:10.1186/2190-8567-3-4
- Kuehl-Kovarik, M. C., Pouliot, W. A., Halterman, G. L., Handa, R. J., Dudek, F. E., & Parin, K. M. (2002). Episodic bursting activity and response to excitatory amino acids in acutely dissociated gonadotropin-releasing hormone neurons genetically targeted with green fluorescent protein. *Journal of Neuroscience*, *22*, 2313-2322.
- Kuo, C. -C., & Bean, B. P. (1994). Na⁺ channels must deactivate to recover from inactivation. *Neuron*, *12*, 819-829.

- Kusano, K., Fueshko, S., Gainer, H., & Wray, S. (1995). Electrical and synaptic properties of embryonic luteinizing hormone-releasing hormone neurons in explant cultures. *Proceedings of the National Academy of Sciences of the United States of America*, *92*, 3918-3922.
- Layman, L. C. (1999) Genetics of human hypogonadotropic hypogonadism. *American Journal of Medical Genetics*, *89*, 240-248.
- LeBeau, A., Goor, F. V., Stojilkovic, S., & Sherman, A. (2000). Modeling of membrane excitability in gonadotropin releasing hormone secreting hypothalamic neurons regulated by Ca^{2+} mobilizing and adenylyl cyclase-coupled receptors. *The Journal of Neuroscience*, *20*, 9290-9297.
- Lee, K., Duan, W., Sneyd, J., & Herbison, A. E. (2010). The Slow Calcium-Activated Afterhyperpolarization Currents Control Burst Firing Dynamics in Gonadotropin-Releasing Hormone Neurons. *The Journal of Neuroscience*, *20*(18), 6214-6224.
- Lee, K., Liu, X., & Herbison, A. E. (2012) Burst firing in gonadotropin-releasing hormone neurons does not require ionotropic GABA or glutamate receptor activation. *Journal of Neuroendocrinology*, doi: 10.1111/j.1365-2826.2012.02360.x
- Liu, X., & Herbison, A. E. (2008). Small-conductance calcium-activated potassium (SK) channels control excitability and firing dynamics in gonadotropin-releasing hormone (GnRH) neurons. *Endocrinology*, *149*, 3598-3604.
- Liu, X., Lee, K., & Herbison, A. E. (2008). Kisspeptin Excites Gonadotropin-Releasing Hormone Neurons through a Phospholipase C/Calcium-dependent Pathway Regulating Multiple Ion Channels. *Endocrinology*, *149*, 4605-4614.
- Liu, X., Porteous, R., d'Anglemont de Tassigny, X., Colledge, W. H., Millar, R., Petersen, S. L., & Herbison, A. E. (2011). Frequency-Dependent Recruitment of Fast Amino Acid and Slow Neuropeptide Neurotransmitter Release Controls Gonadotropin-Releasing Hormone Neuron Excitability. *The Journal of Neuroscience*, *31*(7), 2421-2430.
- MacColl, G., Quinton, R., & Bouloux, P. M. G. (2002). GnRH neuronal development: insights into hypogonadotropic hypogonadism. *Trends in Endocrinology & Metabolism*, *13*(3), 112-118.

- Martinez, d. I. E. G., Choi, A. L., & Weiner, R. I. (1992). Generation and synchronization of gonadotropin-releasing hormone (GnRH) pulses: Intrinsic properties of the GT1-1 GnRH neuronal cell line. *Proceedings of the National Academy of Sciences of the United States of America*, *89*, 1852-1855.
- Meeks, J. P., & Mennerick, S. (2007). Action Potential Initiation and Propagation in CA3 Pyramidal Axons. *Journal of Neurophysiology*, *97*, 3460-3472.
- Mellon, P. L., Windle, J. J., Goldsmith, P. C., Padula, C. A., Roberts, J. L., & Weiner, R. I. (1990). Immortalization of hypothalamic GnRH neurons by genetically targeted tumorigenesis. *Neuron*, *5*, 1-10.
- Messenger, S., Chatzidaki, E. E., Ma, D., hendrick, A. G., Zahn, D., Dixon, J., Thresher, R. R., malinge, I., Lomet, D., Carlton, M. B. L., Colledge, W. H., Caraty, A., & Aparicio, S. A. J. R. (2005). Kisspeptin directly stimulates gonadotropin-releasing hormone release via G protein-coupled receptor 54. *Proceedings of the National Academy of Sciences of the United States of America*, *102*(5), 1761-1766.
- Moenter, S. M. (2010). Identified GnRH neuron electrophysiology: A decade of study. *Brain Research*, *1364*, 10-24.
- Moenter, S. M., DeFazio, A. R., Pitts, G. R., & Nunemaker, C. S. (2003). Mechanisms underlying episodic gonadotropin-releasing hormone secretion. *Frontiers in Neuroendocrinology*, *24*, 79-93.
- Nagai, T., Sawano, A., Park, E. S., & Miyawaki, A. (2001). Circularly permuted green fluorescent proteins engineered to sense Ca^{2+} . *Proceedings of the National Academy of Sciences of the United States of America*, *98*, 3197-3202.
- Nevian, T., Larkum, M. E., Polsky, A., & Schiller, J. (2007). Properties of basal dendrites of layer 5 pyramidal neurons: a direct patch-clamp recording study. *Nature Neuroscience*, *10*(2), 206-214.
- Nunemaker, C. S., DeFazio, R. A., Geusz, M. E., Herzog, E. D., Pitts, G. R., & Moenter, S. M. (2001). Long-Term Recordings of Networks of Immortalized GnRH Neurons Reveal Episodic Patterns of Electrical Activity. *Journal of Neurophysiology*, *86*, 86-93.

- Numemaker, C. S., DeFazio, R. A., & Moenter, S. M. (2002). Estradiol-sensitive afferents modulate long-term episodic firing patterns of GnRH neurons. *Endocrinology*, *143*, 2284-2292.
- Nunemaker, C. S., DeFazio, R. A., & Moenter, S. M. (2003). Calcium current subtypes in gonadotropin-releasing hormone neurons. *Biology of Reproduction*, *69*, 1914-1922.
- Palk, L., Sneyd, J., Shuttleworth, T. J., Yule, D., & Crampin, E. (2010). A dynamic model of saliva secretion. *Journal of Theoretical Biology*, *(266)*(4), 625-640.
- Palmer, L. M., Clark, B. A., Gründemann, J., Roth, A., Stuart, G. J., & Häusser, M. (2010). Initiation of simple and complex spikes in cerebellar Purkinje cells. *The Journal of Physiology*, *588*(10), 1709-1717.
- Pielecka-Fortuna, J., Chu, Z., & Moenter, S. M. (2008). Kisspeptin Acts Directly and Indirectly to increase Gonadotropin-Releasing Hormone Neuron Activity and Its Effects Are Modulated by Estradiol. *Endocrinology*, *149*(4), 1979-1986.
- Piet, R., de Croft, S., Liu, X., & Herbison, A. E. (2014). Electrical properties of kisspeptin neurons and their regulation of GnRH neurons. *Frontiers in Neuroendocrinology*, <http://dx.doi.org/10.1016/j.yfrne.2014.05.006>
- Purvis, L. K., & Butera, R. J. (2005). Ionic current model of a hypoglossal motoneuron. *Journal of Neurophysiology*, *93*, 723-733.
- Roberts, C. B., Best, J. A., & Suter, K. J. (2006). Dendritic processing of excitatory synaptic input in hypothalamic gonadotropin releasing-hormone (GnRH) neurons. *Endocrinology*, *147*, 1545-1555.
- Roberts, C. B., Campbell, R. E., Herbison, A. E., & Suter, K. J. (2008). Dendritic action potential initiation in hypothalamic gonadotropin-releasing hormone neurons. *Endocrinology*, *149*, 3355-3360.
- Roberts, C., O'Boyle, M., & Suter, K. (2009). Dendrites determine the contribution of after depolarization potentials (ADPs) to generation of repetitive action potentials in hypothalamic gonadotropin releasing-hormone (GnRH) neurons. *Journal of Computational Neuroscience*, *26*, 39-53.

- Sasaki, T., Matsuki, N., & Ikegaya, Y. (2011). Action-Potential Modulation During Axonal Conduction. *Science*, *331*, 599.
- Schmidt-Hieber, C., Jonas, P., & Bischofberger, J. (2008). Action potential initiation and propagation in hippocampal mossy fibre axons. *The Journal of Physiology*, *586*(7), 1849-1857.
- Schwanzel-Fukuda, M., & Pfaff, D. W. (1989). Origin of luteinizing hormone-releasing hormone neurons. *Nature*, *338*, 161-164.
- Seminara, S. B., Messager, S., Chatzidaki, E. E., Thresher, R. R., Acierno, J. S., Shagoury, J. K., Bo-Abbas, Y., Kuohung, W., Schwinof, K. M., Hendrick, A. G., Zahn, D., Dixon, J., Kaiser, U. B., Slaugenhaupt, S. A., Gusella, J. F., O'Rahilly, S., Calton, M. B. L., Crowley, W. F., Aparicio, S. A. J. R., & Colledge, W. H. (2003). The GPR54 Gene as a Regulator of Puberty. *The New England Journal of Medicine*, *349*, 1614-27.
- Shu, Y., Duque, A., Yu, Y., Haider, B., & McCormick, D. D. (2007). Properties of Action-Potential Initiation in Neocortical Pyramidal Cells: Evidence From Whole Cell Axon Recordings. *Journal of Neurophysiology*, *97*, 746-760.
- Shu, Y., Hasenstaub, A., Duque, A., Yu, Y., & McCormick, D. A. (2006). Modulation of intracortical synaptic potentials by presynaptic somatic membrane potential. *Nature*, *441*, 761-765.
- Sim, J. A., Skynner, M. J., & Herbison, A. E. (2001). Heterogeneity in the basic membrane properties of postnatal gonadotropin-releasing hormone neurons in the mouse. *The Journal of Neuroscience*, *21*, 1067-1075.
- Smith, J. T., Li, Q., Yap, K. S., Shahab, M., Roseweir, A. K., Millar, R. P., & Clarke, I. J. (2011). Kisspeptin Is Essential for the Full Preovulatory LH Surge and Stimulates GnRH Release from the Isolated Ovine Median Eminence. *Neuroendocrinology*, *152*(3), 1001-1012.
- Sneyd, J., & Dufour, J. F. (2002). A dynamic model of the type-2 inositol trisphosphate receptor. *Proceedings of the National Academy of Sciences of the United States of America*, *99*, 2398-2403.
- Spergel, D., Kruth, U., Hanley, D., Sprengel, R., & Seeburg, P. (1999). GABA- and Glutamate-Activated Channels in Green Fluorescent Protein-Tagged Gonadotropin-Releasing Hormone Neurons in Transgenic Mice. *Journal of Neurophysiology*, *19*, 2037-2050.

- Stafford, L. J., Xia, C., Ma, W., Cai, Y., & Liu, M. (2002). Identification and Characterization of Mouse Metastasis-suppressor *KiSS1* and Its G-Protein-coupled Receptor. *Cancer Research*, *62*, 5399-5404.
- Stuart, G. J., & Häusser, M. (2001). Dendritic coincidence detection of EPSPs and action potentials. *Nature Neuroscience*, *4*, 63-71.
- Suter, K. J., Wuarin, J. P., Smith, B. N., Dudek, F. E., & Moenter, S. M. (2000). Whole-cell recordings from hypothalamic slices reveal burst firing in gonadotropin-releasing hormone (GnRH) neurons identified with green fluorescent protein (GFP) in transgenic mice. *Endocrinology*, *141*, 3731-6.
- Terasawa, E., Keen, K. L., Mogi, K., & Claude, P. (1999). Pulsatile Release of Luteinizing Hormone-Releasing Hormone (LHRH) in Cultured LHRH Neurons Derived from the Embryonic Olfactory Placode of the Rhesus Monkey. *Endocrinology*, *140*(3), 1432-1441.
- Terasawa, E., Schanhofer, W. K., Keen, K. L., & Luchansky, L. (1999). Intracellular Ca^{2+} Oscillations in Luteinizing Hormone-Releasing Hormone Neurons Derived from the Embryonic Olfactory Placode of the Rhesus Monkey. *The Journal of Neuroscience*, *19*(14), 5898-5909.
- Uenoyama, Y., Inoue, N., Pheng, V., Homma, T., Takase, K., Yamada, S., Ajiki, K., Ichikawa, M., Okamura, H., Maeda, K. -I., & Tsukamura, H. (2011). Ultrastructural Evidence of Kisspeptin-Gonadotrophin-Releasing Hormone (GnRH) Interaction in the Median Eminence of Female Rats: Implication of Axo-Axonal Regulation of GnRH Release. *Journal of Neuroendocrinology*, *23*, 863-870.
- van Goor, F., Krsmanovic, L., Catt, K., & Stojilkovic, S. (1999a). Coordinate regulation of gonadotropin-releasing hormone neuronal firing patterns by cytosolic calcium and store depletion. *Proceedings of the National Academy of Sciences of the United States of America*, *96*, 4101-4106.
- van Goor, F., Krsmanovic, L., Catt, K., & Stojilkovic, S. (1999b). Control of Action Potential-Driven Calcium Influx in GT1 Neurons by the Activation Status of Sodium and Calcium Channels. *Molecular Endocrinology*, *13*, 587-603.
- van Goor, F., LeBeau, A., Krsmanovic, L., Sherman, A., Catt, K., & Stojilkovic, S. (2000).

- Amplitude-dependent spike broadening and enhanced Ca^{2+} signaling in GnRH-secreting neurons. *Biophysical Journal*, 79, 1310-1323.
- Vidal, A., & Clément, F. (2010). A Dynamical Model for the Control of the Gonadotrophin-Releasing Hormone Neurosecretory System. *Journal of Neuroendocrinology*, 22, 1251-1266.
- Weiss, J., Crowley, W. F. Jr., & Jameson, J. L. (1989). Normal structure of the gonadotropin-releasing hormone (GnRH) gene in patients with GnRH deficiency and idiopathic hypogonadotropic hypogonadism. *The Journal of Clinical Endocrinology & Metabolism*, 69(2), 299-303.
- Zhang, C., Bosch, M. A., Rønnekleiv, O. K., & Kelly, M. J. (2013). Kisspeptin Activation of TRPC4 Channels in Female GnRH Neurons Requires PIP2 depletion and cSrc Kinase Activation. *Endocrinology*, 154(8), 2772-2783.
- Zhang, C., Roepke, T. A., Kelly, M. J., & Rønnekleiv, O. K. (2008). Kisspeptin Depolarizes Gonadotropin-Releasing Hormone Neurons through Activation of TRPC-Like Cationic Channels. *The Journal of Neuroscience*, 28(17), 4423-4434.
- Zhang, C., Rønnekleiv, O. K., & Kelly, M. J. (2013). Kisspeptin inhibits a slow afterhyperpolarization current via protein kinase C and reduces spike frequency adaptation in GnRH neurons. *American Journal of Physiology - Endocrinology and Metabolism*, 304(11), E1237-E1244.
- Zhang, X., & Spergel, D. (2012). Kisspeptin Inhibits High-Voltage Activated Ca^{2+} Channels in GnRH Neurons via Multiple Ca^{2+} influx and Release Pathways. *Neuroendocrinology*, 96, 68-80.

